

The design of a hard rock permittivity and loss sensor to be integrated with borehole radar

Beukes Kotzé



UNIVERSITEIT • STELLENBOSCH • UNIVERSITY
jou kennisvennoot • your knowledge partner

**Thesis presented in partial fulfillment of the requirements for the degree of Master of Science in
Engineering at the University of Stellenbosch**

**Supervisors: Prof KD Palmer
Prof JH Cloete**

April 2004

Declaration

I, the undersigned, hereby declare that the work contained in this thesis is my own original work and that I have not previously in its entirety or in part submitted it at any university for a degree.

Signature: 

Date: 09/03/2004

Abstract

The use of ground penetrating radar, and especially borehole radar in underground mines, is becoming increasingly attractive. This is due to the improvements in the user friendliness of this system. Borehole radar is able to sense accurately geological faults and structures hidden inside the rock body and this information is of value to geologists.

In the quest to increase the accuracy of the radar, it was realized that the borehole trajectory and surrounding rock properties are needed. This thesis discusses a rock permittivity and loss sensor which is designed to be deployed in cylindrical hard rock boreholes with diameter of about 50 mm. The sensor consists of electrodes to produce capacitance that is dependant on the rock properties, and electronics to measure this dependency. The biggest problem foreseen is that the probe will not be in direct contact with the rock body.

Cylindrical Electrodes were designed using numerical simulations and physical models. Sensitivity and noise attributes received attention.

Electronic components were used to sense the small capacitance produced by the electrodes. The resulting signals are slow changing "DC" voltages from which an indication of the needed properties could be extracted.

The system was integrated and tested in both laboratory and mine conditions. Test-result-based improvements were introduced and led to satisfactory working of the probe. However, the deployment method will need attention before this probe can be used in field conditions.

Opsomming

Die kommersiële gebruik van boorgatradar begin al hoe meer aantreklik word, in skag myne, aangesien die radar al hoe meer gebruikersvriendelik word. Die radar kan geologiese eienskappe in ontwikkelende dele van die myn uitwys. Die inligting is van groot waarde vir die betrokke geoloë.

Om die akkuraatheid van die radar inligting te verhoog, is die boorgat trajek en eienskappe van die rots wat die gat omring nodig. Die fokus van die studie is om 'n sensor te ontwikkel wat die rots permitiwiteit en verliese meet en weergee. Die voorgestelde oplossing bestaan uit elektrodes wat 'n kapasitor vorm wat afhanklik is van die bogenoemde rots eienskappe en elektronika om die verandering te meet. Die grootste uitdaging is weens die feit dat die probe nie in direkte kontak met die rots sal wees nie.

Elektrodes is ontwikkel deur middel van numeriese simulاسies en fisiese modelle. Aandag is gegee aan sensitiwiteit en ruis eienskappe.

Elektroniese komponente is gebruik om die verandering in klein waardes van kapasitansie waar te neem en as 'n stadig veranderende "GS" waarde weer te gee.

Die sisteem is geïntegreer en in beide laboratorium en myn omstandighede getoets. Verbeterings is aangebring na toetse en bevredigende resultate is verkry. Nog aandag moet wel geskenk word aan ontplooiings meganismes.

Acknowledgements

Firstly I would like to thank my Heavenly Father for the strength, peace and joy that I have received so abundantly during the work on this project. May this be to glorify Your Name.

Prof Keith Palmer for endless ideas and practical solutions.

Prof Johannes Cloete for the amazing enthusiasm in all aspects of life.

The "dudes" in molshoop. Paul, Brian, Tim, Lötter, Stephan, Wernich. Not one day passed that you did not unselfishly help me in one way or the other. Bachelors beware!!

Wessel Croukamp and Ullrich, for the precision work that was a stable foundation to build on.

Pieter Henning, my flatmate, for an invaluable bounce board to test ideas on. Here's to surfing after work!!!

Thanks to my late father, he was my inspiration, and thanks to my mother who always supports me with enthusiasm.

Lastly to Jenine, my fiancé: Thanks for all the support you have given me.

Ek het jou lief.



Table of contents

Table of contents	VI
Table of figures	VIII
List of tables	XI
Symbols used	XII
1. Introduction.....	1
1.1 Background to Borehole Radar	1
1.2 Problem definition and proposed solution	2
1.3 Layout of this document	3
2. Electrode design.....	4
2.1 Computer simulations	4
2.1.1 Introduction	4
2.1.2 The guard electrode concept[7].....	5
2.1.3 Numerical simulations of electrode configurations.....	7
2.2 Electrode design: Physical models.....	18
2.2.1 Three different probes built to produce physical tests.....	18
2.2.2 Correlation between CST and physical probes.....	20
2.3 Conclusions: designing of electrodes	21
3. Electronics.....	22
3.1 The sensing of capacitance.....	22
3.1.1 Sinusoidal drive signal: Phase and amplitude detectors.....	22
3.1.2 Sinusoidal drive signal: Resonant tank	23
3.1.3 Saw tooth drive signal	24
3.1.4 Square wave driving method.....	26
3.1.5 Implementation of non-sinusoidal drive schemes and results obtained.....	28
3.1.6 Conclusions on the sensing of capacitance	33
3.2 Choosing final electrode and drive configuration	34
3.2.1 Saw driven based sensor	34
3.2.2 Square driven based sensor.....	35
3.2.3 Most suitable sensor	35
3.3 Square signal generator	37
3.3.1 Oscillator	37
3.3.2 Buffer stage.....	37
3.4 Buffer and amplifier for signal received from electrodes	38
3.5 Sampling of amplified signal.....	40
3.6 Conditioning of DC signals	45
3.6.1 Low-pass filter.....	45
3.6.2 DC shifting of output signal.....	46



3.7	Comprehensive and detailed schematic	46
3.8	Field deployable prototype	48
3.7.1	Physical assembly of electrodes and housing for electronics	48
3.7.2	Printed circuit board design and electronics	49
4	Testing of rock probe	51
4.1	Sample and hold chain accuracy	51
4.2	Tests in simulated borehole conditions	52
4.2.1	Test setup	52
4.2.2	Method followed in test	53
4.2.3	Results	54
4.2.4	Attributes resulting from tests: Characteristic of step response	58
4.2.5	Attributes resulting from tests: Loss test	60
4.2.6	Conclusions on "bazooka" tests	61
4.3	Test using a characterized rock core	62
4.3.1	Introduction	62
4.3.2	Results obtained	64
4.3.3	Test on resolution of probe	66
4.4	Discussion of test results	68
5	Conclusions	71
5.1	Overview	71
5.2	Properties of sensor under laboratory conditions	71
5.3	Problems associated with mine conditions	72
5.4	Future research possibilities	73
	Bibliography	74
	Appendix A: Mine tests	76
	Conclusions on mine tests:	83
	Appendix B: Detailed figure of "Bazooka"	84

Table of figures

Figure 1-1 Schematic of Radar deployment	1
Figure 2-1 Positioning of guard electrode and possible field lines.....	5
Figure 2-2 An electrode configuration with capacitances shown as lumped elements	6
Figure 2-3 Diagram of the ideal position of probe inside the borehole	8
Figure 2-4 Cylindrical electrodes with changed material	10
Figure 2-5 Square electrodes showing drive elements.....	10
Figure 2-6 Square electrodes showing layers.....	10
Figure 2-7 Linear relationship between frequency and current for simulated probe	12
Figure 2-8 Electrodes placed far apart.....	13
Figure 2-9 Electrodes placed far apart with small guard	13
Figure 2-10 Electrodes placed close to each other	13
Figure 2-11 Section through electrodes showing the critical dimensions X, Y and Z.....	14
Figure 2-12 Electrodes with (2,26,2) dimensions.....	15
Figure 2-13 Electrodes with (10,10,10) dimensions	15
Figure 2-14 Electrodes with (14,2,14) dimensions.....	15
Figure 2-15 Electrodes with (9,2,9) dimensions.....	15
Figure 2-16 Test one: Effect of guard length to sensed capacitance	16
Figure 2-17 Test one: Effect of guard length to probe sensitivity	16
Figure 2-18 Test two: Separation of active electrodes - effect on capacitance	17
Figure 2-19 Test two: Separation of active electrodes - effect on sensitivity.....	17
Figure 2-20 Probe 1 with large guard and rock core placed alongside	19
Figure 2-21 Probe 3 with small guard spacing.....	19
Figure 3-1 Major subsystems of sensor to be developed	22
Figure 3-2 Schematic of resonant tank sensing method showing all critical elements.....	23
Figure 3-3 Example of a possible saw tooth signal	24
Figure 3-4 Model of sensor with current sensing resistor added.....	24
Figure 3-5 Output signal indicating attributes connected to capacitive and resistive parts.....	25
Figure 3-6 Example of possible square waveform.....	26
Figure 3-7 Model of sensor with lumped elements inserted to produce capacitive voltage division	26
Figure 3-8 Resulting waveform for square drive method.....	27
Figure 3-9 Saw tooth drive method with no amplification	28
Figure 3-10 Amplifier added to electrodes	29
Figure 3-11 Output waveform	30
Figure 3-12 Generator A producing a "rough" signal.....	31
Figure 3-13 Generator B producing a "smooth" signal	31
Figure 3-14 Smooth signal generator	31
Figure 3-15 Square wave method.....	33



Figure 3-16 Saw driven based sensor: Sampled data.....	34
Figure 3-17 Saw driven based sensor: Averaged data.....	35
Figure 3-18 Schematic of oscillator buffer stage	37
Figure 3-19 Model of sensor with lumped elements (repeated from Figure 3-7).....	38
Figure 3-20 Schematic of electrode signal amplifier.....	39
Figure 3-21 Sample and hold scheme: First sample	40
Figure 3-22 Sample and hold scheme: Second sample	40
Figure 3-23 Simplified schematic of sensor with sample and hold components	42
Figure 3-24 Control signals for sample and hold components	43
Figure 3-25 Detailed schematic of sample and hold scheme.....	44
Figure 3-26 Butterworth low-pass filter	45
Figure 3-27 Schematic of DC level shifter	46
Figure 3-28 Comprehensive schematic	47
Figure 3-29 Sectional cut through probe to describe mechanical assembly	48
Figure 3-30 Picture of mechanically strong probe	49
Figure 3-31 Populated printed circuit board with major components isolated.....	49
Figure 4-1 Accuracy of sampling chain: Channel 1	51
Figure 4-2 Accuracy of sampling chain: Channel 2	52
Figure 4-3 Picture of "bazooka" on test site.....	53
Figure 4-4 Bazooka placed for the touching tests	53
Figure 4-5 Indication of capacitance with water level changing.....	56
Figure 4-6 Indication of losses with water level changing.....	56
Figure 4-7 Ability (of lack thereof) of probe to sense rock in a water filled hole	57
Figure 4-8 Sketch one: Homogeneous air	58
Figure 4-9 Sketch two: Water level at guard.....	58
Figure 4-10 Sketch three: water level at sense electrode.....	58
Figure 4-11 Sketch four: Homogeneous water	58
Figure 4-12 Response of probe to step function: Capacitance.....	59
Figure 4-13 Response of probe to step function: Resistance.....	60
Figure 4-14 Effect of saline water on received waveform.....	60
Figure 4-15 Test setup for measuring the borehole core.....	63
Figure 4-16 Close-up picture of the active probe elements and the core.....	63
Figure 4-17 Sensed permittivity of rock core	64
Figure 4-18 Permittivity of Bleskop marker used as reference for tests.....	64
Figure 4-19 Sensed losses of rock core	65
Figure 4-20 Losses of the Bleskop marker used as reference for tests.....	65
Figure 4-21 The actual received signal that was sampled.....	66
Figure 4-22 Sensitivity test setup: Chrome and pyroxenite interface	67
Figure 4-23 Sensed permittivity of chrome and pyroxenite interface	67



Figure 4-24 Sensed losses of chrome and pyroxenite interface.....	68
Figure 4-25 Transfer of probe for the two tests performed: Permittivity	69
Figure 4-26 Transfer of probe for the test performed: Losses	70

List of tables

Table 2-1 Mediums implemented in layers	8
Table 2-2 Results for FEKO simulations	9
Table 2-3 Test results: Capacitance values for different configurations and different mediums	20
Table 2-4 Sensitivity tradeoff between CST simulations and physical tests	21
Table 2-5 Capacitance value tradeoff between CST simulations and physical tests: Probe 3	21
Table 3-1 Verification of results by using lumped elements	32
Table 3-2 Tradeoff between two sensors	36
Table 3-3 Summary of probe to be developed	36
Table 3-4 Components used to generate control signals	44
Table 3-5 Transfer characteristics of Butterworth filter	46
Table 4-1 Step-by-step sequence of experiment	54
Table 4-2 Results for first part of test: Centred versus probe touching one side - permittivity	54
Table 4-3 Results for first part of test: Centred versus probe touching one side – Losses	55
Table 5-1 Product specification under laboratory test situations	71



Symbols used

Symbol	Definition of symbol	Units	Value
ϵ	The absolute permittivity of a material	F/m	
ϵ_0	Reference permittivity of vacuum ^[1, page 52]	F/m	8.85×10^{-12}
ϵ_r	Permittivity as a factor of the permittivity of vacuum		
ϵ_r'	The real part of permittivity contributing to the storage of electricity		
ϵ_r''	The imaginary part of permittivity contributing to the losses in the system		
ϵ_{r1}	Relative permittivity of first material used		
ϵ_{r2}	Relative permittivity of second material used		
Tan δ	Description of dielectric loss ^[2, page 285] Tan $\delta = \epsilon_r'' / \epsilon_r'$		
Q	Quality factor Q = 1 / Tan δ		
v	Voltage of the form $v = K \sin(\omega t)$		



1. Introduction

1.1 Background to Borehole Radar

Borehole radar is able to accurately sense geological faults and structures hidden inside a rock body at distances up to 50 m from suitable boreholes, typically of diameter 50 mm. It is a specialized sub-discipline of ground penetrating radar. The main application of this radar is to aid geologists in surveying and quantifying an ore body in hard-rock deep mining. This survey information is used to estimate the amount of ore in the mine as well as locations of geological faults that can lead to accidents. Pilot holes (approximately 47 mm in diameter) are drilled in a fan-like manner in the developing areas of a mine. The cores retrieved from these holes are used with the experience of the geologist to form a map of the geological structure. The spacing between the holes is large in relation to the geological attributes and thus the data received is spatially under sampled^[3]. The radar is used to fill these gaps between the holes on the geologist's map.

An overview of the working of the radar system will be given now. In Figure 1-1 a schematic is presented with the major components of the radar.

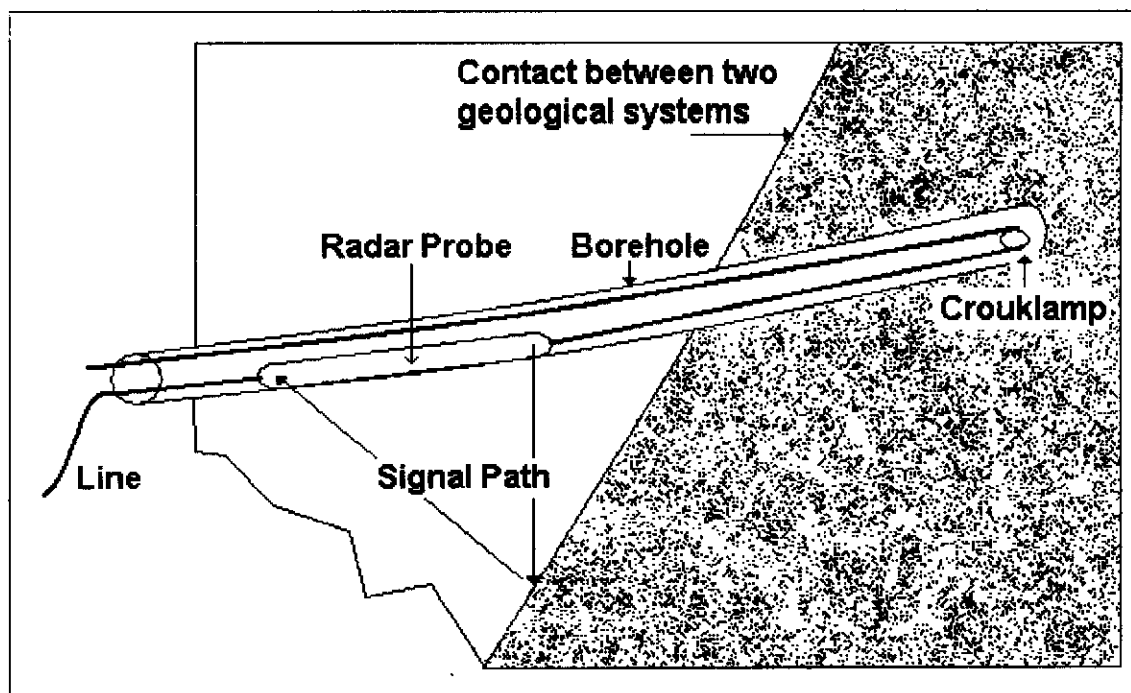


Figure 1-1 Schematic of Radar deployment

The radar probe is deployed by winching the probe into the borehole at a constant velocity. The dyneema line that is wrapped around the Crouklamp is used to haul the probe into the hole. Strengthened fiber optic

cables are connected to the other end of the probe and are used to extract the probe. The transmitted radar pulses are reflected from in-homogeneities in the rock body and are received and digitized inside the probe. Data is sent out through the fiber optic cables and is stacked and saved on a hand held computer at the collar of the hole. The trajectory of the borehole is used to generate a reference coordinate system for the radar. By doing this, the position of the geological attribute is pinpointed in the rock body. The constant velocity at which the probe is winched produces a continuous profile of the rock. Frequency content of the radar pulse is 10 – 100 MHz.

Borehole radar progressed vastly from the mid 1980's and the rate accelerated in the past 3 years to such an extent that the whole system has been streamlined by improving the accuracy and sensitivity through characterizing the system transfer function. These improvements necessitated a new look at the peripheral elements: deploying the probe easily and effectively and getting accurate borehole trajectory and rock properties. The Crouklamp and winches were developed to ease the deploying of the probes. The Sindlehead navigator was developed to measure borehole trajectory^[4]. Measuring the properties of the hard rock is required to improve radar performance and is the focus of this document.

1.2 Problem definition and proposed solution

A traditional indication of the rock layers penetrated by the hole and their properties are obtained from a study of the borehole core. This log of the specific hole is sometimes not accurate or not available. The electrical properties of the rock, which are the focus of the sensor, are also of importance as the geologist is at present not equipped to log these electrical properties. This information is crucial for the following reasons. Firstly, the speed of propagation is linked to the electrical properties of the rock. This effect is important in relating radar pulse delay to distance traveled. Secondly, the information on the location of the layers can be used to verify and improve the mines geological models. The displacement of the radar probes is known, but it will be helpful if this information can be verified. Thirdly, if the hole is filled either fully or partially with water, the exact location of the water level will be known. Fourthly, the reflecting mechanisms are not entirely understood and a dedicated sensor may shed more light on the layers or the transition between layers that produce the radar reflections.

The sensor to be developed here must be able to sense the properties of the rock, especially the hard rock permittivity and conductivity. The sensor must be deployable in a borehole in a way similar to the radar. Commercial probes measuring properties of materials are available but these sensors have open electrodes and must be in direct contact with the material^[5]. This will not be the case with the sensor to be designed.

The limitations of conditions underground are extreme and the sensor will have to overcome these limitations. The sensor must be placed inside a probe to protect it from water, dirt and moisture. This

probe has an inside diameter of some 30 mm. The difference in probe and hole sizes means that the electrodes may not be in even, close contact to the rock body. This spatial separation comes about as the borehole is not smooth or free of rubble and can cause the probe to get stuck if it is not small enough. As previously mentioned, the holes may be filled with water which could impair the sensor's working. This must be catered for. As with the radar, the sensor must use a local power source inside the probe, this is usually done with a battery pack. Batteries do have limited power and the voltage must be regulated to create stable power supply. The data will be sampled and stored on the Sindlehead navigator as the two probes are expected to work in conjunction with each other. Temperature stability is also necessary as the rock temperature can rise up to 70 °C in deep mining conditions.

To create coupling to the rock body, electrodes are introduced. Custom designed electrodes will be used to implement this. The electrodes will be controlled by electronics located inside the probe.

1.3 Layout of this document

The sensor can be divided into two parts: One is the electrodes that will be able to produce signals which are sensitive to the rock properties, and the second is the electronics used to drive the electrodes and receive output signals. Chapter two focuses on the design of the electrodes. The iterative process of finding the best electrode configuration was done with the aid of two software packages (FEKO and CST Microwave Studio). Two sets of electrodes were made according to the results obtained with the software and were tested. Chapter three describes the design of the necessary electronics. Sections of this chapter include: Introducing the different drive options and choosing the optimal one; the internal sampling/sensing of the received signal and the conditioning of this signal. Chapter four explains the various tests done on the sensor and the results obtained from these tests. Chapter five is dedicated to the conclusions and recommendations.

2. Electrode design

2.1 Computer simulations

2.1.1 Introduction

One of the simplest ways to obtain the dielectric properties of a material is to use it as a dielectric for a capacitor, if this is done the properties of the rock will be transformed to a electrical easily sensed quantity. Two important considerations in this chapter is the use of fringing fields to penetrate the rock as well as the use of a guard electrode to improve sensitivity. At this point the use of cylindrical electrodes is introduced as this will be compatible with the cylindrical borehole environment.

To illustrate the effect of a dielectric on a capacitor the parallel plate capacitor model can be used ^[6, page226]. If two conducting planes are positioned parallel to each other with known area and spacing, the capacitance can be computed empirically.

$$C = \frac{A\epsilon_0\epsilon_r}{d} \quad (2.1)$$

In this equation ϵ_r is the relative permittivity of the material filling the space between the electrodes. Here it is assumed that the field is essentially uniform with negligible fringing. This applies if d is much less than the smallest area dimension.

Reversely, the permittivity can be calculated if the capacitance can be measured easily and accurately with sensing equipment and with known geometry. The quality factor can also be measured and gives an indication of the losses in the system. Measuring devices will be handled in chapter three. Furthermore, it can be shown (and is shown in equation 2.2) that this direct relation between dielectric constant and capacitance holds for all electrode configurations ^[6, page 223].

$$C = \frac{\iint (\bar{D} \cdot \bar{n}) da}{v}$$

If dielectric is electrically linear $\rightarrow \bar{D} = \epsilon \bar{E}$ (2.2)

$$\therefore C = \frac{\iint \epsilon (\bar{E} \cdot \bar{n}) da}{v} = \frac{\epsilon \iint (\bar{E} \cdot \bar{n}) da}{v}$$

As previously mentioned, practicalities place limitations on the design. Two of these limitations influence the electrodes. Firstly, the measurement must be taken in the borehole. This rules out the placing of rock between the electrodes, the fields must be forced into the rock using other methods. The only solution seems to be to penetrate the rock by the fringing fields of the electrodes. The problem is that fringing fields

are a small percentage of the total fields and decrease quickly away from the electrodes. This effect is made worse by the second limitation: the probes will not be in direct contact with the rock.

The fringing effect as well as the decaying effect mentioned in the above paragraph, can be seen in Haus & Melcher page 233^[6]. Although the fields outside the plates are weak, they do spread out quite far. If a material with an elevated ϵ_r is brought close to the edge of the plates, the fringing fields will increase and so will the capacitance. This effect will be the corner stone of the sensor.

2.1.2 The guard electrode concept^[7]

The increase in capacitance due to fringing fields penetrating high ϵ_r materials can be measured, but it is possible to separate these fields into fringing and local (not fringing), which will increase the sensitivity of the sensor substantially. This separation of fields can be done by inserting a grounded (guard) electrode between the two electrodes of the capacitor (that resemble the sensor). By doing this, the strong fields will be produced between the driven electrode and the grounded guard electrode, while the fringing fields will bypass the guard electrode and terminate on the sensing electrode. Figure 2-1 presents a guarded electrode configuration. The field lines in Figure 2-1 are hand drawn and are only an approximate indication of the strength and position of the field lines that will produce the capacitance.

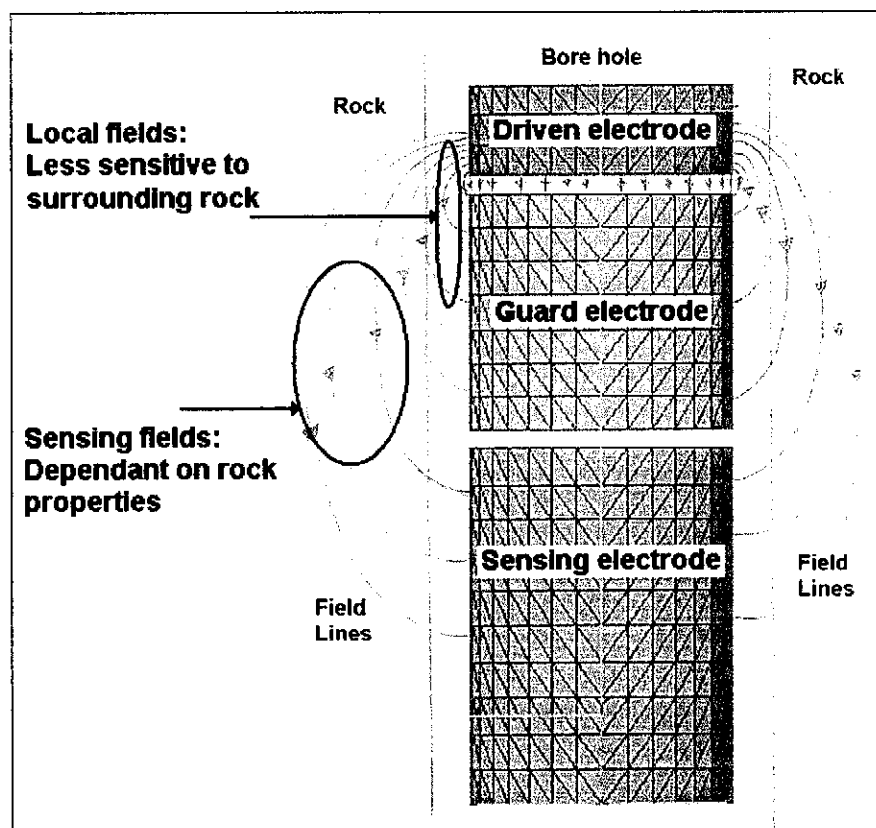


Figure 2-1 Positioning of guard electrode and possible field lines

For this scheme to work, the sensing electrode must be held at a quasi-ground potential to enable the fields to be formed as if the guard and sensing electrodes were attached. The capacitance between the driven and guard electrodes (denoted C_g) will be substantially higher than the capacitance produced between the driven and sensing electrodes (denoted C_{sense}). Most of the fields terminating on the sensing electrode penetrated the rock body and the C_{sense} will be a stronger function of the rock properties. The capacitances created with this configuration is displayed as lumped elements in Figure 2-2.

The capacitance that will be sensed can be divided into lumped elements (described in Figure 2-2) which are produced by the respective fields denoted in Figure 2-1. C_h is produced by the local fields inside the hole and will not be affected by the rock properties. C_r is produced by the displayed sensing fields and will be influenced directly by the rock properties. The value that will be sensed (C_{sense}) is the sum of C_h and C_r . C_g is produced between the driven and guard electrode and is produced in such a way that it will not influence the capacitance that is to be sensed. Schematic representation in Figure 2-2 introduces the first simplified model to describe the electrodes.

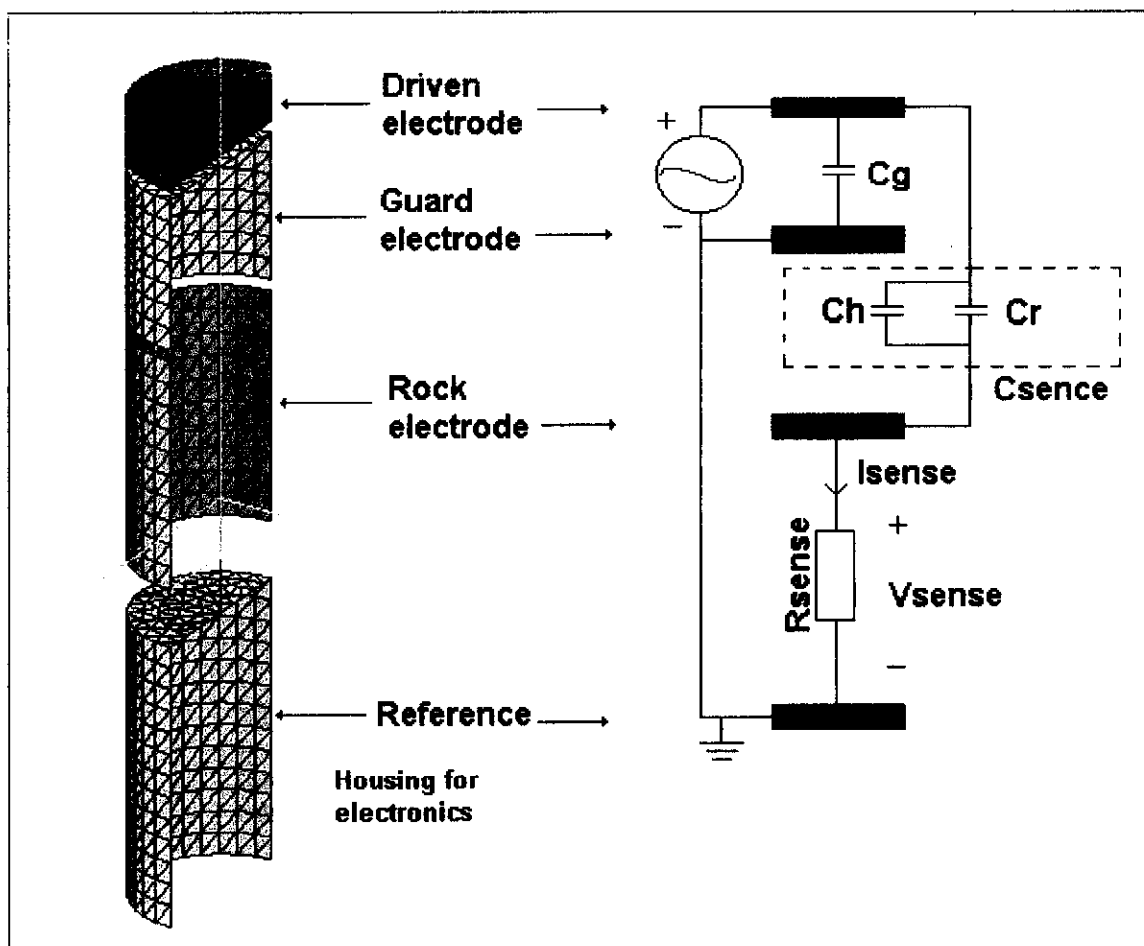


Figure 2-2 An electrode configuration with capacitances shown as lumped elements

All the following simulations done had the guard electrode configuration implemented.

2.1.3 Numerical simulations of electrode configurations

2.1.4.1 Introduction to FEKO and CST

Computer-based analysis of geometries was introduced to speed up the design process as it is faster and easier to change an attribute in a software program than to change a physical model. There were two software packages available to the author. These two packages use different methods to discretize and simulate the geometries. The one was FEKO which is a MOM (Method of moments) based code and the other is CST (Computer Simulation Technology) Microwave Studio which is a FEM (Finite element method) based code. A brief summary of each method will follow.

MOM: The code discretize the interfaces between materials of a three dimensional geometry as triangles and surface/boundary conditions are applied to form the characteristics of the geometry. This code (and specifically FEKO) is thus effective in simulating planar geometries.

FEM: This code discretizes the volume of the geometry (tetrahedral for CST) and uses power and potential relations to characterize the geometry. The code is therefore more suitable for bulky geometries.

Both these simulation packages are optimized to solve electrodynamic problems. Due to the fact that the sensor to be simulated is electrically small and not resonant, attention must be given to the mesh size to ensure that the results are dependable

2.1.4.2. FEKO simulations and results

The guarded electrodes were simulated in FEKO^[8], Figure 2-2 gives a schematic of this configuration. The model excitation element was placed between the guard and the driven electrodes. This is a theoretical port needed by the code to extract the capacitance and is implemented by a sinusoidal drive element as explained. The guard was connected to the housing/reference by a conducting wire located on the axis of the sensor. A 50 Ω load was placed between the sensing (rock) electrode and the ground node to sense the current which in turn indicated the capacitance measured. A voltage division analysis, below, shows that this choice is valid.

Voltage division assuming phasors, $e^{j\omega t}$ (2.3)

$$\frac{\bar{V}_{sense}}{\bar{V}_{drive}} = \frac{R_{sense}}{R_{sense} + j \frac{1}{\omega C_{sense}}}$$

IF $\omega C_{sense} \gg R_{sense}$

$$|\bar{V}_{sense}| = \frac{R_{sense}}{1} |\bar{V}_{drive}| \frac{1}{\omega C_{sense}}$$

eg. $R_{sense} = 50 \Omega$, $f = 1 \text{ MHz}$, $C_{sense} = 1 \text{ pf}$

$$X_{sense} = \frac{1}{\omega C_{sense}} \approx 159.2 \text{ k}\Omega \gg 50 \Omega \quad \text{and} \quad |V_{sense}| = 0.314 \times 10^{-3}$$

$$\therefore |\bar{V}_{drive}| = 10 \text{ V} \quad \text{yields} \quad |\bar{V}_{sense}| \approx 3.1 \text{ mV}$$

which is essentially at ground potential.

The differential voltage between the sense electrodes and housing is small relative to the drive voltage and this implies that the sense electrode is at quasi-ground potential for low frequencies, in the 1 MHz range.

The active electrodes (sensing, driving and guard electrodes) were created as explained in the guard electrode section. Meshing is produced by the FEKO mesher and consists of triangles that form the transition between two materials or the location of metal (MOM discretizing). Three layers of dielectrical mediums were inserted to simulate the borehole conditions. Between the electrodes (radius of 14 mm) one layer of material was inserted and given the properties of air, the second was made to simulate the inside of the borehole. The transition between the "hole" and "rock" (third) layer was at 'n radius of 20 mm. Figure 2-3 gives a radial cut of the centered probe in a borehole.

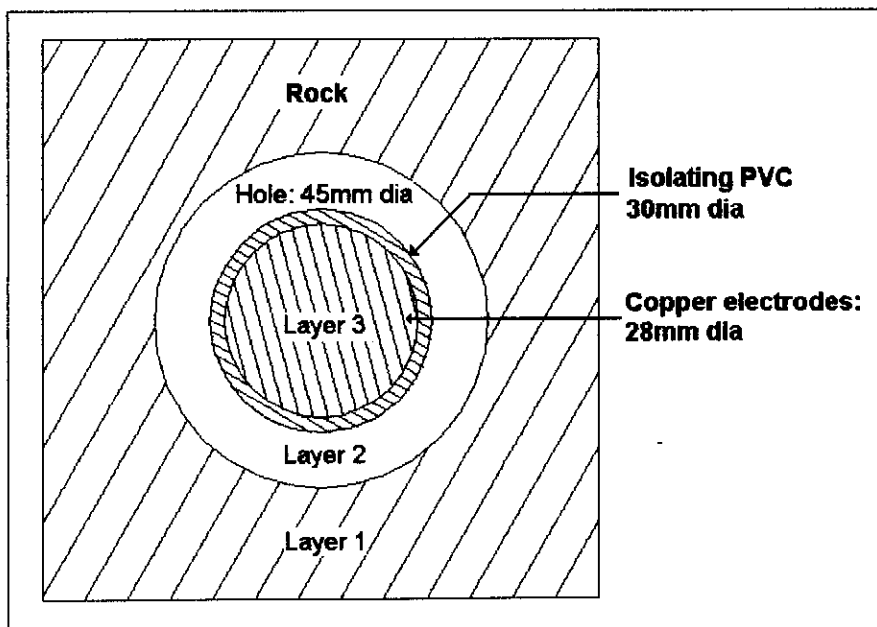


Table 2-1 Mediums implemented in layers

Layer 1	Air
Layer 2	Air Water
Layer 3	Simulated rock ϵ_r from 1 to 20

Figure 2-3 Diagram of the ideal position of probe inside the borehole

In the ideal situation the "rock" layer must extend to infinity, but this could not be done with the code and the "rock" medium had to be bounded to comply with the code. The rock layer was made three times the diameter of the sensor in all directions and has absorbing boundaries. The axial length of the electrodes was chosen by preliminary tests and a thorough investigation is given in section 2.4.5.

The simulation was repeated with different values of ϵ_r for the rock material. These values were chosen to be in the 8 to 14 range as the rock properties are expected to lie in this range. The results obtained from this data did not follow a definite trend and interpretation of the data was troublesome. Usable data was obtained by averaging capacitance simulated over frequency. To present the data the "increase ratio of permittivity" ($\epsilon_{r2} / \epsilon_{r1}$) of the "rock" medium will be given against the corresponding "increase ratio" of the simulated capacitance for the according permittivities. If the sensor had an ideal linear transfer function, the capacitance change will be in the same ratio. In this fringing field situation it was expected that the ratio of capacitance would be smaller than the permittivity ratio but larger than one.

Table 2-2 Results for FEKO simulations

"Increase ratio" of permittivity Ratio of $\epsilon_{r2} / \epsilon_{r1}$ (given in brackets)	Simulated ratio of capacitance (averaged over frequency). Expected to be between one and the value stated in column 1.
1.14 (8/7)	4.6
1.12 (9/8)	2.97
1.11 (10/9)	0.77
1.1 (11/10)	1.68
1.09 (12/11)	1.01
1.08 (13/12)	1.59
1.07 (14/13)	1.12

The averaged data produced some useful information. The ratio of capacitance was consistently higher than one and became more accurate with higher permittivity. The reason for the inconsistent results could be due to the fact that the geometry is not entirely suited for FEKO analysis. This explanation is based on the large (bad) condition number given by the FEKO solver. This number gives an indication of the accuracy of the results and is given in the report file created after the simulation. This number was in the 10^{13} range where as FEKO suggest that it must be less than 10^{10} . This factor became less as the permittivity increased and this could explain why the results in Table 2-2 became more accurate as permittivity increased. The number also decreased as the meshing was made finer, but a much more powerful computer is needed to make the meshing significantly smaller.

FEKO simulation did not produce accurate results and dictated the use of CST.

2.1.4.3 Geometry used for CST simulations.

The CST Microwave Studio electrodes were created similarly to the electrodes created in FEKO. The problem of building a circular geometry with square blocks (tetrahedral in the case of CST) is that there must be a high number of small cubes to approximate the circular geometry. Figure 2-4 shows the cylindrical electrodes created (dark) and the lighter squares indicate how CST changed the geometry to implement it with squares for simulation. If there is too little squares the changed geometry will no longer resemble the intended geometry. The meshing was made smaller and stable results were obtained, this however took a lot of time and processing power. As the meshing favors square geometries, the electrodes were implemented using equivalent rectangular boxes as shown in Figure 2-5 and Figure 2-6.

The capacitance between the two geometries (square and cylindrical) changed, but the fundamental factors stayed the same. (Factors include: Frequency response, ϵ_r dependence and axial geometrical changes). An effort was made to decrease the difference between the two shapes by making the outside circumference of the square and cylindrical electrodes the same. This system was changed and there was a factor two difference between the two geometries according to the simulation. The two simulations followed the same trends in all of the results obtained and thus the decision was made to simulate all the different situations with square electrodes. The simulation time was decreased dramatically and the only factor greatly affecting the meshing was the electrically critical parts in the system (previously the geometry also greatly influenced the meshing). The layers of different materials are shown in Figure 2-6 and are the same as explained for the FEKO simulations.

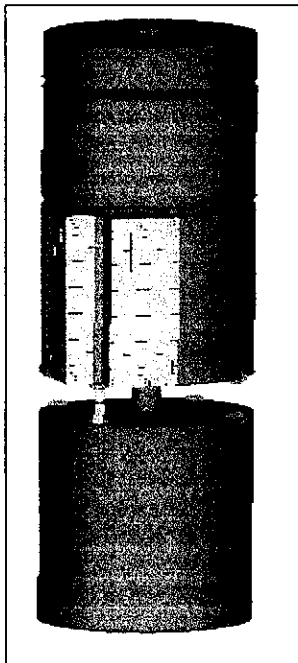


Figure 2-4 Cylindrical electrodes with changed material

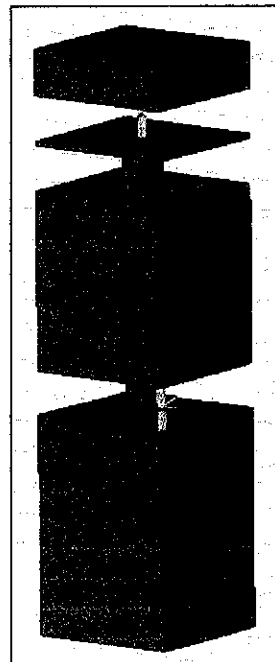


Figure 2-5 Square electrodes showing drive elements

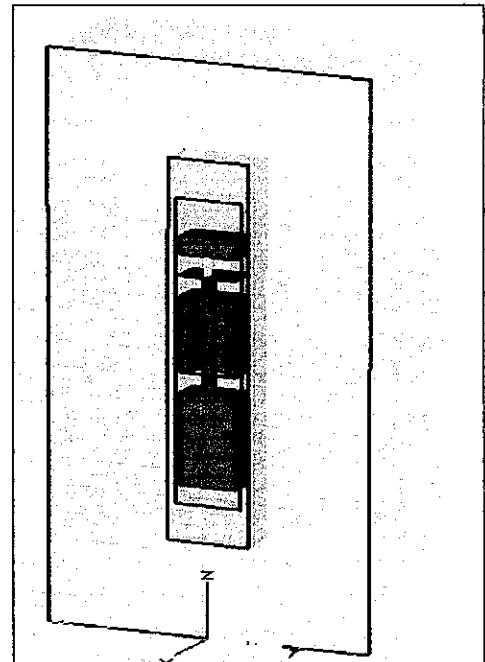


Figure 2-6 Square electrodes showing layers

Some reference to the “critical” parts of the geometry is made. These areas are close to an edge of the electrodes or where there are small parts (relative to the geometry). The built-in mesh generator discretizes the geometry and displays the mesh so that the user can check the meshing. The meshing density can be adjusted by parameters in the mesh properties control box, there are also some special cases that can be addressed. These special cases include finer meshing in dielectric mediums (necessary for the wavelength decreases in high ϵ_r materials), special meshing at round corners and other more specialized features^[9]. The package also includes a function “Adaptive mesh refinement” (AMR) that basically does a convergence test on the simulation results. The AMR function uses previous simulation results to automatically refine the mesh in places that need finer mesh. The two simulation results are related and the size of the error can be specified and was taken as -40 dB in relation to the previous results, for these simulations (advised, default number). The lumped resistor (as in FEKO) was changed to a port with the same input impedance for CST handles ports easier than FEKO and there is no change in attributes. Symmetry was also included and it is important to note that the ports are not duplicated according to the symmetry. The rock must be specified as infinite but there is no boundary in the code that can implement this and a finite amount of rock was inserted around the sensor. This rock stretches at least three times the corresponding sensor size on the corresponding axis in all directions. The wall implemented at the end of the rock is a fully absorbent wall.

2.1.4.4. Simulations done to test the general validity of CST results

Two tests were performed on the electrodes to check the program for irregularities and the ability to produce repeatable results. This is important for obtaining confidence in using the code. Test one is simply to check for correlation between a simulation with no layers and a surrounding permittivity of air to a simulation with all the layers inserted, but the layers are given the same properties as air. CST was able to produce exactly the same result for both the layered and un-layered simulations. The results are so similar that inserting a figure will be of no use as the graphs will lie on top of each other.

Test two will simulate the probe over frequency with loss-less materials and will check that the results are consistent with what is expected from basic circuit analysis.

$$I = j2\pi fCV \quad (2.4)$$

with C and V constant I increases linearly with frequency

The current was sensed by the 50Ω port connecting the sensing and reference electrodes as in Figure 2-2. Figure 2-7 displays this linear relationship.

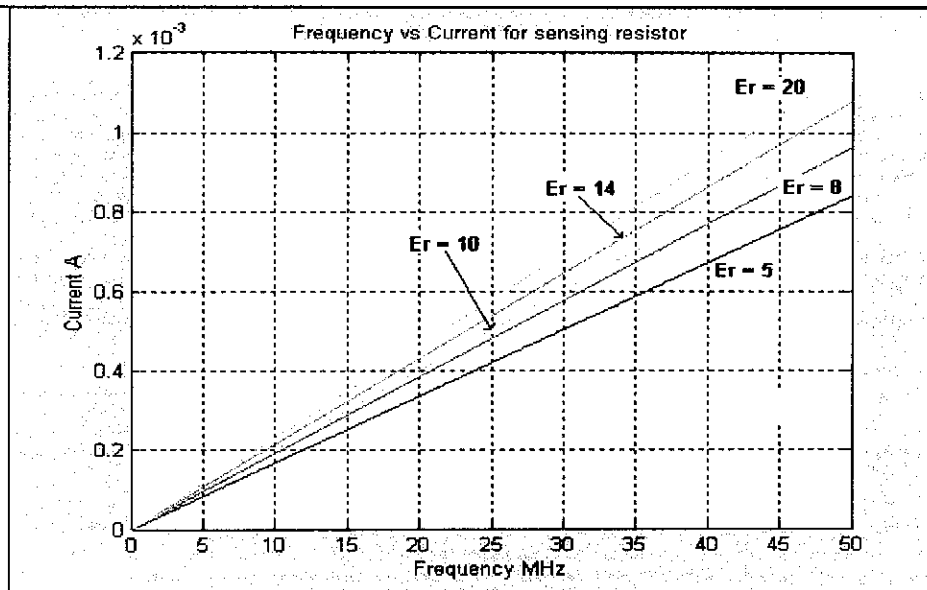


Figure 2-7 Linear relationship between frequency and current for simulated probe

The CST simulation was done five times with different "rock" properties as indicated in the figure and the linear relationship was repeatable. In addition to this, the increase in permittivity gives an increase in capacitance (the slope of the lines increased), which strengthens confidence in the numerical model.

These tests do not declare the CST results as absolutely accurate, but give a representation of the real life situation and gives the user some confidence in the results that were obtained.

2.1.4.5 Optimum electrode spacing through CST simulations

The only dimensions of the probe that can be designed, are the length/spacing of the electrodes. The radius of the sensor is limited by the probe size that is determined by the borehole diameter and adequate clearance to prevent the probe from getting stuck. The optimal electrode size and spacing is obtained when the best trade-off between sensitivity and capacitance size is reached. Sensitivity is measured by the effect that a change in rock ϵ_r produces a change in the output signal (the output signal is a measured voltage directly proportional to rock capacitance). Here, larger is better as the sensor is to have a strong relation to the rock body. The size of the capacitance to be measured is crucial to the ability to sense this value practically.

Existence of this optimum point is expected as there are two extremes that oppose each other. On the one hand, if the sensing and driven electrodes are placed far from each other, the capacitance will be a strong function of the rock properties, but this capacitance will be too small to measure. On the other hand, if the active electrodes are brought close to each other, the capacitance will be large and easy to measure, but no significant penetration of the rock will be produced. To produce a practical grasp of the effect described above, hand drawn pictures similar to Figure 2-1 will be introduced with possible field lines inserted. Three pictures are presented, each with different electrode sizes.

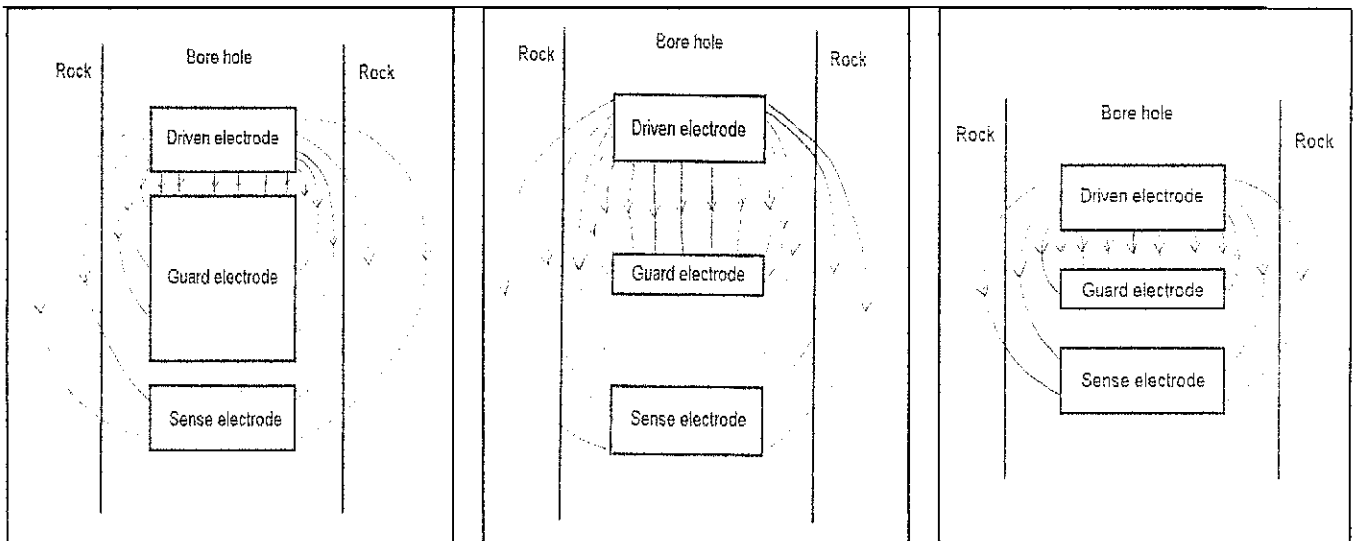


Figure 2-8 Electrodes placed far apart

Figure 2-9 Electrodes placed far apart with small guard

Figure 2-10 Electrodes placed close to each other

Figure 2-8 displays the situation where the electrodes are far apart and the perceived capacitance is expected to be small. Figure 2-10 displays the situation where the electrodes are close to each other and large capacitance but less sensitivity is expected. Figure 2-9 was inserted to try and speculate what the influence of the guard length will be. From the figure, the guard length will not have that big an effect on the sensed capacitance, but the simulations will give a more accurate representation.

To quantify this problem, Figure 2-11 is introduced. In this figure dimensions X, Y and Z are placed to denote the attributes that are to be changed. For the first time a detailed figure of the electrodes is shown and an explanation is due. The driven electrode is positioned at the end of the probe. It was designed this way to decrease the distance that the small sensed signal must travel from the sensing electrodes to reach the electronics. The electronics are housed inside the reference electrode. The drive signal is produced by the electronics inside the housing and are fed to the far side of the sensor by coaxial cables. The signal driving this electrode will be explained fully in chapter three. To connect all of this, two semi-rigid coaxial cables are used as shown in Figure 2-11, the active electrodes are as before. The sum of these dimensions ($X + Y + Z$) controls the separation of the active elements and the dimension Y controls the length of the guard electrode.

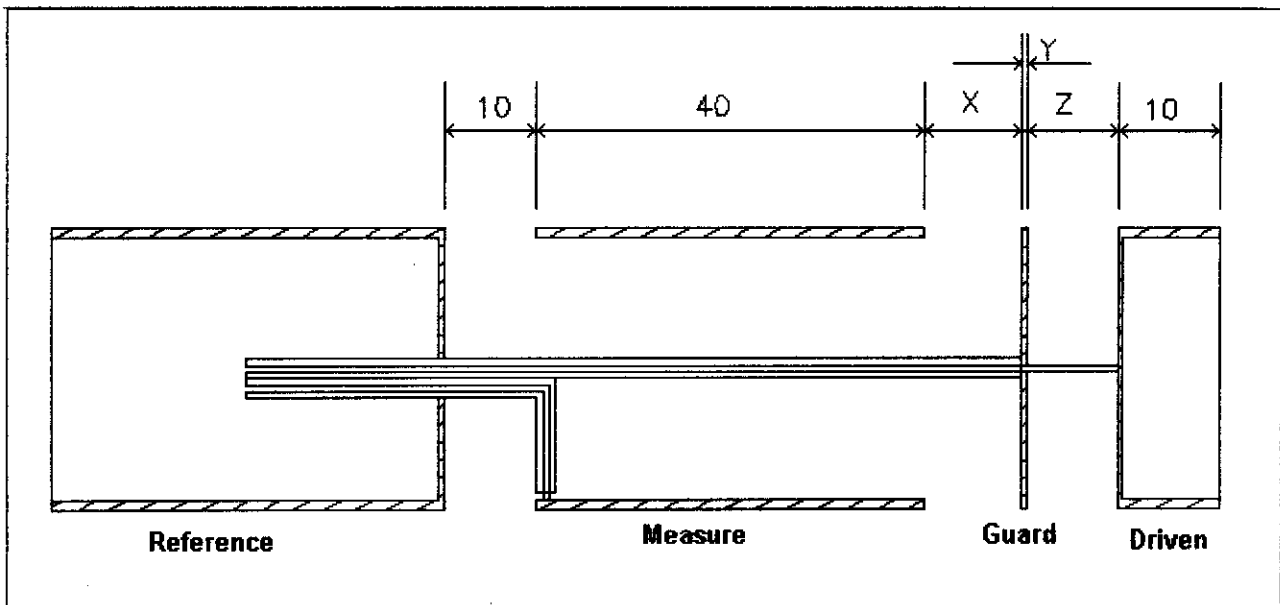


Figure 2-11 Section through electrodes showing the critical dimensions X, Y and Z

The next four pictures are introduced to explain the simulation a little more and to produce graphical information on the exact test conditions. The figures were produced by CST graphical environment and were the actual electrodes used in the simulations. The view presented is a sectional view through the axis of the geometry. The sizes quoted in the headings are in the (X,Y,Z) notation (will be explained in the next paragraph) and refer to the electrode size.

In the graphs to follow the electrode sizes for specific simulations are inserted in a way similar to that of coordinates of a rectangular system for example (14,2,14) indicates the (X,Y,Z) dimensions respectively.

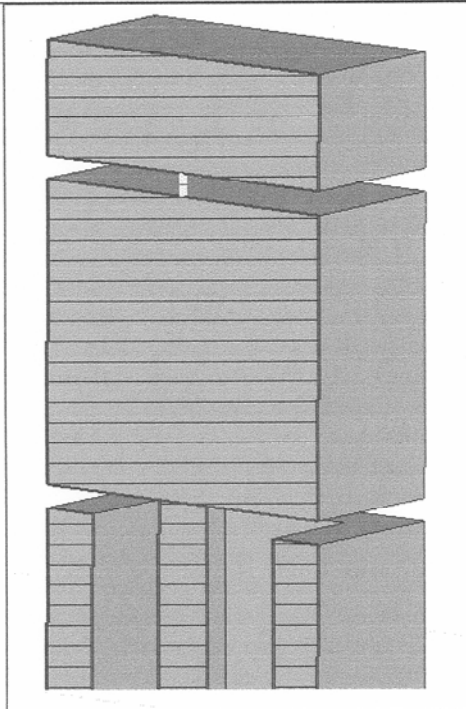


Figure 2-12 Electrodes with (2,26,2) dimensions

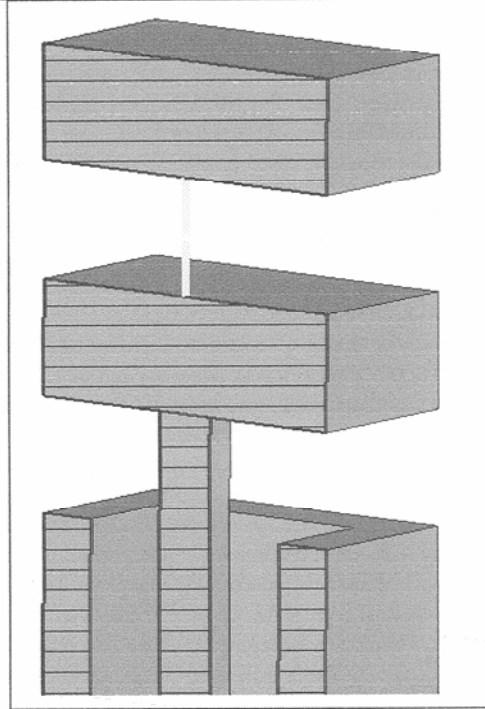


Figure 2-13 Electrodes with (10,10,10) dimensions

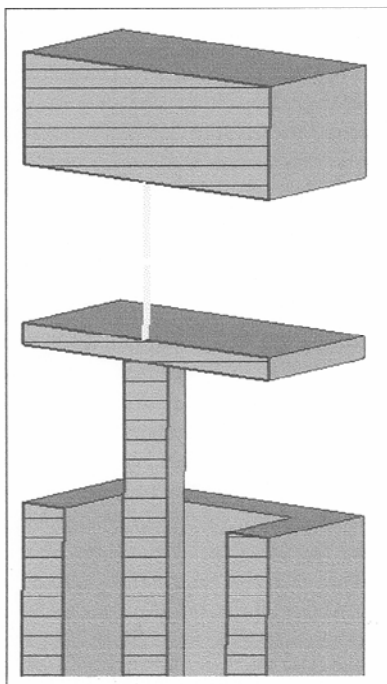


Figure 2-14 Electrodes with (14,2,14) dimensions

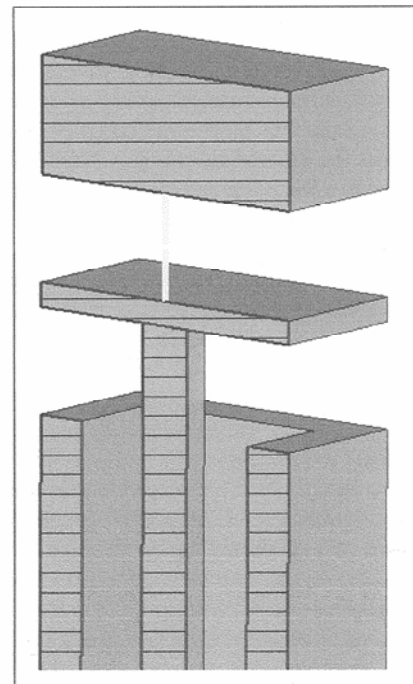


Figure 2-15 Electrodes with (9,2,9) dimensions

Two sets of tests were completed, the one held the total separation ($X + Y + X = 30$ mm) constant and adjusted the guard length (Y) and the second decreased the total separation and held the guard length constant ($Y = 2$ mm). The one simulation (2,32,2) was done only for completeness and don't have a 30 mm total length. For each spacing, a set of results indicating the capacitance versus the permittivity of the rock body was produced.

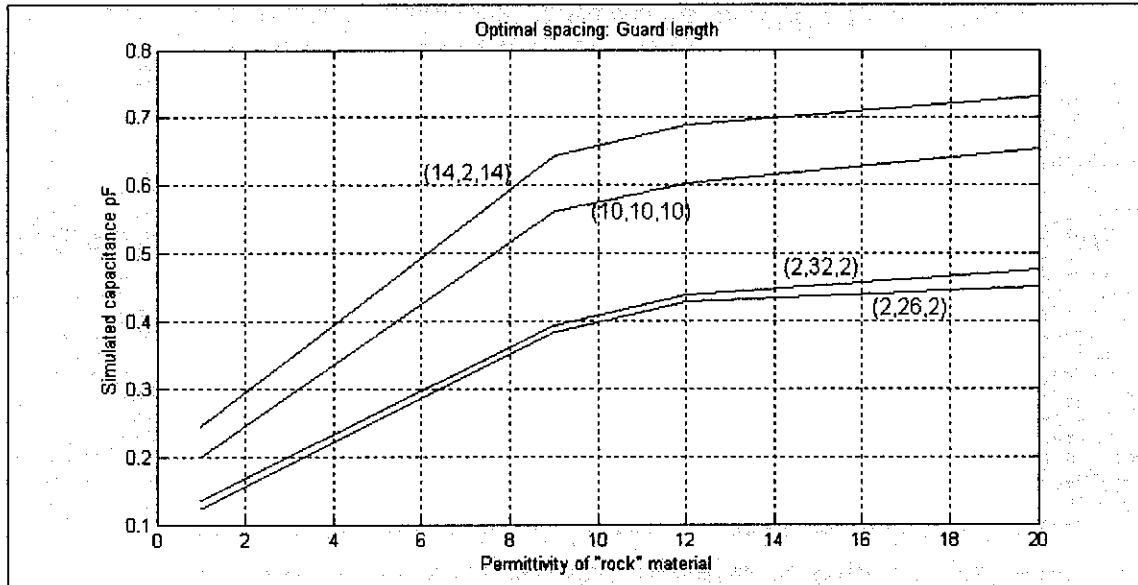


Figure 2-16 Test one: Effect of guard length to sensed capacitance

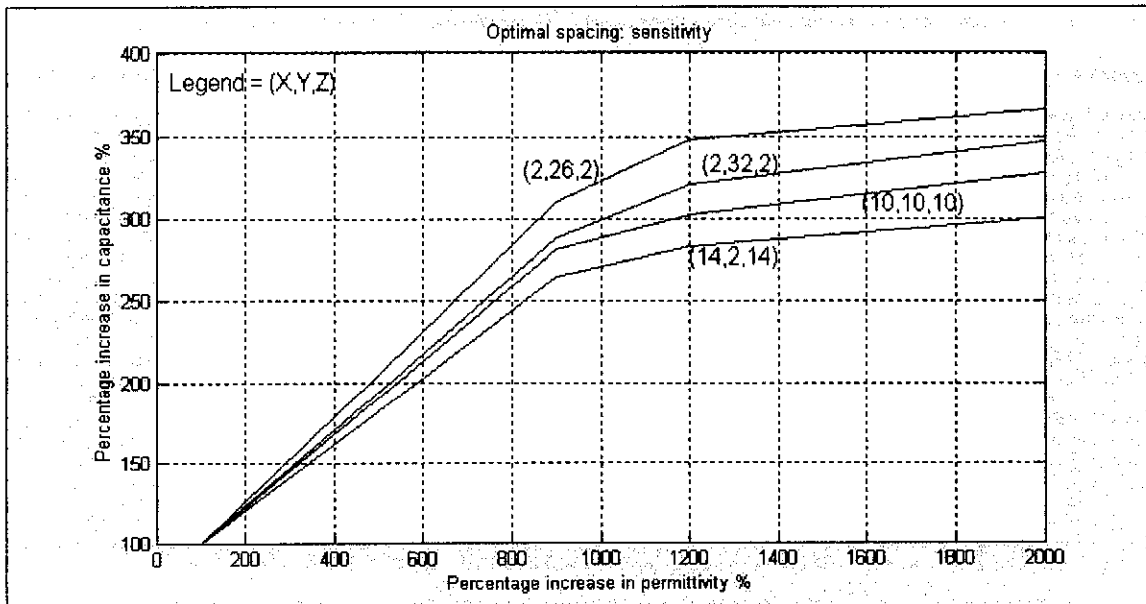


Figure 2-17 Test one: Effect of guard length to probe sensitivity

From these two graphs it can be seen that the guard electrode length does have an affect on the sensitivity of the sensor. The payoff in the two characteristics (explained above: sensitivity and capacitance size) can clearly be seen as the small guard length (14,2,14) produces large capacitances



(Figure 2-16) and less sensitivity (Figure 2-17). The large guard length (2,28,2) produces good sensitivity (Figure 2-17) and smaller capacitance size (Figure 2-16).

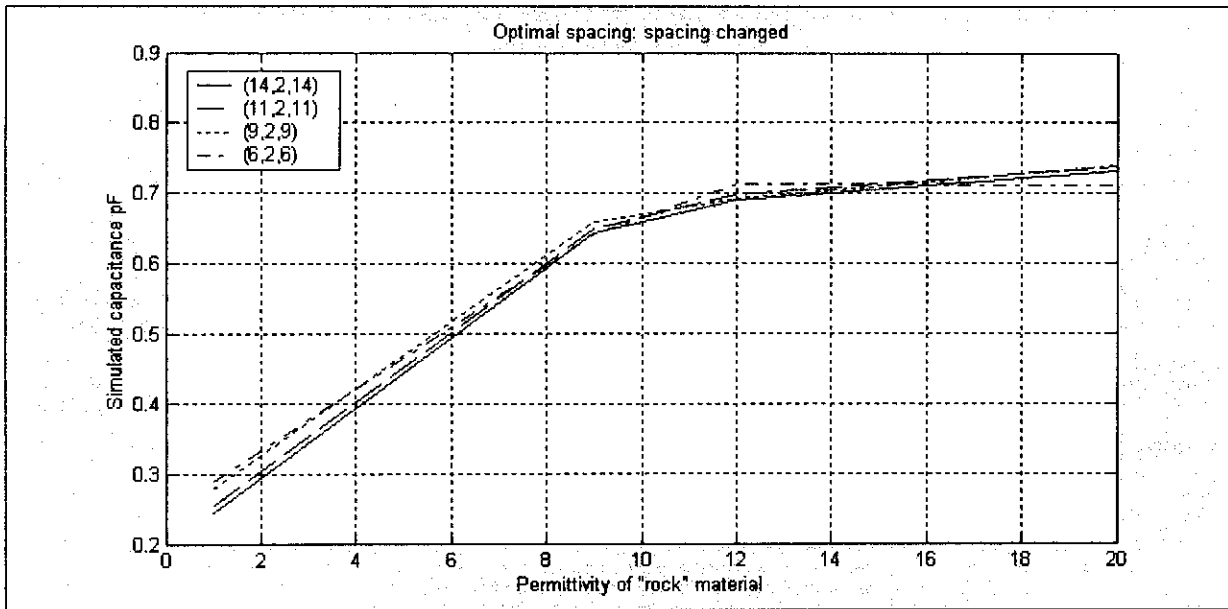


Figure 2-18 Test two: Separation of active electrodes - effect on capacitance

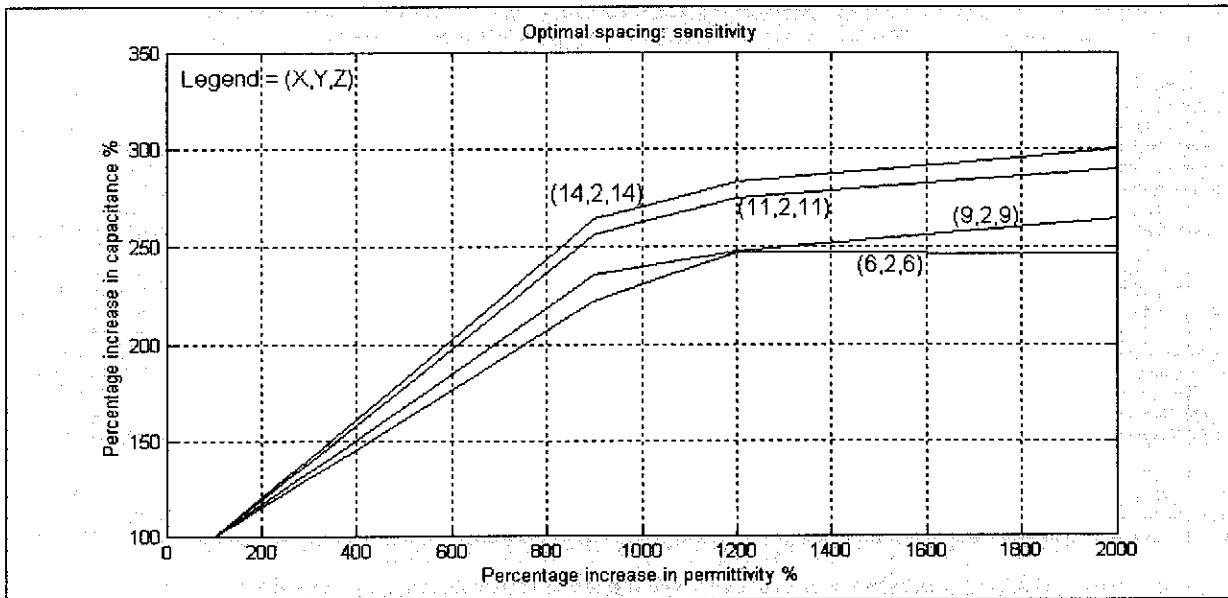


Figure 2-19 Test two: Separation of active electrodes - effect on sensitivity

There are two definite trends that can be isolated. Firstly, there is not a sharp defined "optimum" point in the simulations. Instead, a usable range that is clearly defined could be extracted from these results. Sensors with attributes ranging from (14,2,14) to (2,26,2) will work satisfactory. If a "best" spacing is to be chosen, it will be the (10,10,10) value according to the average performance in all tests. The change was gradual and no small change in geometry will effect the working of the sensor greatly. The second point is



directly connected to Figure 2-18. It can be seen that decreasing the total spacing $X+Y+Z$ decreases the sensitivity but does not increase the capacitance of the system. This is quite interesting and is probably connected to the fact that the guard electrode influences the electric fields. Other factors include:

- Capacitance to be measured is in the range 0.1 to 0.8 pf.
- Difference between an ϵ_r of 9 and 12 (typical of two rock types) is in the order of 10 %.
- The transfer function ($\epsilon_r(\text{rock})$ versus capacitance) for the electrodes is not linear and it behaves asymptotically. This asymptote seems to be in the vicinity of three times the capacitance value for air.

The actual CST capacitance value was extracted by saving the S parameters and then converted to ABCD parameters. The B parameter then gives the capacitance directly^[10, page 208]. All these traces are for 1 MHz signals, a wide variety of frequencies were simulated and the results are not shown here for the deviation from the results discussed above is small.

2.2 Electrode design: Physical models

In this section the building and testing of three electrode configurations are presented. These probes were made to be used for testing only and are not structurally strong enough for final use. They were assembled from 30 mm diameter copper piping cut to size and was held in position by a PVC pipe with a sectional cut (Figure 2-20). The electrodes were electrically connected by semi-rigid coaxial cables. The method used to extract the capacitances will be explained fully in chapter three.

2.2.1 Three different probes built to produce physical tests

Three probes were built according to the CST simulations to produce a workable prototype sensor and to verify the effect of geometrical changes. Two probes were built with large total spacing ($X + Y + Z = 30$ mm) with the guard electrode differing in length. One of the probes was made to have the "optimum" geometry (10,10,10) as explained in section 2.1.4.5. The third probe was created with small total spacing.

The probes:

- (2,26,2) – long guard electrode, large total spacing (Probe 1 - shown in Figure 2-20)
- (10,10,10) – medium length guard electrode, large total spacing (Probe 2)
- (10,0.1,10) – small guard electrode, small total spacing (Probe 3 – shown in Figure 2-21)

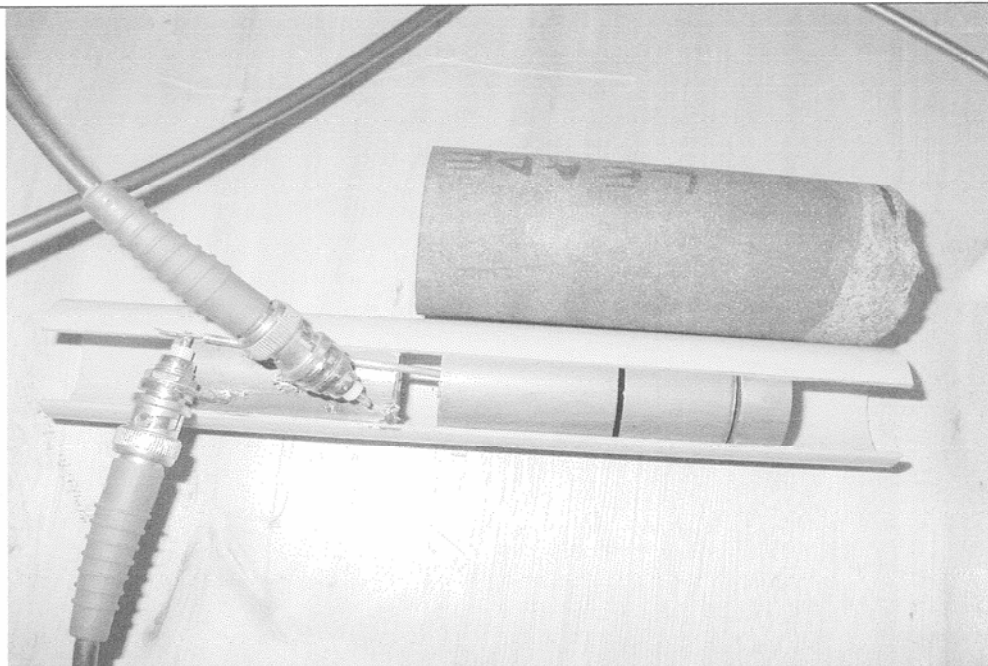


Figure 2-20 Probe 1 with large guard and rock core placed alongside

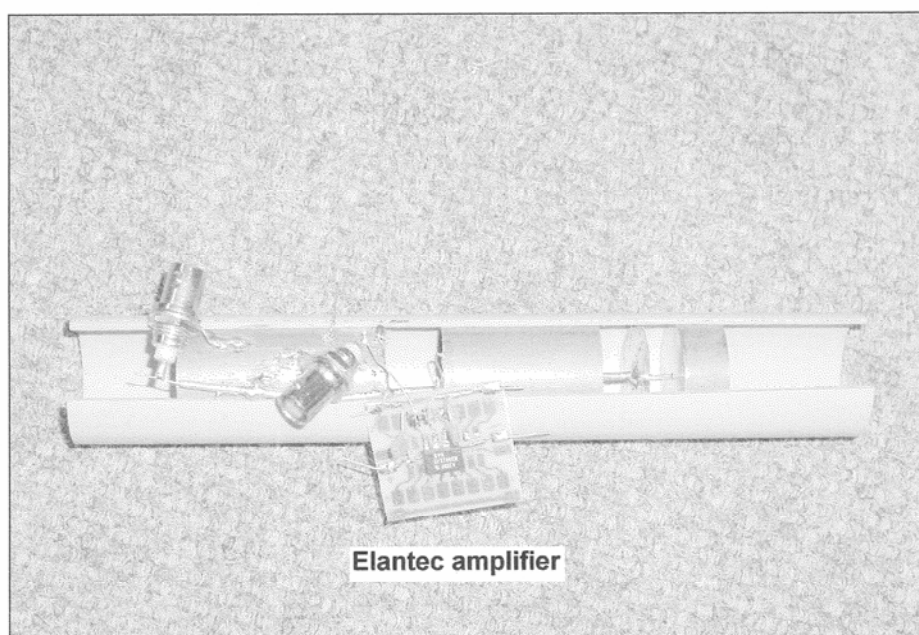


Figure 2-21 Probe 3 with small guard spacing

The current that flows on the “measure” electrode is sensed by the Elantec amplifier which converts it to a voltage (the detailed electronics will be presented in chapter three). The transfer function is known and thus the capacitance can be deducted directly from the Elantec amplifier output voltage. Two generators were used to drive the electrodes, as their noise characteristics are different and this had an effect on the measurements. One of the generators (generator A) was capable of large drive signal but produce a noisy

signal. The other generator (generator B) had a smoother signal but smaller output strength (this will be explained fully in chapter three).

To increase the permittivity of the system, a rock core was placed alongside the sensor (shown in Figure 2-20). This core consists of chromitite from the bushveld igneous complex and is rich in platinum group metals and chrome. It's properties at 1 MHz are $\epsilon_r = 20$ and loss tangent of 0.55^[11]. This is a simplistic way to produce elevated capacitances and simulate borehole situations, but it turned out to be useful. To produce the reference air test, the sensor was placed on a 10 cm high piece of expanded polystyrene with all the cables to the reference side of the sensor. The rock was placed on the polystyrene next to the sensor for the chrome leader tests.

Table 2-3 Test results: Capacitance values for different configurations and different mediums

Dimension (X, Y, Z)	Air	Chrome leader	Ratio of C_{ϵ_r}/C_{air}
(2,26,2) – generator B	0.1 pf	0.436 pf	4.42 times
(2,28,2) – generator A	0.113 pf	0.494 pf	4.36 times
(10,10,10) – generator B	0.260 pf	0.573 pf	2.2 times
(10,0.1,10) – generator B	0.5 pf	0.875 pf	1.77 times
(10,0.1,10) – generator A	0.4 pf	0.73 pf	1.8 times

The trend postulated and simulated by CST follows: Larger guard electrode implies more sensitive readings and a smaller total spacing implies larger capacitance values. Total capacitance measured was in the 0.1 to 0.9 pf range, as CST simulations suggested.

The two properties that were measured are the permittivity and the losses. The effect the permittivity has on the sensor was simulated and tested extensively. It was noted that the capacitance is affected by the amount of electric fields penetrating the rock body and that the losses are affected by the same mechanism. As the simulation take up excessive time and will never represent the practical situation perfectly, it was decided not to do the loss simulations, but to build the probes according to the permittivity results. The effect that the losses have on the system could be noted in the practical tests and a detailed description will follow in chapter three.

2.2.2 Correlation between CST and physical probes

As already mentioned, the test results followed the trend given by CST. The following table gives a tradeoff between the sensitivity predicted by CST and the measured values. The values in the table are the ratio between the capacitance measured (or simulated) for the elevated ϵ_r and the capacitance measured for air.

Table 2-4 Sensitivity tradeoff between CST simulations and physical tests.

Probe geometry (X, Y, Z)	CST (C_{er}/C_{air})	Tests(C_{er}/C_{air})
(2,26,2)	3.5 times	4.4 times
(10,10,10)	3 times	2.2 times
(10,0.1,10)	2.75 times	1.8 times

The actual CST capacitance value was extracted by saving the S parameters and changing it to ABCD parameters. The B parameter then gives the capacitance directly. The following table gives this result for one of the electrode configurations (Probe 3), adjacent to the simulated results.

Table 2-5 Capacitance value tradeoff between CST simulations and physical tests: Probe 3

	$\epsilon_r = 1$ (air)	$\epsilon_r = 20$ (rock)
CST	0.288 pf	0.74 pf
Tests	0.5 pf	0.875 pf

The CST simulation and test results do not correlate by a factor of 1.5 but the following points can be noted:

- The CST simulations are based on a square geometry while the test sensors are cylindrical (simulated difference between cylindrical and square was 2 times)
- With the CST simulations, the probe is in the center of the hole without the “plastic pipe” touching the rock. The measurements are made with a rock core lying next to the sensor.
- The CST sensor is surrounded by rock
- The values are small and rounding in the code can have an effect.

2.3 Conclusions: designing of electrodes

It was possible to create a sensor that will be sensitive enough to sense a rock body that is removed between 0 and 10 mm from the electrodes. The capacitances produced are small and pose a challenge to the electronics that will be used to measure the differences. The software packages that were used, did speed up the designing process and gave good insight into the problem. The three probes that were built expanded this insight and created the foundation on which the electronics can be designed. The characteristics of each of these probes were discussed and, as will be shown in the next chapter, this information will be invaluable to the choices that are to be made.

3. Electronics

The previous chapter focused on all the passive elements of the sensor. This chapter introduces the active part of the sensor. The order in which the materials will be presented will be the same as the signal path as given in Figure 3-1.

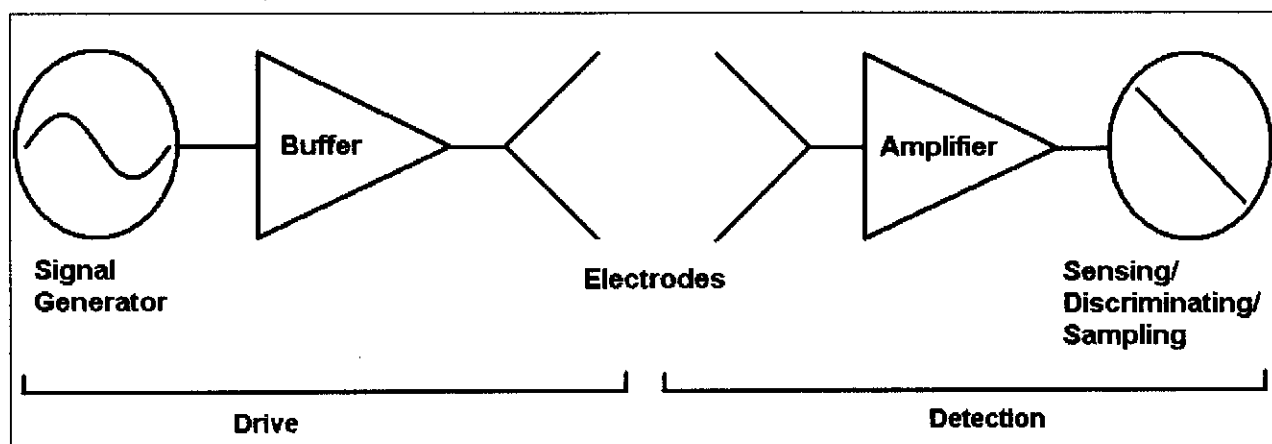


Figure 3-1 Major subsystems of sensor to be developed

Firstly, the driving method and signals are introduced. The wide range of uses for capacitors implies various methods to measure them, some of these methods will be explained and the most attractive ones will be used in prototypes. Secondly, the amplifier and electrode output configuration will be discussed. The capacitance value that is to be measured is small and therefore care must be taken in constructing this configuration. Thirdly, the sampling of the primary signal will be introduced. Fourthly, the conditioning of the signal will be handled, and lastly a field deployable sensor will be presented.

3.1 The sensing of capacitance

To drive the electrodes, a method had to be devised to sense small values of capacitance (0.1-1 pf). Sensitive network analyzers and RLC measuring devices were available, but these will not be able to fit into the borehole and therefore there is a need to make small, accurate sensing electronics. A study on ways to measure capacitance and losses was done and four suitable methods were found. The next section will be dedicated to introducing each of these methods and choosing suitable schemes.

At the heart of a sensing scheme is the signal driving the electrodes. The characteristics of this driving signal will command the way in which the data is extracted.

3.1.1 Sinusoidal drive signal: Phase and amplitude detectors

This is the standard way to find the impedance of a system^[12, page 186]. The drive port of the sensor is excited with a stable sinusoidal signal. Both the drive and the resulting signal (at the sense port of the sensor) are fed into the phase and amplitude comparator IC and the voltage and phase relationship is produced as a

varying DC voltage. These detectors are commercially available but expensive. The modules are designed to work over an extended range of phase and amplitude. The small capacitance and high resistance terms will introduce small changes in the phase and large changes in amplitude and it is feared that the sensitivity of this module will not be ideal.

3.1.2 Sinusoidal drive signal: Resonant tank

This method is based on an ingenious circuit by W.H. Steyn^[13]. He used this method to sense the capacitance of wood to obtain an indication of the moisture content. The basic principle of operation is to keep a RLC resonance network in tune by compensating for any loss or gain in capacitance from the measuring probe by adjusting the voltage across a tuning diode. This adjustment is done in closed loop by using a phase detection technique^[13]. The voltage across the tuning diode will give a highly sensitive indication of the changes in capacitance of the probe.

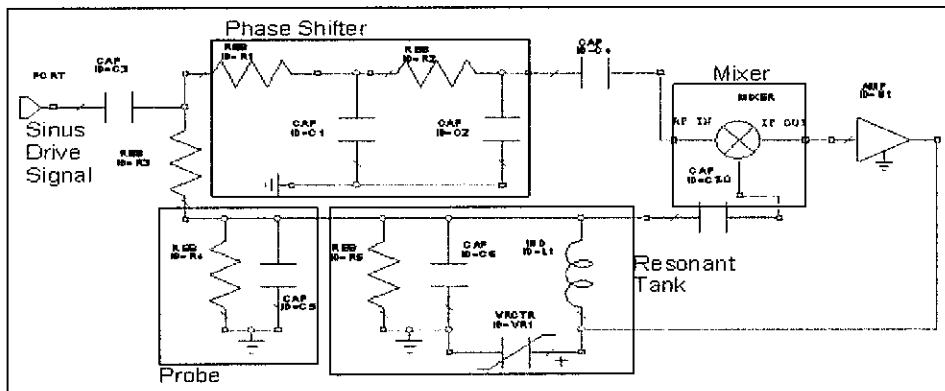


Figure 3-2 Schematic of resonant tank sensing method showing all critical elements

Figure 3-2 is a schematic of the electronics used in the wood probe. The input signal is a buffered stable oscillation and is divided into two paths. The first path is shifted by a constant factor of 90° and is connected to the first mixer port. The other path has no delay if the RLC tank is in resonance and is connected to the other mixer port. If a mixer is driven out of phase, the output will be zero and the system will be stable. If the characteristics of the resonant tank are changed by the sensor sensing a different value of capacitance, a phase shift will occur and the phase difference between the mixer's ports will not be 90° out of phase and the mixer will produce an output voltage. This voltage will be amplified and will cause the varactor diode to pull the tank into resonance again. The resonant components (L1 and varactor) are necessary to increase the perceived capacitance of the sensor.

This method is attractive as it produces a large output function from small changes in capacitance, however this specific method will not be able to sense the losses of the system.

3.1.3 Saw tooth drive signal

Non-sinusoidal drive signals were also investigated and the first to receive attention is the saw tooth shaped signal, e.g. Figure 3-3.

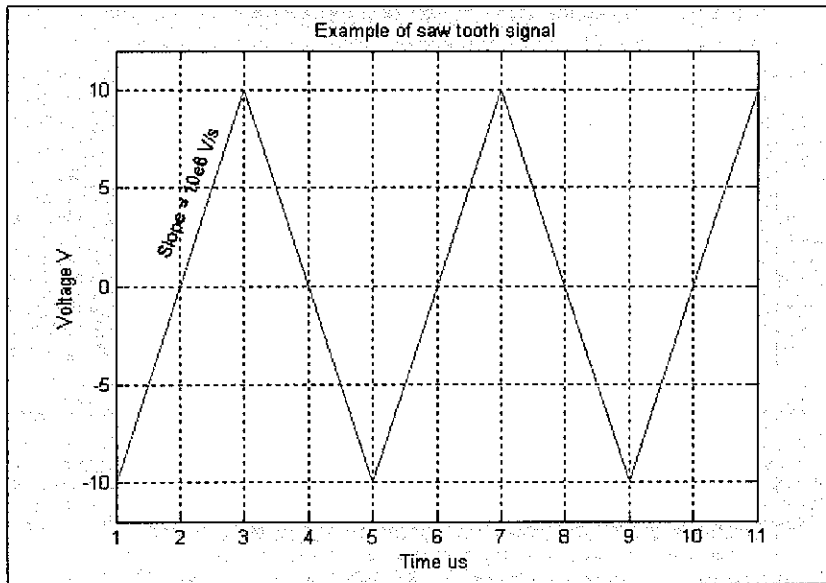


Figure 3-3 Example of a possible saw tooth signal

There are two deciding factors in creating a signal like this: firstly the frequency (200 kHz for signal in graph) and secondly the amplitude of the signal (10 V for signal in graph). To explain how this signal can be used to extract the data from the sensor, the model of the sensor will be used and a schematic of the model is shown in Figure 3-4. C1 in the model is C_n and C_r of Figure 2-2 in parallel to form the capacitance that will be affected by the permittivity. R1 is a resistor that produces the loss factor that will be measured if the rock body is lossy. Although the model is not comprehensive, it is accurate enough.

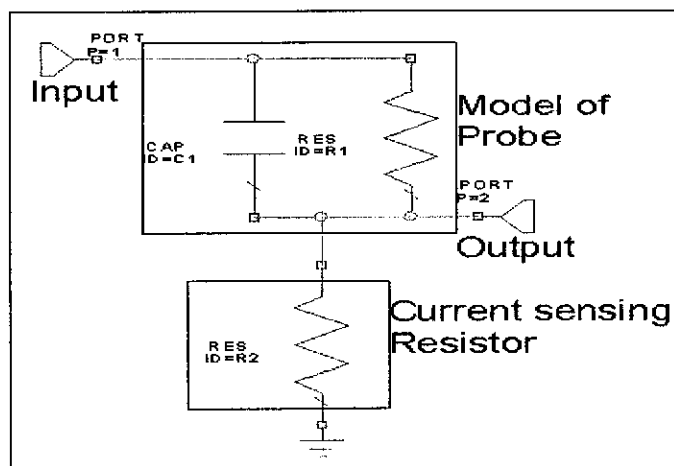


Figure 3-4 Model of sensor with current sensing resistor added



If the signal shown in Figure 3-3 is applied to the input port, the current in the sensing resistor will be defined by:

$$\begin{aligned}
 i_{sense} &= i_{C1} + i_{R1} \\
 V_{C1} &= V_{R1} = V_{input} \text{ if sensing resistor is small} \\
 i_c &= C1 \frac{dV_{input}}{dt} = \pm C1 * \text{slope} \\
 i_r &= \frac{V_{input}}{R1}
 \end{aligned} \tag{3.1}$$

The current is converted to a voltage (by R2) and is displayed in Figure 3-5. The jump is attributed to the voltage differentiation over the capacitor and the slope is attributed to the voltage over the resistive part of the model.

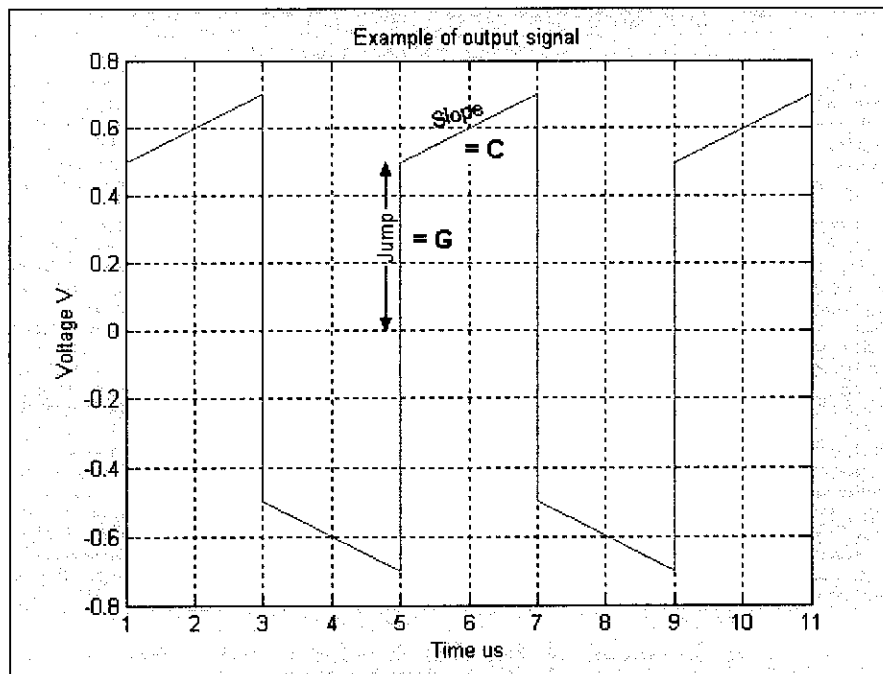


Figure 3-5 Output signal indicating attributes connected to capacitive and resistive parts.

If the sensor is driven with the above scheme the capacitive and resistive parts of the model can be extracted from the output waveform (Figure 3-5) as explained in equation 3.1.

The advantage of this scheme is that there are no complex integrated circuits necessary and it is simple. The downside is the complex input waveform.

3.1.4 Square wave driving method

The second non-sinusoidal drive scheme is implemented by a square waveform and as with the previous method, the ideal waveform will be shown in Figure 3-6.

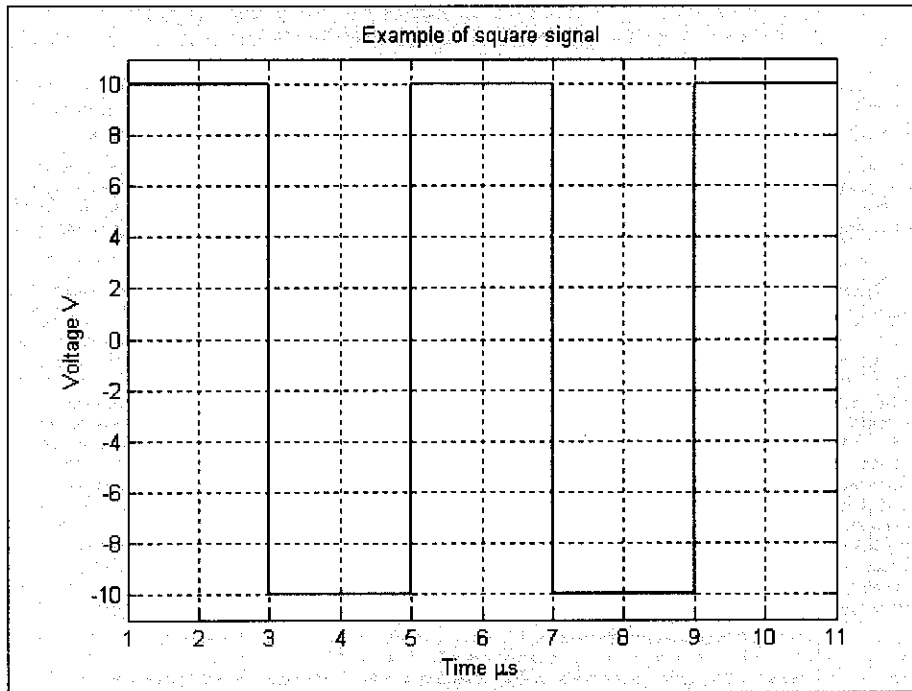


Figure 3-6 Example of possible square waveform

This waveform can be reproduced if the frequency and amplitude are known, again these factors will influence the output signal. To explain the working of the scheme, the model of the sensor will be given as before, this time with two extra lumped elements.

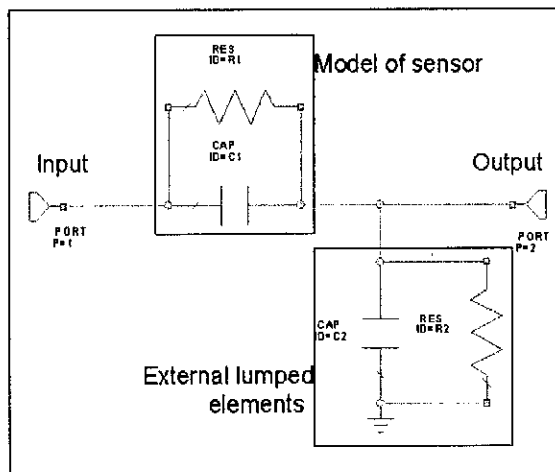


Figure 3-7 Model of sensor with lumped elements inserted to produce capacitive voltage division



If both the resistors are ignored for a while and the theoretical situation is imagined where the output impedance is infinite, the output voltage will be the same as the input but with amplitude scaled by a factor. This factor will be a function of the ratios of the two capacitors:

$$V_{out} = \frac{C_{Sensor}}{C_{Sensor} + C_{Lumped}} V_{in} \quad (3.2)$$

This relationship is obtained by the analogy between resistors and capacitors. If the resistive part of the sensor is added for a moment (output resistance still infinite) the resistor will produce a DC current path. This current will be integrated by the lumped capacitor and will produce a linear increase in voltage. The resulting voltage at the output will then look exactly the same as with the saw drive method:

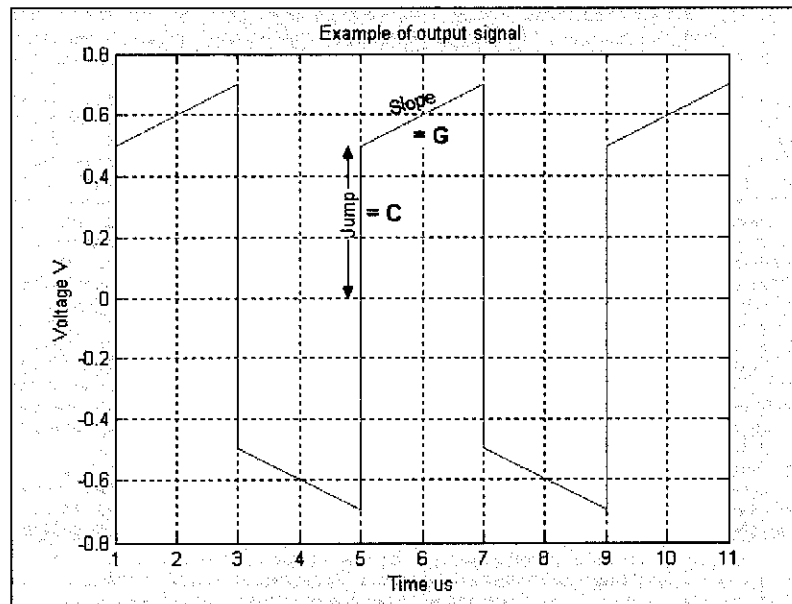


Figure 3-8 Resulting waveform for square drive method

The jump is due to the capacitive voltage division and the slope is due to the resistive element integrating the DC current. Now, if the real world is taken into account, the lumped resistor must be added as shown in Figure 3-7 to simulate the output resistance. As result of the very small capacitances, this resistance must be large (in the MΩ range) to make the natural decay long in relation to the square wave period. The transfer function for the whole system was calculated and follows:

$$V_{out}(t) = A \times V_{in}(t_0) - A \times V_{in}(t_0) e^{-\frac{t}{\tau}} + \frac{K \times V_{in}(t_0) \times t}{R_r} \quad (3.3)$$

$$\tau = R_{lumped} \times C_{lumped}$$

$$A \approx \frac{C_r}{C_r + C_s}$$



One approximation had to be made to produce this equation: the DC point between the two capacitors was taken as a constant. This will be valid if the sum of the integration and natural decaying term is small which, as will be seen in the next section, was the case.

3.1.5 Implementation of non-sinusoidal drive schemes and results obtained

The simplicity of the non-sinusoidal drive schemes made it easy to test the electrodes with standard lab signal generators. By doing this, the performance of the two methods could be tested and quantified before any electronics had to be designed. It was convenient to have this information in the beginning phase of the design. The results given at the end of chapter two were extracted from raw data, which will be shown now, by using the abovementioned methods.

3.1.5.1 Results obtained with saw tooth drive method

The first tests were done on the electrodes without any output amplification (a picture of this was shown in Figure 2-20). These results are shown in Figure 3-9.

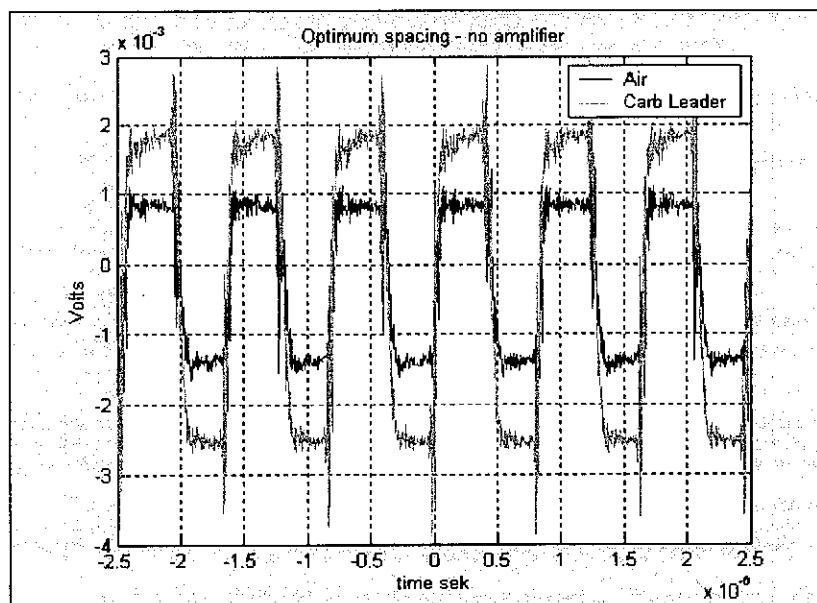


Figure 3-9 Saw tooth drive method with no amplification

Test conditions:

- Input signal: frequency 1 MHz, 12 V_{0-p} saw tooth.
- Probe 3 was used in this experiment for its large capacitance values.
- The output was connected to the oscilloscope with 50 Ω impedance.
- The signal was averaged by a factor of 16.

Remarks on Figure 3-9:

- A high frequency was used to increase the amplitude of the signal, as the amplitude of the signal is directly proportional to the frequency. This was necessary as the signal was not detectable in the noise at lower frequencies.
- The signal was averaged to retrieve usable data. The averaging decreased the noise by a factor of four. Without this averaging factor, the characteristics used to extract the capacitance information cannot be identified.
- The increase in amplitude from air ($\epsilon_r = 1$) to rock sample (chrome leader $\epsilon_r = 20$) was in the order of 1.7 times. The losses of the chrome leader were high and a hint of a slope can be seen in the figure.

These were the first results obtained from the sensor and to improve on them, an amplifier was inserted to increase the size of the signal and to limit the bandwidth of the system. For this an Elantec 2280 operational amplifier/buffer was used. The gain bandwidth product of this component is 250 MHz. The gain was fixed to 10 times amplification with a resulting bandwidth of approximately 25 MHz. The electrode with the amplifier inserted is shown in Figure 2-21. This change resulted in a big improvement as can be seen in Figure 3-10.

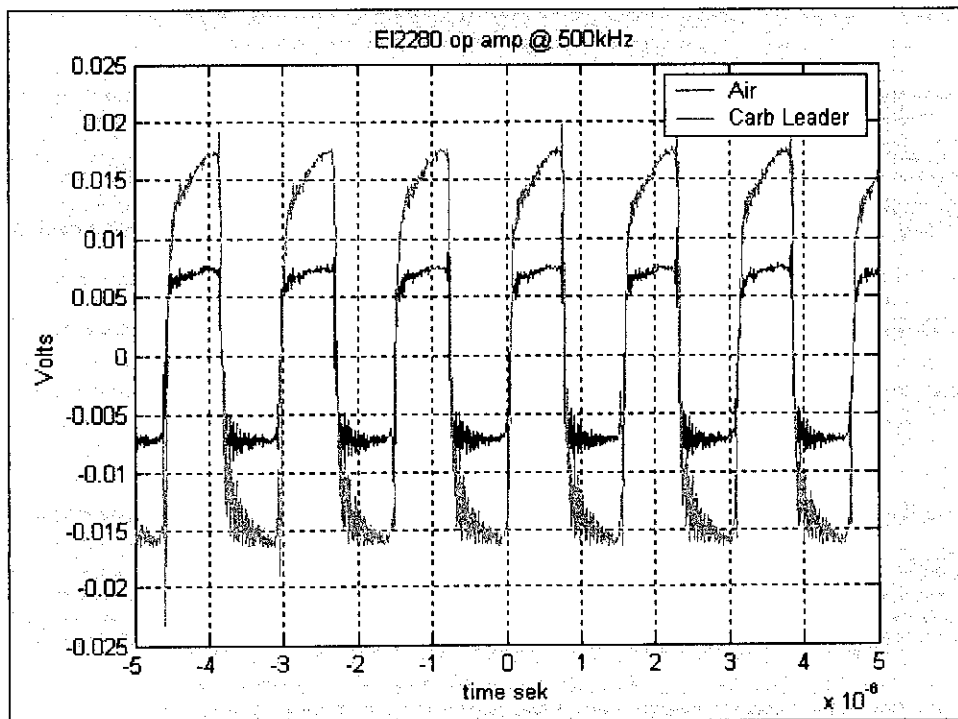


Figure 3-10 Amplifier added to electrodes

Test conditions:

- Input signal: frequency 500 kHz, the other parameters are the same as in Figure 3-9, averaged by 16.
- The Elantec amplifier was added.

Remarks on Figure 3-10:

- The signal to noise ratio is larger.
- The first effect of the loss term can be seen in the change in the slope of the traces.

Introducing the amplifier enabled the system to be more sensitive to smaller capacitance values. Hence the larger electrodes (probe 1 and 2) were introduced with their smaller capacitance values but stronger transfer functions (see Table 2-4). The result was the trace displayed in the Figure 3-11.

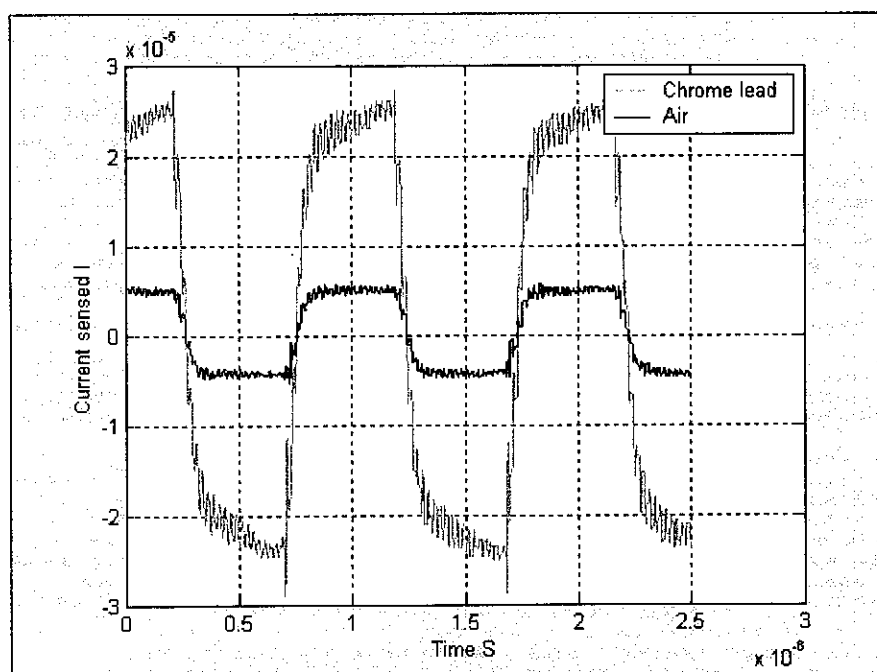


Figure 3-11 Output waveform

Test conditions:

- Input signal: frequency 1 MHz, 12 V_{o-p} saw tooth.
- Probe 2 was used for these measurements.
- The measured output voltage was transformed into current and is displayed to ease correlation with equation 3.1.

Remarks on Figure 3-11:

- Sensitivity was increased by using more sensitive electrodes.
- The noise was still present and Figure 3-11 displays averaged data (factor of 16).

An effort was made to decrease the amount of noise in the system. The major source of noise was the signal generator used to drive the electrodes. The saw wave signal is not smooth and is generated by a digital counter counting up and down. The size of the steps produced by the digital counting is displayed in Figure 3-12 and Figure 3-13.

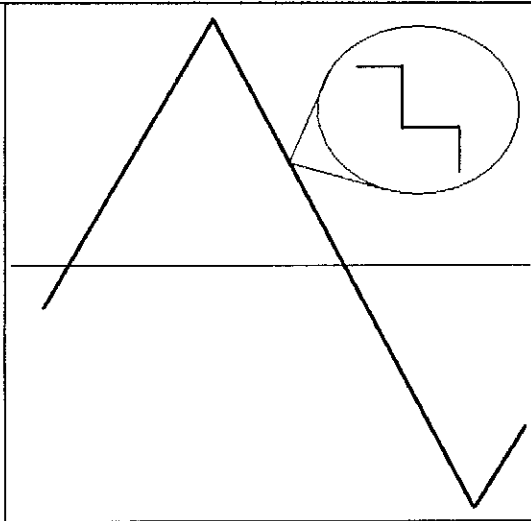


Figure 3-12 Generator A producing a "rough" signal

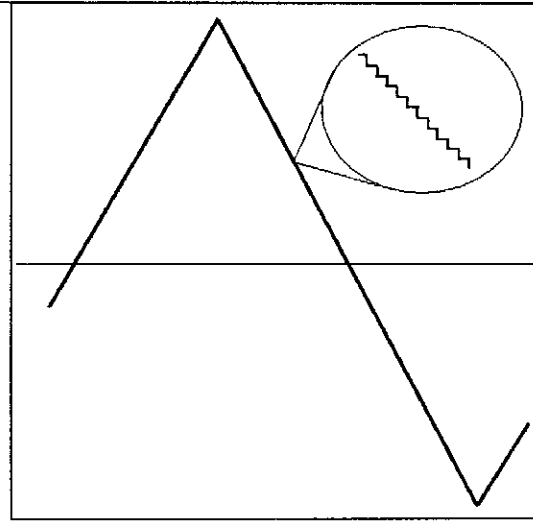


Figure 3-13 Generator B producing a "smooth" signal

This slope is differentiated by the capacitance of the system and if a noisy signal is differentiated, the noise is made worse. A better generator was obtained with a smooth saw signal, this proved to be effective (Figure 3-14).

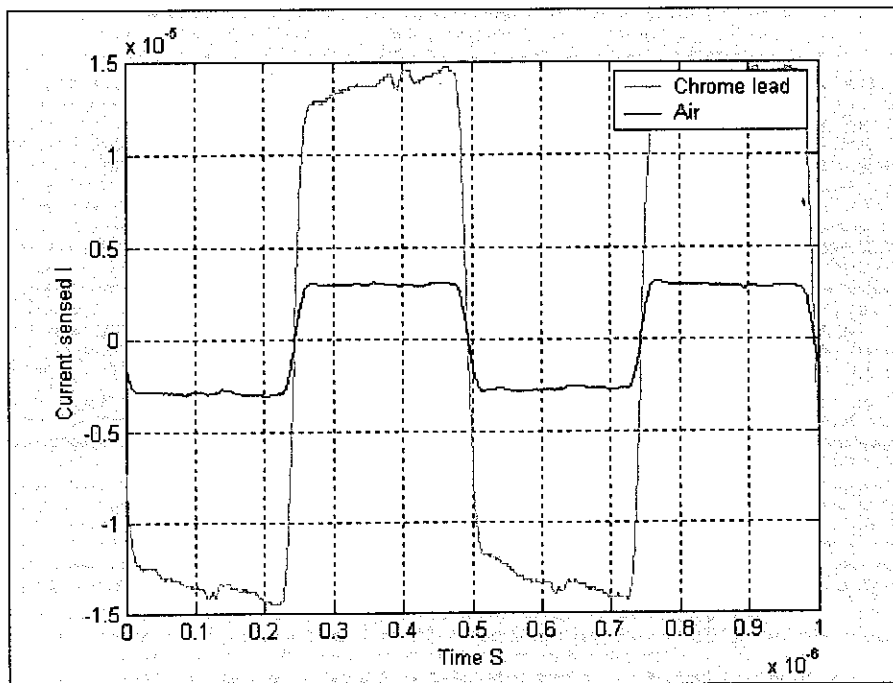


Figure 3-14 Smooth signal generator

Test conditions:

- Input signal: frequency 2 MHz (minimum frequency of signal generator), 2.5 V_{o-p} saw tooth.
- Data displayed was averaged by 16.



Remarks on Figure 3-14:

- Current was extracted using the amplifier's transfer function.
- The noise was considerably less. The "squiggle" in the middle of the pulse coincides with the time that the signal goes through zero and the non-linearity there produces the effect.

This configuration was used to extract the data given in section 2.2 as explained in section 3.1.3. To test and verify the data extraction method, a capacitor and resistor were soldered over the electrodes to implement a known quantity. This was done with both a 3.3 pf and 3.9 pf capacitor as well as a variable resistor at the quoted values. The same method was used to extract the values of the lumped elements as was used to extract the data and the test results and Table 3-1 gives the results.

Table 3-1 Verification of results by using lumped elements

Element inserted	Measured value	Difference between measured and expected	Difference between measured and expected
3.3 pf lumped cap	3.92 pf	0.63 pf	16%
3.9 pf lumped cap	4.62 pf	0.73 pf	15.8%
270 k Ω resistor	281 k Ω	11 k Ω	3.9%
580 k Ω	534 k Ω	46 k Ω	8.61%
860 k Ω	939 k Ω	79 k Ω	8.4%

The total measured capacitance was larger than the inserted lumped element due to capacitance formed between the electrodes and capacitor leads. The capacitor leads shift part of the driven plane closer to the measure electrode and this may increase the capacitance of the sensor and produce a capacitance of the order 0.6 pf. The resistance value was also on the mark and inside 10 % accuracy. It can be seen that the measuring method is accurate.

3.1.5.2 Square wave drive method

Using the previous method, the noise in the system was decreased to a level that is acceptable. An effort was made to decrease the noise even more and the square wave drive method was introduced. This method implements voltage division and integration of charge, both these actions are not as susceptible to noise as differentiating. It is also much easier to generate a clean square waveform. This method was implemented with a LF351 operational amplifier. The reason for using this package is the small input bias current (50 pA) and hence the large input resistance (needed). The op-amp was made to have a gain of 2 (non-inverting configuration). The input parasitic capacitance was used as the lumped capacitance (shown in Figure 3-7). A 1 M Ω lumped resistor was inserted. A larger resistor value could have been chosen but larger values induced oscillations.

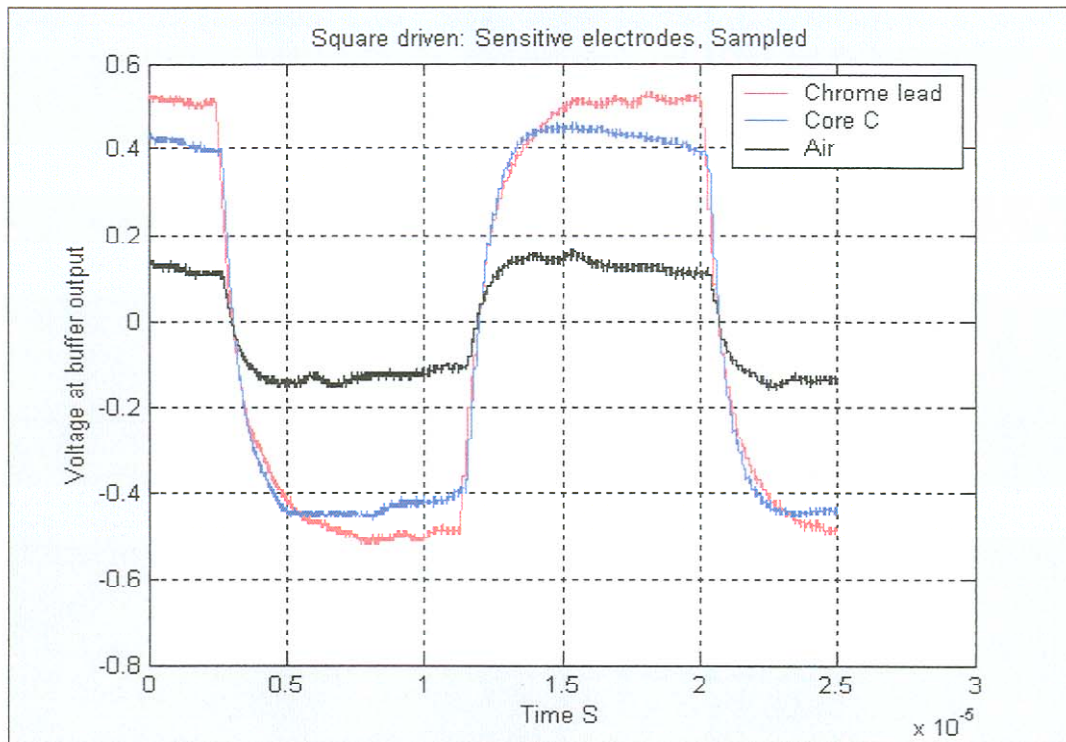


Figure 3-15 Square wave method

Test conditions:

- Input signal: frequency 57 kHz, 12 V square wave.
- Another rock core was introduced and denoted core D. This rock has permittivity similar to the chrome leader's but with less losses.
- Data displayed was sampled and not averaged.

Remarks on Figure 3-15:

- A wider range of frequencies is possible with this method and the frequency could be lowered.
- As expected, there was considerably less noise in the system.
- The natural decaying of the signal can be seen in the traces. The resistance term influenced the chrome leader's slope in such a way that the slope is now positive.

3.1.6 Conclusions on the sensing of capacitance

The process described in this section followed the chronological steps in gaining information on the various drive schemes. This gives a clear understanding of the origin of the sensor as well as the critical attributes required for desired functioning. The information gained in this section laid the foundation on which the final configuration was based.

3.2 Choosing final electrode and drive configuration

To make this final decision, two separate sensors were assembled and tested, keeping the advantages of each part in mind.

3.2.1 Saw driven based sensor

This sensor was specially made for the saw tooth drive signal. The output configuration (shown in Figure 3-4) does not decrease the sensitivity of the sensor, as was the case with the square input configuration. This implies that a sensor with lower sensitivity can be used. The size of the capacitance is crucial as the signal to noise ratio for this scheme is small. Keeping this in mind, the small guard spacing (Figure 2-21) was used as it has the highest capacitance value. This may help to improve the signal to noise ratio. The signal was amplified as mentioned above and the resulting waveform is presented in Figure 3-16.

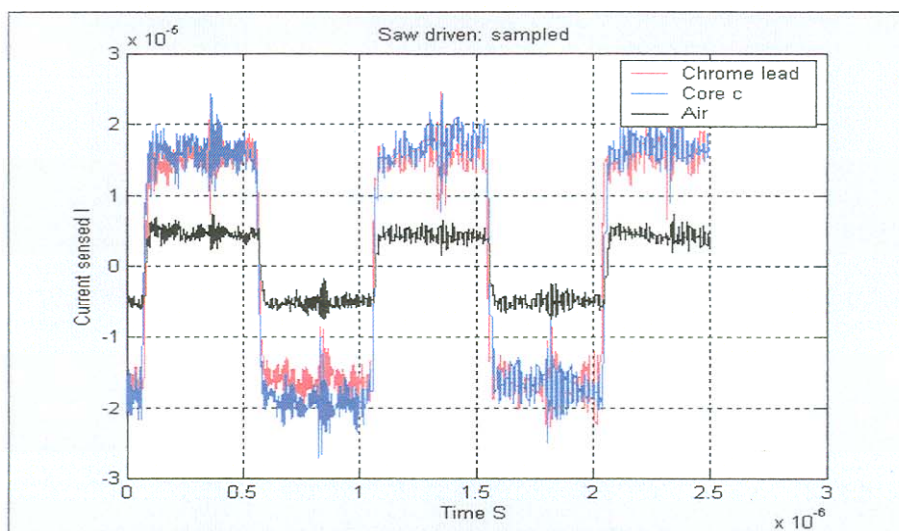


Figure 3-16 Saw driven based sensor: Sampled data

For the first time it was possible to retrieve sampled data that is presentable from the saw driven scheme. From Figure 3-16 the characteristics that were expected could be noted. If the data was averaged by a small factor, the results were good, the waveform had sharp transitions and a smooth and predictable slope. The sensitivity of the sensor to the difference between air and the chrome leader core was three. The difference between two different rock cores is not apparent but is shown in the averaged results.

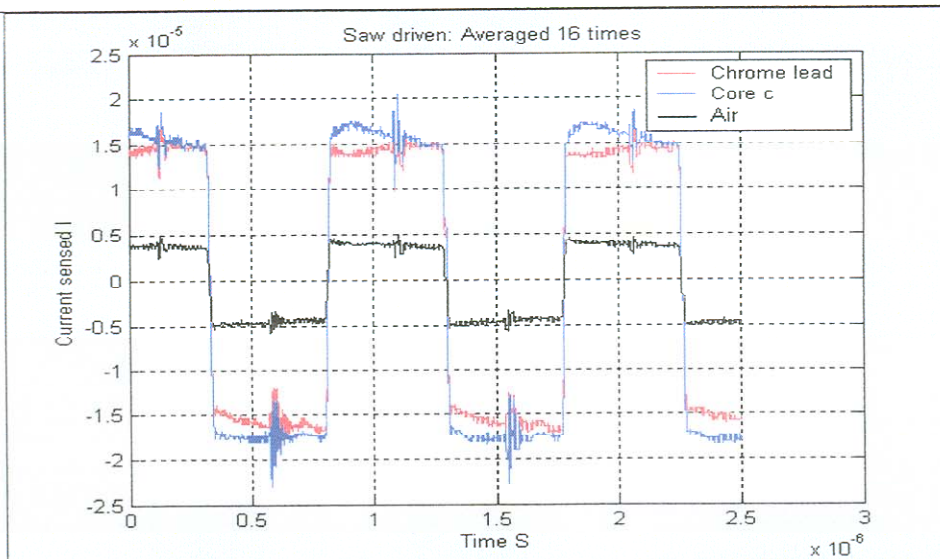


Figure 3-17 Saw driven based sensor: Averaged data

3.2.2 Square driven based sensor

This method relies on the fact that there is voltage division between the two capacitances shown in Figure 3-7. This division will lower the sensitivity of the sensor. To explain it, equation 3.4 will be used. From this equation it can be seen that a change in C_{sensor} will introduce a change in output voltage but the C_{lumped} will affect the change. An example of this will now be given.

$$\frac{C_{\text{Sensor}}}{C_{\text{Sensor}} + C_{\text{Lumped}}} = \frac{0.1}{0.1 + 3.3} = 0.0294 \text{ (For example)}$$

If C_{Sensor} is increased with factor 3 to 0.3

$$\Rightarrow \frac{0.3}{0.3 + 3.3} = 0.0833 \tag{3.4}$$

$$\therefore \frac{0.0833}{0.0294} = 2.83 \text{ Times}$$

Thus the driving method influences the sensitivity of the sensor. The signal to noise ratio for this scheme is acceptable and the size of the capacitance produced by the electrodes is not that crucial. For these reasons the large spacing with large guard electrodes was used with this method. The resulting waveform can be seen in Figure 3-15.

3.2.3 Most suitable sensor

The two sensors will now be compared in tabular form (Table 3-2)



Table 3-2 Tradeoff between two sensors

Saw driven based sensor	Square driven based sensor
The signal to noise ratio is large enough to display the effects of large changes in capacitance, but for smaller changes averaging is needed.	The signal to noise ratio is large enough to make sensitive readings without averaging.
Output signal must be amplified at least 10 times	The output does not need amplification, but a specialized amplifier is necessary (low input bias current)
Sensitivity approximately 3 times (ratio of voltage produced with air to voltage produced with chrome core)	Sensitivity approximately 3 times (ratio of voltage produced with air to voltage produced with chrome core)
The saw tooth signal is difficult to generate as a dedicated generator IC is needed to produce a clean triangular wave. Natural responses or slew rates of amplifiers could be used but is not accurate enough.	To generate a clean square wave is simple.
Frequency of operation is limited by the minimum detectable amplitude of the received signal as the amplitude is directly proportional to frequency. This lower limit is at 1MHz. The upper limit is produced by the components used.	Frequency of operation is broad and is limited by the components used (upper limit) and the lower limit is reached if the natural decaying is to much.
The transfer function of the system is simple and the values of capacitance and resistance can easily be extracted from the waveform	The transfer function is complex and it is more troublesome to extract the capacitance and resistance values. The input of the specialized amplifier plays a large role in the output waveform and the input characteristics are not accurately known. This implies that the sensor will need to be calibrated.

As can be seen, the choice in final probe is not easy as both configurations do have positive and negative attributes. The good noise properties, wide frequency range and simple signal generator made the square driven probe the most attractive.

Table 3-3 Summary of probe to be developed

Drive signal	Square
Frequency range	20 kHz to 2 MHz
Electrode sizes	(2,26,2)
Sensitivity (voltage for rock/voltage for air)	Three times

3.3 Square signal generator

3.3.1 Oscillator

The first part of a signal generator is the oscillator used to produce the reference frequency. Crystal oscillators are frequency stable and the norm to use. They are also commercially available as packages that only need power and one external capacitor. The crystal was specified to be 1 MHz. From this frequency, a whole range of frequencies can be created by logical counters. A four bit counter (74HC161) was used as the frequency divider producing 500, 250, 125 and 62.5 kHz (and 1 MHz as a matter of fact). Both these ICs use 5 V DC power and produce logical signals. This signal amplitude has to be increased and driving capability must be added. The sampling components will limit the operating frequency and, as will be seen in section 3.5, the frequency was limited at 125 kHz.

3.3.2 Buffer stage

To produce this, a transistor output stage was added. The schematic of this stage is shown in Figure 3-18.

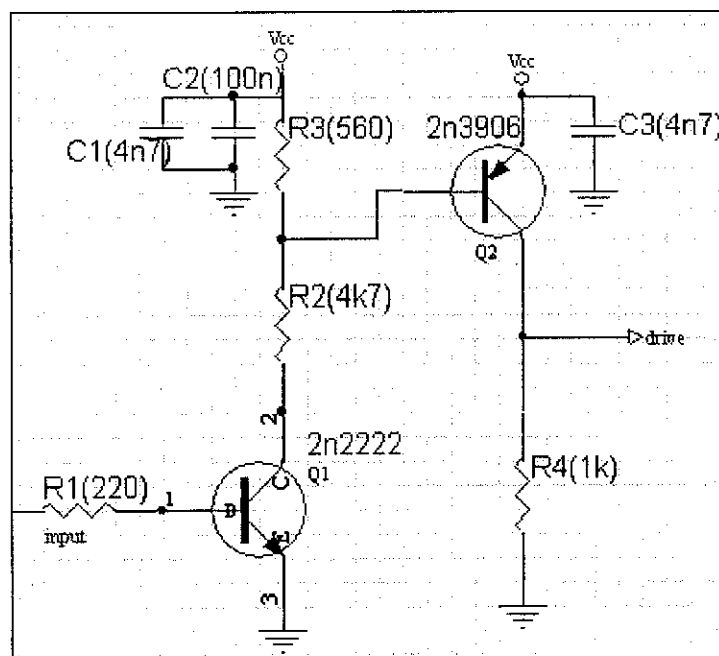


Figure 3-18 Schematic of oscillator buffer stage

One transistor could have been used to implement the necessary drive capability but the on and off characteristics are not the same. If one transistor is used, the rising edge of the square wave is produced by the switching off characteristic of the transistor. This is slow (300 ns) in comparison with the on characteristic of the transistor (35 ns). To harness the on characteristic of the transistor to create the fast rise time, a PNP transistor is used with the NPN transistor generating the necessary drive signal. The falling edge of the signal is now slow. This will not be a problem as only the positive cycle will be used for sampling (sampling will be done in section 3.5). If the input of Figure 3-18 is driven with a 50 % duty cycle

5V signal, the output waveform is 11.8 V 45 % duty cycle(12 V DC power supply) with a rise time of 35 ns and a fall time of 300 ns. R1 is inserted to limit the current that will be pulled from the logic gate when the transistor is switched on. There is, however, enough current to have the transistor on hard. Very little overshoot was noted and the noise of the signal is the same as the DC voltage.

3.4 Buffer and amplifier for signal received from electrodes

The input characteristics of the amplifier that are used to buffer the signal, are the major factors in deciding which component to use. The model of the sensor and lumped elements was given in Figure 3-7 and will be duplicated here for ease of reference. The lumped capacitor was implemented by the input parasitic capacitance of the operational amplifier used in preliminary tests. The value of this capacitance directly influences the voltage of the resulting signal as was shown in equation 3.1. The smaller this capacitance value is, the larger the generated output voltage will be. In addition to this, the input bias current must be small (pA range) to produce a large input resistance. The major reason for changing the amplifier is the low bandwidth associated with the LF351.

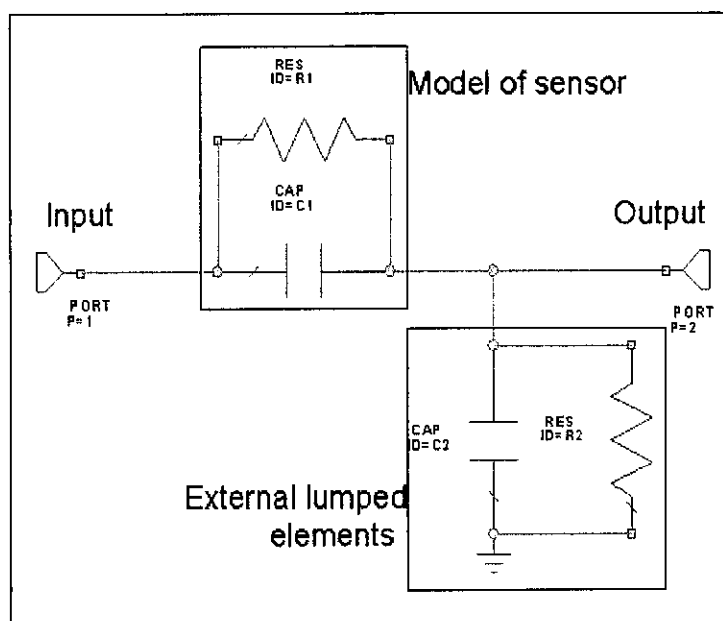


Figure 3-19 Model of sensor with lumped elements (repeated from Figure 3-7)

After extensive internet searches, a Burr-Brown amplifier OPA602, which has the necessary attributes, was found: High bandwidth (6.5 MHz), low input bias current (1 pA) and low input capacitance (1pF). In addition to these factors, the IC is available in South Africa and is inexpensive (R190)^[14]. The component is housed in a compact SOIC package.

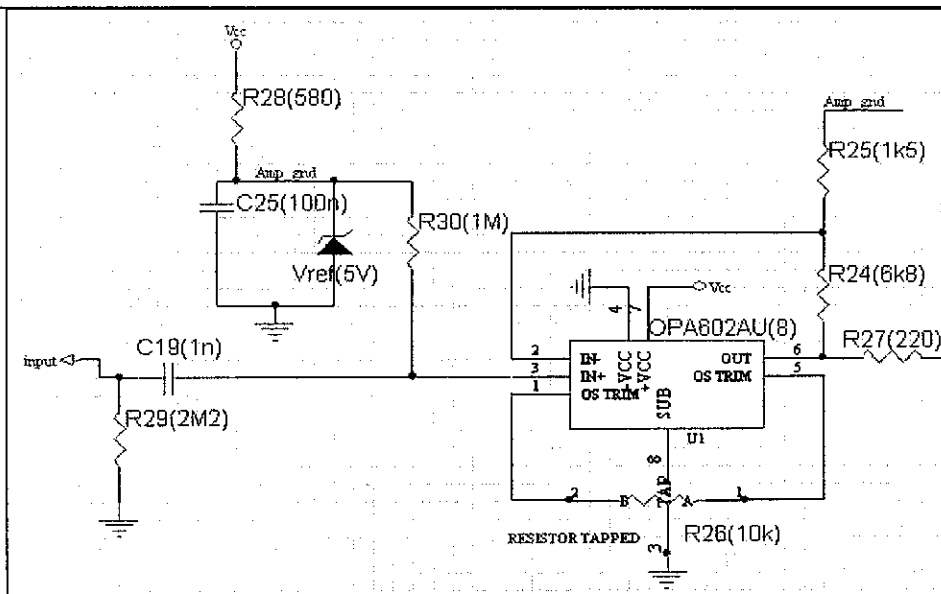


Figure 3-20 Schematic of electrode signal amplifier

In Figure 3-20, the implementation of the amplifier is shown. The sensing electrode is connected to the input terminal shown in the figure. The input resistance that the electrode will perceive is R28 and R30 in parallel. From the values in the figure, the input resistance is 680kΩ. R28, C25 and V_{ref} (LM 336) produce a 5V reference to create a virtual ground for the amplifier. The LM 336 is a cheap, temperature stable zener diode that can be used as a fixed voltage reference (no external components) or as a 4-6V adjustable voltage reference (variable resistor added). This virtual ground is connected to the input of the amplifier by R30. This large value is necessary to keep the large input resistance. It will not influence the reference voltage as the current consumed by the input of the amplifier is small. The next equation displays this effect.

$$\begin{aligned}
 I_{Bias} &= 1\rho A, R30 = 1M \\
 V_{Delta} &= 1^{-12} * 1^6 = 1\mu V
 \end{aligned}
 \tag{3.5}$$

The amplifier is connected in the non-inverting configuration by R24 and R25 and the gain is given by the next equation^[15, page 502]

$$A_v = 1 + \frac{R24}{R25} = 1 + \frac{1.5k}{6.8k} = 5.5 \text{ Times} \tag{3.6}$$

The bandwidth of the amplifier is then decreased to 1.2 MHz. This will be enough to result in a sharp signal. The slew rate of the amplifier is quoted as 35 V/μs. If the amplified signal has an amplitude of 1 V (as will be seen later, was the case) the delay time will be 29 ns. This theoretical delay is in the same range as the drive signal's rise time.



3.5 Sampling of amplified signal

Thus far in the document, the extraction of the actual data has not received any attention. If a sinusoidal drive method is used, the output from the mixer/detector will produce a DC voltage that is directly proportional to the attributes that are to be measured. This can then easily be digitized and stored inside the Sindlehead navigator. If a non-sinusoidal method is used, the amplified signal from the electrodes will be sampled and stored for later processing and interpretation. There are two ways to implement the digitizing, one is to use a micro-processor with analogue to digital converters and on-board memory and the other option is to use sample and hold components. The rate at which modern micro-processors can store data has increased to such an extent that even small components can sample and process data at a rate of up to two million samples per second (Ms/s). This will be fast enough to sample, for example, a 200 kHz signal. The data can then be sent over to the Sindlehead receiver in digital format. The actual traces can then be reconstructed and data extracted well. This seems easy to implement, but using a 2 Ms/s rate to measure the changes of a probe moving slowly along a borehole seemed to be an overkill. The use of sample and hold ICs was then introduced. These components take a snapshot of the input (of the IC) voltage the instant the hold command is given. The value is held on the output until another hold command is given. The repetitive characteristic of the waveform makes it ideal to be sampled in this way. If the hold command is given at the same point in the cycle each time, the square waveform can be sampled to a DC voltage. If two of these components are used and fired at different times in the cycle, it will be possible to reproduce a simplification of the original signal. This scheme is shown in Figure 3-21 and Figure 3-22.

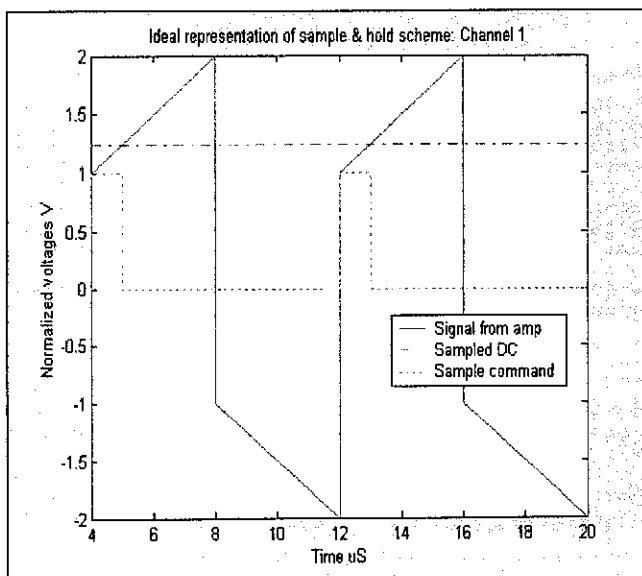


Figure 3-21 Sample and hold scheme: First sample

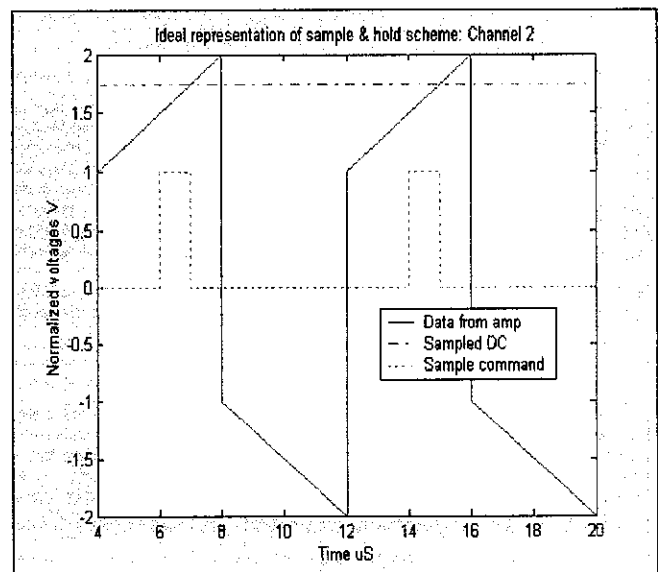


Figure 3-22 Sample and hold scheme: Second sample

These figures were created in MATLAB and are theoretical examples and not actual data. The hold command is given with the negative edge of the sample signal. The “dash-dot” lines in these figures represent the resulting DC voltages and the solid lines the proposed signal to be sampled. If the positions of the hold commands are known, then the original waveform can be extracted from the DC voltages. The slope of the signal is extracted with the standard equation. From this slope, the amplitude of the “jump” can be calculated and this is the capacitance information. The attributes influencing the slope are complex and the resistance cannot be extracted directly. To produce a measure of the losses, the ratio of the two samples can be taken. This will produce valuable information as the natural decaying is always at the same rate irrespective of the voltage value. The ratio Channel1/Channel2 will be used extensively. If this number decreases, increasing losses are being measured. This way of producing raw data instead of standard units (permittivity and resistance) was introduced as standard units could not be extracted directly from the data. The data produced will be computed in the following way.

Capacitance:

$$\Delta t_{sample} = t_{sample2} - t_{sample1}$$

$$Slope = \frac{ch2 - ch1}{\Delta t_{sample}} \quad (3.7)$$

$$Permittivity = ch1 + t_{sample1} * slope$$

Resistance:

$$Losses = \frac{channel1}{channel2}$$

An investigation into possible usable components highlighted important attributes of these components. The two most important attributes (of the sample and hold (S&H) ICs) are the acquisition time and the aperture delay (or time). The acquisition time is the minimum time that the IC must be in sample mode (the output follows the input) before the hold command can be given. The dotted line in Figure 3-21 can be used as an example of this: if the signal is a logical zero, the IC is in hold mode and the input and output are disconnected. If the signal is a logical one, the IC is in sample mode and the output follows the input. The minimum acquisition time is the shortest pulse needed to produce a stable hold value (stable implies the output voltage is the same as the input voltage at the instant of the falling edge). Two suitable components were found: LF398 with minimum acquisition time of 4 μ s and AD781 with minimum acquisition time of 500 ns. The aperture time is defined as: “The effective delay representing the point in time, relative to the hold command, that the input sample will be sampled”^[16]. This delay time is much shorter than the acquisition time and is 200 ns for the LF398 and 25 ns for the AD781. Another factor that is worth mentioning, is the droop rate. This is the rate at which the hold voltage decreases as time passes. The components are made to have small changes and droop rates of 0.01 μ V/ μ s. As the square wave will be repeated at high frequencies, this would not have been a problem.

It was decided to use the LF398 S&H IC mainly due to its relatively low cost. The LF398 was priced at R41 with the AD781 at R380 ^[17]. The working frequency will be limited by this component. The Analog Devices IC could have been used and it would then be possible to drive the electrodes at 1 MHz. However, there is no extra information at this frequency, in fact, a study by Rüttschlin^[11] showed that the relevant properties of rock (permittivity and losses) are more apparent at lower frequencies.

If the LF398 S&H IC is used in the manner described in Figure 3-21, the working frequency will be limited to 31 kHz. This value was obtained by observing that four pulses would fit into one positive cycle of the signal, thus implying eight pulses of 4 μ s each. This working frequency could not be implemented due to the fact that the natural decaying of the received signal is too high (as explained in section 3.1.4). There was also concern that the frequency was too low and too far away from the radar band.

To increase the working frequency, interleaving of two S&H components per channel was introduced. To explain this method, Figure 3-23 is introduced.

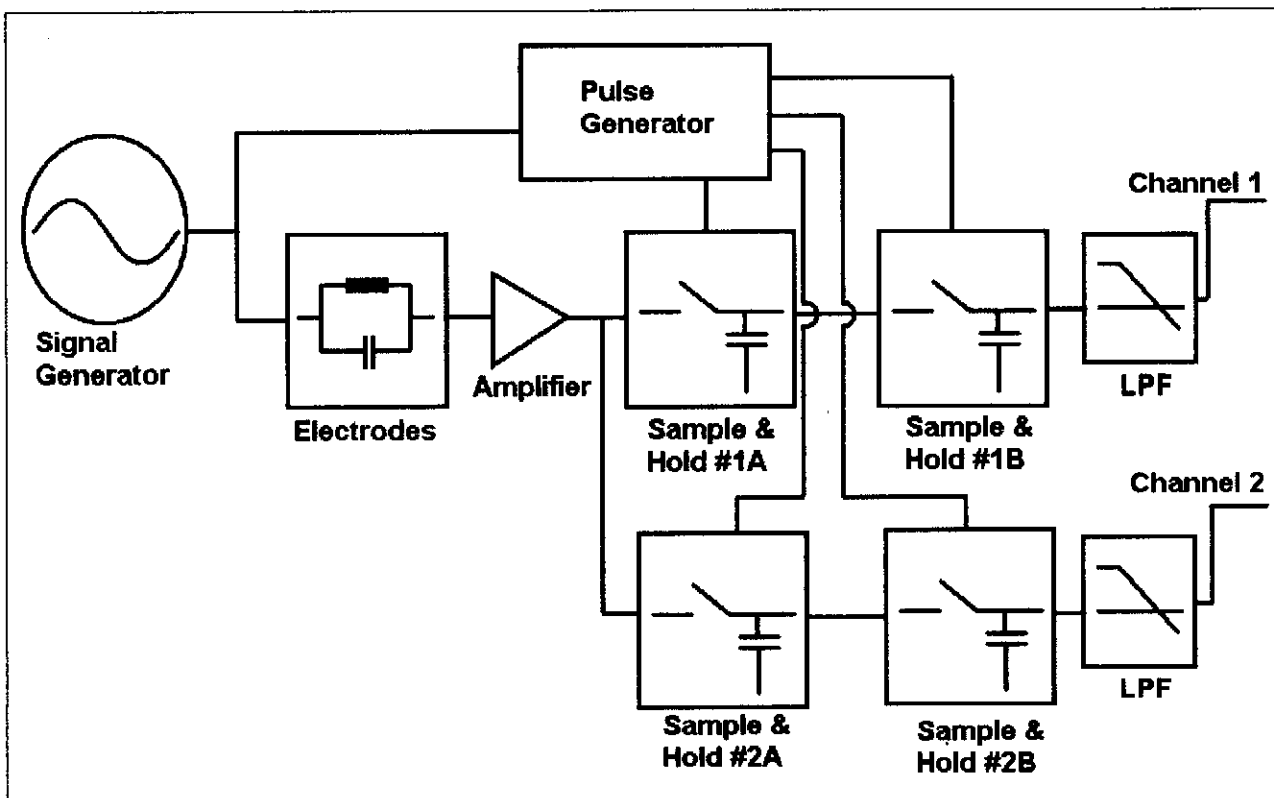


Figure 3-23 Simplified schematic of sensor with sample and hold components

The main objective is to control the two components in one arm in such a way that the hold commands overlap and that a specific component is in the sample mode for just under 50 % of the time. If only one S&H IC was used in one arm and controlled by a 50 % duty cycle signal, the output would not resemble a DC voltage as the component is in the sample mode only half of the time. In the figure above, the B components will see a stable DC voltage the whole time that they are in the sample mode (as the A

components are in hold mode). Then the B components will sample the stable DC voltage and keep the output stable while component A is in the sample mode for the required time. Every time the sample command is given, the input and output voltages of any S&H IC are relatively close to each other. This is not harsh on the components and allows the minimum acquisition time to be decreased to 3 μs . This scheme was implemented and a working frequency of 125 kHz was achieved.

To produce the command signals, four RC circuits with different characteristics were used and were buffered by an inverting buffer with Schmitt inputs (74AHCT14).

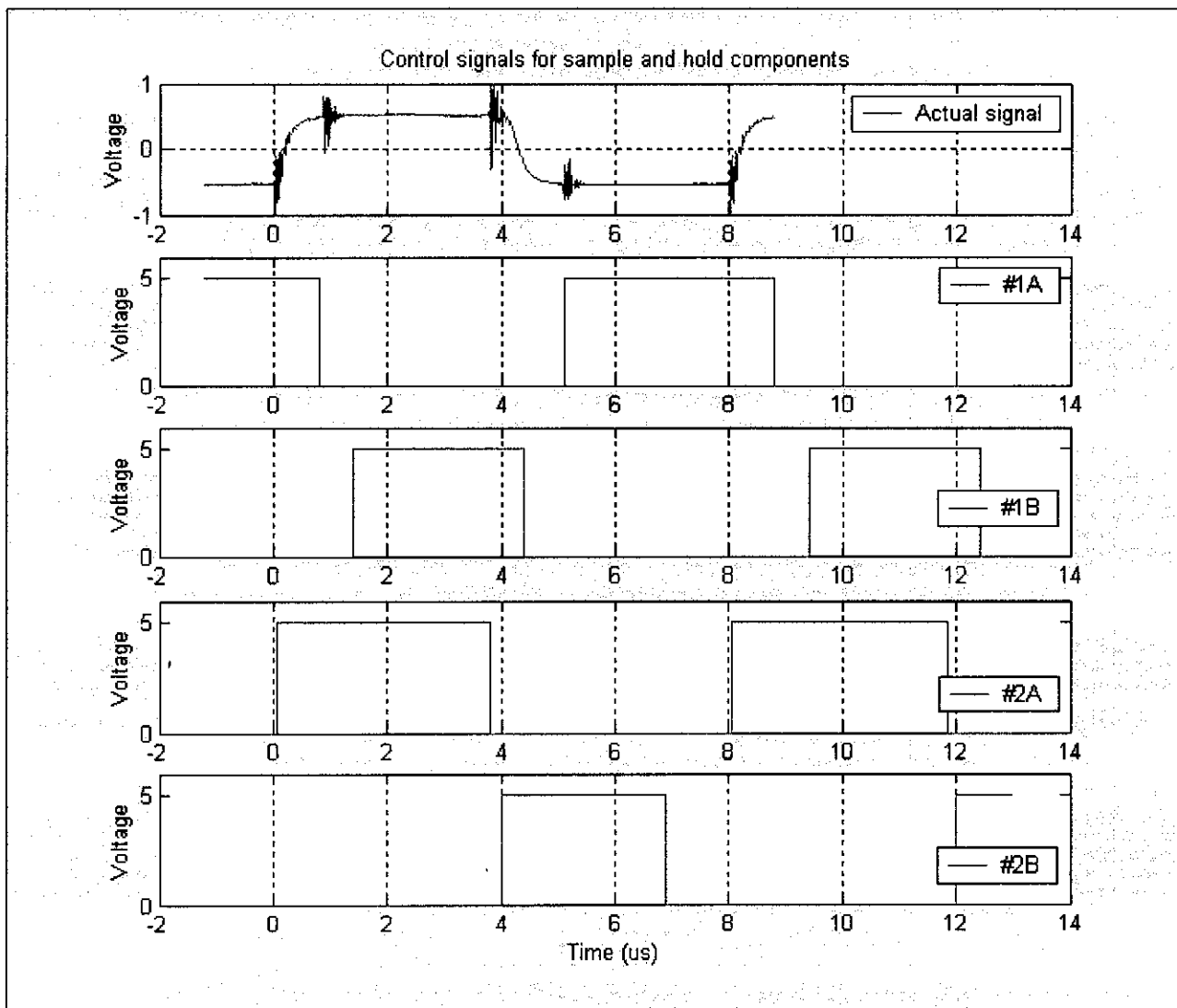


Figure 3-24 Control signals for sample and hold components

Figure 3-24 gives the signals associated with the control of the sample and hold scheme. The first figure (actual signal) is a waveform measured with the probe. The rest of the figures were artificially created in MATLAB to resemble the actual signals driving the various components. The produced drive signals are clean as sharp and fast logical gates were used. The ringing on the actual signal is due to the sampling action.

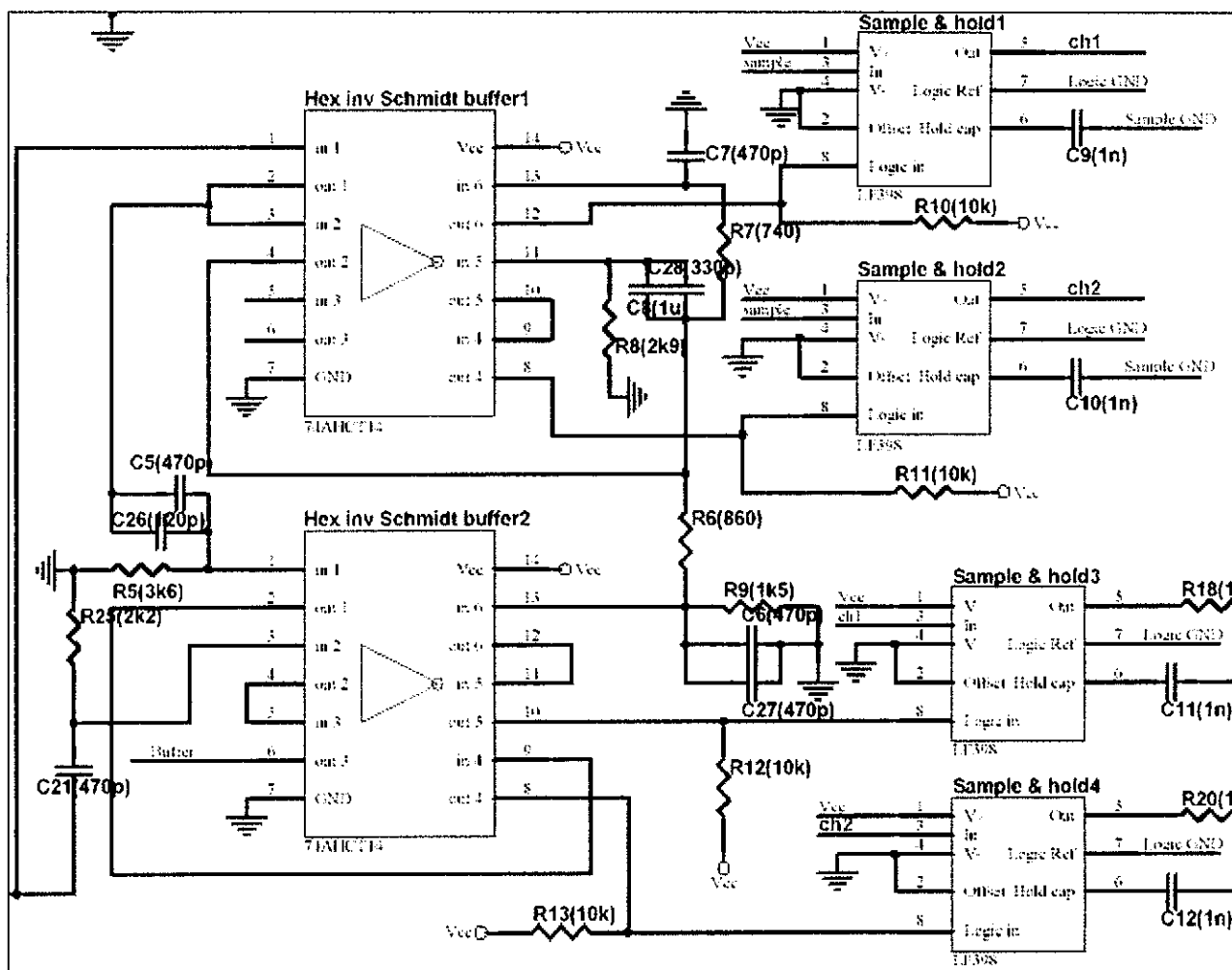


Figure 3-25 Detailed schematic of sample and hold scheme

Figure 3-25 and Table 3-4 indicate the components used to implement the RC delays. These were used to create the waveforms shown in Figure 3-24.

Table 3-4 Components used to generate control signals

Control signal created for:	Components
Channel 1, first sample IC	R7, C7 and 74AHCT14#1
Channel 1, second sample IC	R6, R9, C6, C27 and 74AHCT14#2
Channel 2, first sample IC	R8, C8, C28 and 74AHCT14#1
Channel 2, second sample IC	C5, C26, R5 and 74AHCT14#2

Components R25 and C21 (in Figure 3-25) are used to increase the duty cycle of the drive signal. This is done to cancel the effect of the drive components and to produce a 50 % duty cycle drive waveform. Components C9, C10, C11 and C12 are the only external components the LF398 needs and the value of the hold capacitor determines the acquisition time and droop rates. If a fast acquisition time is needed, this



value must be small. The compromise is that the output droop rate increases. If a low droop rate is required, the capacitor must be large and this produces larger acquisition times. The droop rate for small hold capacitor values is still slow enough for this application and 1nf is the smallest advisable value.

Another limitation on the S&H ICs, is the inability to operate near the voltage rails. Neither the input signal nor the logic drive signal may be less than 3V from the voltage rails. Dual supplies are possible but are not recommended. To solve this problem a logic signal ground was created at 3 V and the drive signal was driven referenced to sample (power) ground. This implies that the sample IC sees a 2 V drive signal. The LF 398 specifies a high at 1.4 V typical, with a maximum of 2.8 V. For this reason, pull up resistors (R10, R11, R12, R13) were inserted at the output of the buffer to marginally increase the output voltage. This proved to be effective and stable sampling was achieved.

3.6 Conditioning of DC signals

3.6.1 Low-pass filter

To produce a low noise, stable output signal, the DC voltages obtained from the sample and hold components were filtered with a two-pole, low-pass active Butterworth filter^[15, page 854]. The cutoff frequency was chosen as 10 Hz as the probe moves at a rate of approximately 10 cm per second when deployed in a borehole. When the probe moves at this rate, a 10 Hz signal will keep up with a rock body resolution of 1 cm. The electrodes will not be able to detect objects smaller than 1cm and this choice is valid. Figure 3-26 displays a schematic of the filter.

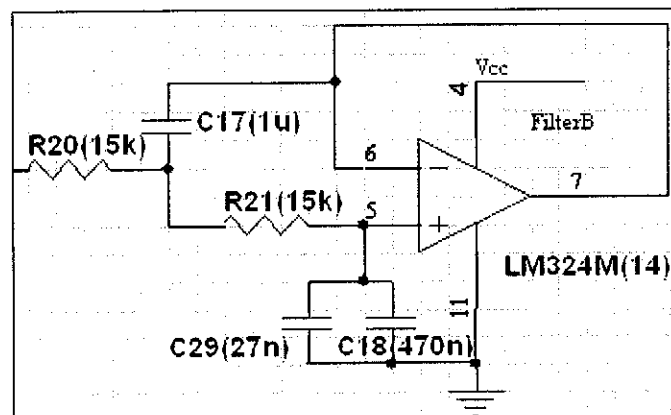


Figure 3-26 Butterworth low-pass filter

The filter was tested with a 3 V amplitude sinus signal and Table 3-5 gives the results.

Table 3-5 Transfer characteristics of Butterworth filter

Frequency	Voltage (sinus signal amplitude)
10 Hz	2.8V
30 Hz	0.48V
50 Hz	0.22V
100 Hz	0.035V

Two of these filters were implemented to filter the two channels

3.6.2 DC shifting of output signal

The analog to digital converters of the Sindlehead navigator will be used to sample the DC voltage supplied by the sensor. These components can sample voltages between 1 and 4 volts and as the rock sensor has a reference voltage of 5 V and increases with permittivity, the two components are not compatible. To produce a voltage range that is suitable to the Sindlehead receiver, the output signal was shifted down by a value of four volts. This implies that the 5 V referenced signal was shifted to a 1 V referenced signal. This was done with two operational amplifiers configured as voltage subtractors with unity gain. The inverting input is connected to a 4 V reference voltage (created with a LM 336 and variable resistor). The non-inverting input is then connected to the 5 V referenced output. The reference is also shifted in exactly the same way as the channels and is also sampled and stored in the Sindlehead. A schematic representation of the shifter is displayed in Figure 3-27. The 4 V reference is used for all three level shifters.

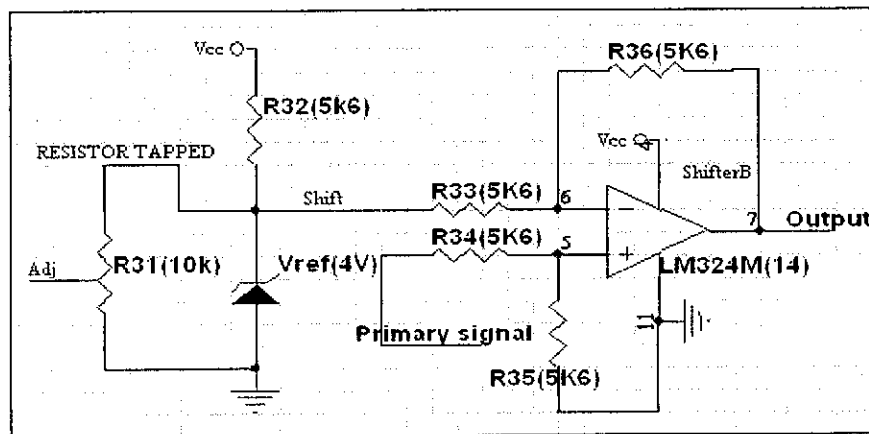


Figure 3-27 Schematic of DC level shifter

3.7 Comprehensive and detailed schematic

The next figure will present the full schematic to explicitly show how each of the subsystems described in sections 3.2 to 3.6 are connected. Peripheral components like power supply and crystal oscillators will be added. The duplicated filters and DC shifters used for the multiple channels are also shown.



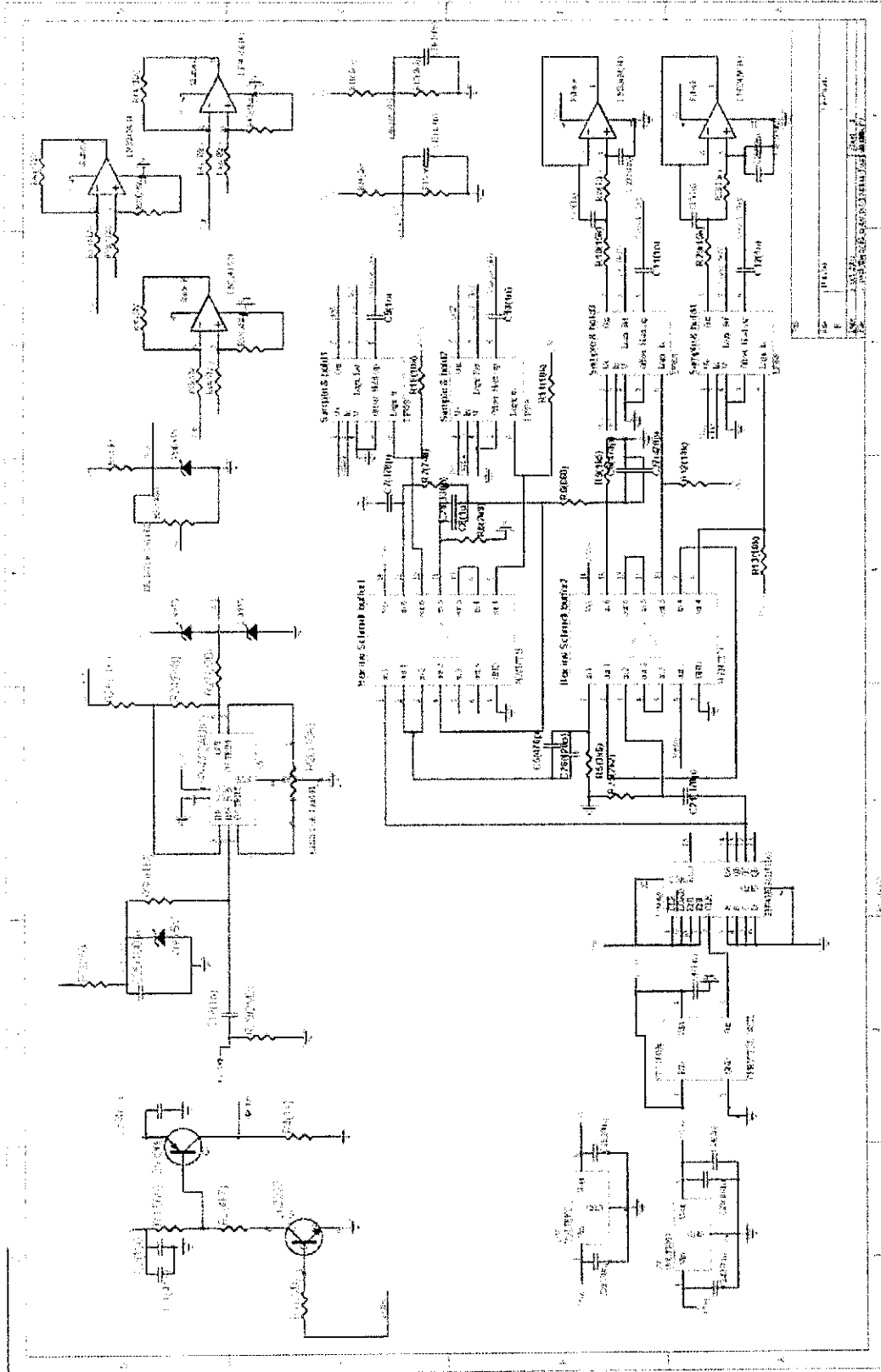


Figure 3-28 Comprehensive schematic

3.8 Field deployable prototype

To take the sensor from workable subsystems to a probe that could be deployed in a practical situation, two aspects needed attention. One is the physical assembly of the electrodes in a mechanically strong way and the second is to integrate all the electronics in a PCB that will fit inside the housing. The probe presented here is the result of one design iteration. The constructed probe was tested in mining conditions. The results of these tests (presented in appendix A) isolated some of the problems that were not foreseen. This information was used to correct the problems that occurred and the next section states the corrected probe.

3.7.1 Physical assembly of electrodes and housing for electronics

Figure 2-11 is repeated here with some changes. This will help in describing the method used to create the mechanically strong probe.

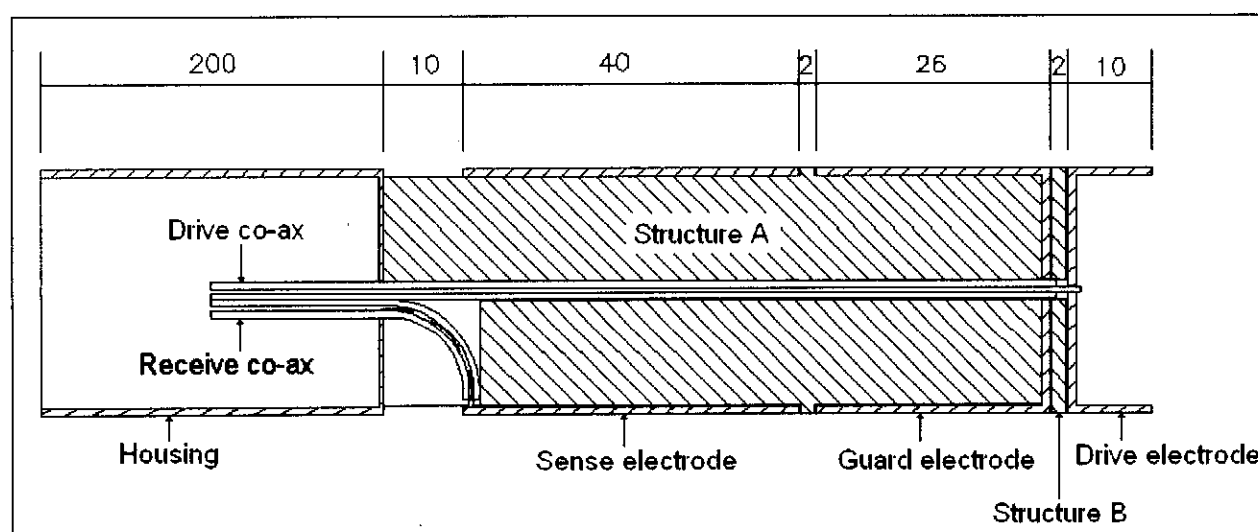


Figure 3-29 Sectional cut through probe to describe mechanical assembly

The raw materials used were copper pipe with outside diameter of 29 mm, plastic machined into cylindrical form, copper that could be machined to make lids, 2 mm semi-rigid coaxial cable and quick drying epoxy. Firstly, structure A consists of plastic that is machined as shown in the figure. It is basically a cylindrical rod with a small edge to separate the sense and guard electrodes. One hole is drilled on the axis. This hole is for the coaxial cable that will produce ohmic connections. The guard electrode is a piece of pipe with a lid soldered to the one side. The guard and sense electrodes are then slid over structure A and glued in position. After positioning in hole, the outer conductor of the drive co-ax is connected to the guard electrode lid to produce the earth connection. The centre conductor of the receive coax is connected to the sense electrode, while the outer conductor is earthed against the housing. The housing consists of a pipe with two lids. The one that is connected to structure A, is soldered and is not removable

while the far end (left hand side in Figure 3-30) can be removed by removing three screws. Structure A is then glued to the housing with the epoxy. Structure B is only a flat, plastic disk with a hole in it. One side is glued to the guard electrode and the other side to the drive electrode. The inner conductor of the drive co-ax is connected to the drive electrode.

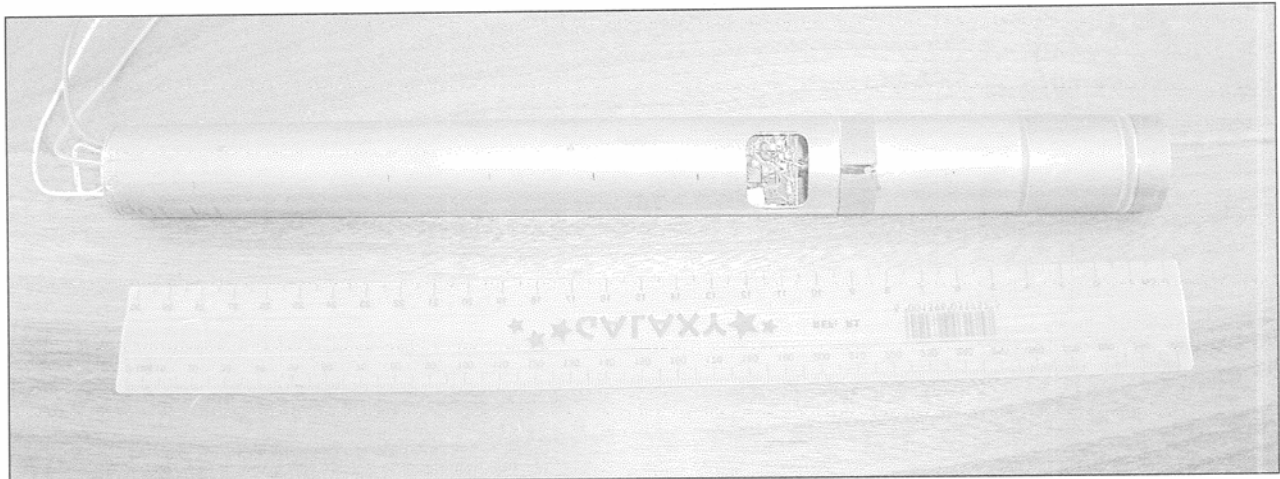


Figure 3-30 Picture of mechanically strong probe

A picture of the probe is given in Figure 3-30. A little window was machined into the housing to enable the user to connect the co-axial cables to the electronics. The groove that was machined into structure A to hold the receive co-ax can be seen just next to the window. Through hole connectors were inserted into the removable lid to produce a path by which the signals can be sent to the Sindlehead navigator. To produce a mechanical connection between the Sindlehead and the rock probe, an omega shaped wire was attached to the housing side of the probe. This connection was also used as the ground return path. The total length of the probe is 31.5 cm.

3.7.2 Printed circuit board design and electronics

Figure 3-31 gives a picture of the electronics.

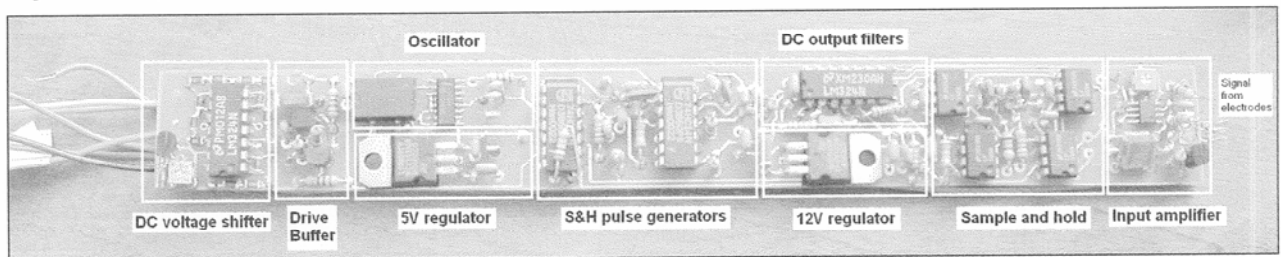


Figure 3-31 Populated printed circuit board with major components isolated

The PCB is 25 mm wide and 215 mm long. It was designed by the author in Protel Design Explorer and manufactured by faculty staff. There are three signal paths:

-
- The drive signal originates at the oscillator and is buffered by the denoted components. The signal is then fed to the electrodes by a co-axial cable on the other side of the board connected just to the left of the drive buffer.
 - The S&H control signals also originate from the oscillator and move to the right hand side of the board. They are used to drive the sample components.
 - The signal received from the electrodes is fed into the input amplifier at the right end of the board and is directed to the left where the signal will be sampled. The sampled signal is filtered and is then connected to the DC voltage shifter. The reason why the DC voltage shifter is so out of place, is due to the fact that it was added to the design after the mine tests were done. From the DC voltage shifter the desired output signals are obtained.

In the picture, there are seven wires attached to the board. In normal working conditions only five connections will be necessary: Channel 1, Channel 2, reference, battery plus and battery minus. The two extra connections were only inserted for testing purposes.

The PCB was attached to the electrodes to produce the desired sensor. The sensor produced usable results and these will be discussed in the next chapter.

4 Testing of rock probe

The reasons for the tests on the probe are firstly to see whether the functionality that is obtained is in line with solving the problem discussed in the introduction. Secondly, it is needed to characterize the probe in such a way that the information obtained is useful and thirdly to find out what the strong points of the sensor are.

Three sets of tests were performed on the probe. The first test was simple and set out to prove that the sampling of the signal is accurate. In the second test, the borehole conditions were simulated to try and recreate working conditions. As the borehole test does not use materials with the same properties as the rock, the third test was done on actual rock cores to see how this affected the sensor.

4.1 Sample and hold chain accuracy

To perform this test, the signal at the S&H input was displayed on the scope and the value at the instant when the hold command is given, was noted, this is denoted "expected". The measured DC output value was also noted and is denoted "measured". The "measured" and "expected" data are plotted on the same axis in Figure 4-1 and Figure 4-2 to display the similarity of the two data sets.

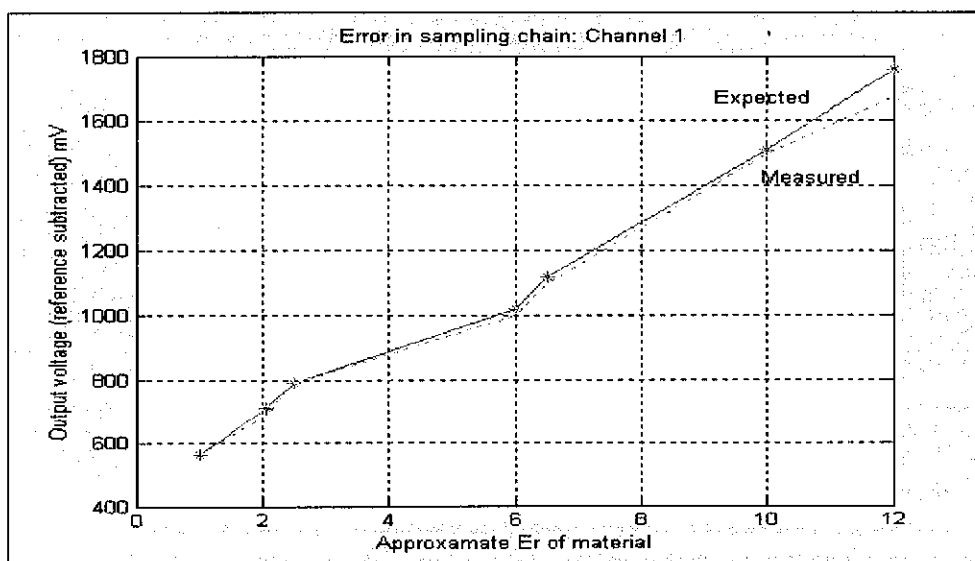


Figure 4-1 Accuracy of sampling chain: Channel 1

As can be seen from these figures, the sampling chain is accurate for there are no notable differences between the expected and measured values.

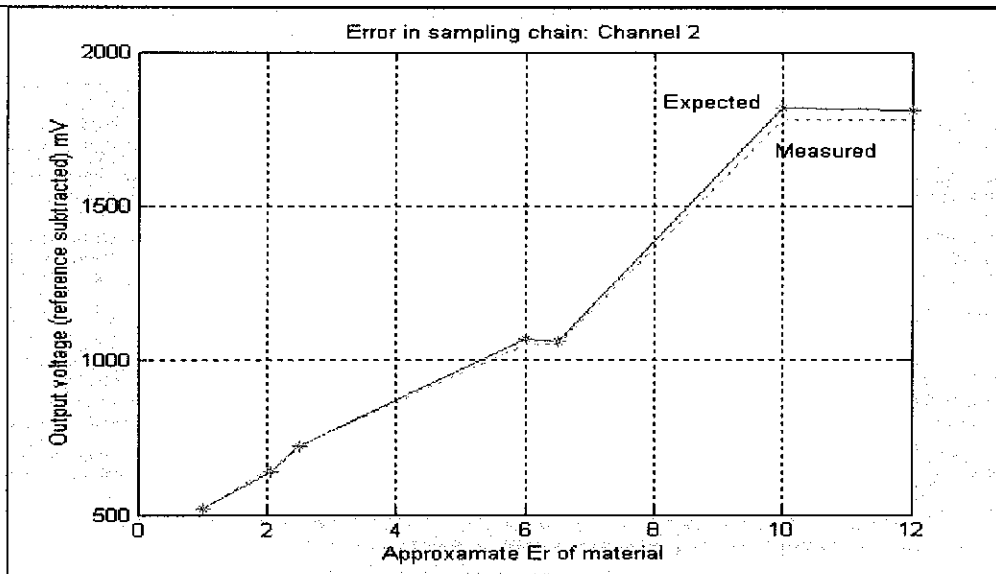


Figure 4-2 Accuracy of sampling chain: Channel 2

4.2 Tests in simulated borehole conditions

The aim of this experiment is to obtain the transfer function of the sensor in a laboratory environment which is similar a mine borehole environment.

4.2.1 Test setup

This experiment was done using a specially designed watertight container nicknamed the "bazooka". A detailed drawing of the bazooka is attached in appendix B. This container consists of concentric PVC pipes that can be filled and drained with fluids or granular solids to simulate borehole conditions. In mining boreholes there are two volumes that must be taken into account. Firstly, the probe will not be in direct contact with the rock as the borehole's diameter is larger than the probe's diameter. This volume (between the hole and the rock) can either be filled with water, or, by default, with air. To simulate this, the "bazooka" has a 40 mm diameter PVC pipe in the middle of the structure and this is loosely referred to as the borehole (volume B in appendix B). A large 110 mm diameter drain pipe was used to produce the structural strength and the volume that will correlate with the rock body (volume A in appendix B). The probe is held in a stationary position while the fluid level is changed. This is not the same as the situation in the mine as the probe will be moved in the borehole. If this is done, the probe will stay in exactly the same position in relation to the radial geometry of the container while the tests are performed. The water will produce a clean step in permittivity which is sensed by the probe and therefore this test will produce the step response of the sensor. The materials used to fill this "bazooka" are specifically selected for their electrical properties.

Substances used:

1. By default an air "filled" bazooka was used to create a reference.
2. Tap water with an ϵ_r of 81.
3. Saline tap water with an ϵ_r of 81 and elevated losses.
4. Granular polypropylene with solid ϵ_r of 2.25.

4.2.2 Method followed in test

The experiment was done twice: Firstly with the probe centred inside the bazooka and secondly introducing asymmetry – making the probe touch one side to simulate a probe inside an inclined borehole (touching test). The DC output voltages were measured at specific water levels with standard digital multi-meters and logged by hand. Table 4-1 gives a detailed sequence of actions taken. The probe was inserted into the "bazooka" with known electrode position.

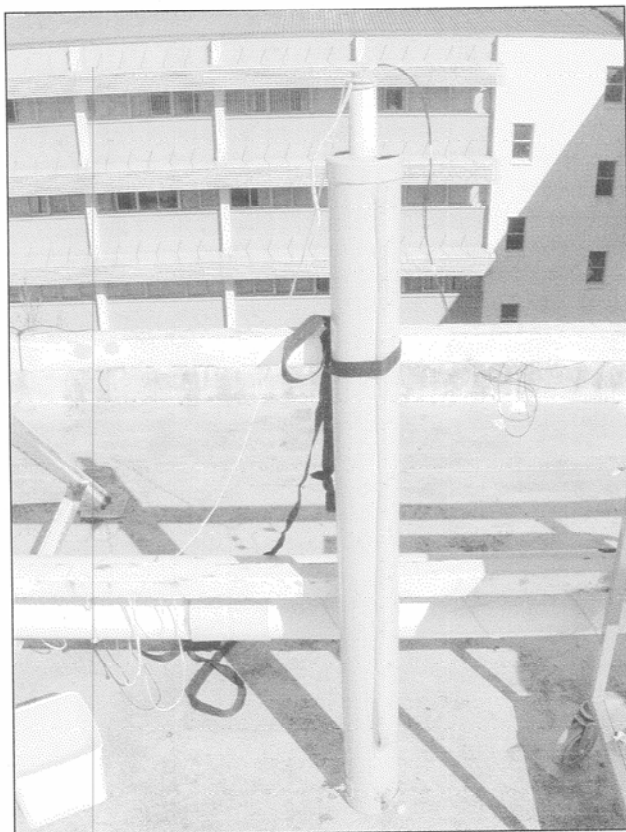


Figure 4-3 Picture of "bazooka" on test site

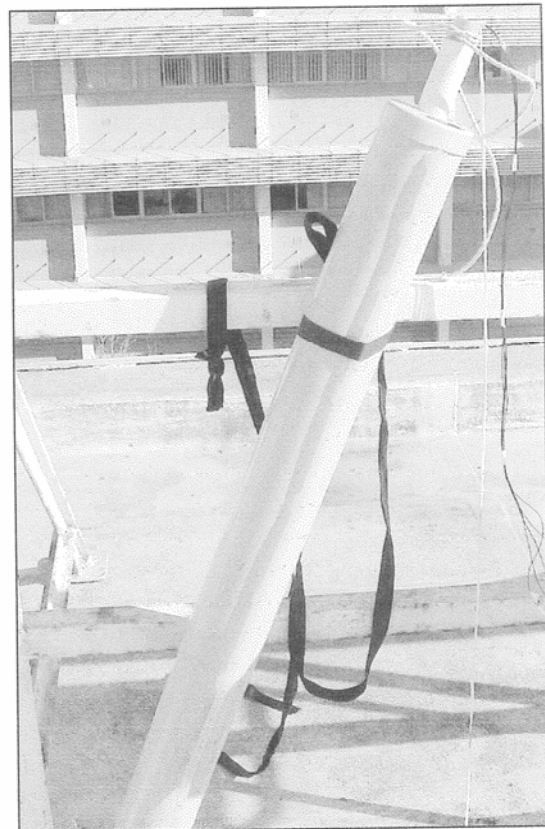


Figure 4-4 Bazooka placed for the touching tests

The pictures in Figure 4-3 and Figure 4-4 give an indication of the test site, the "bazooka" used and how it was positioned to produce the various tests. The inner pipe was used to simulate the borehole, the small

plastic pipe was used to verify the water level inside volume A, the two plugs at the bottom were used to drain the volumes and the holes in the top were used to fill the volumes.

Table 4-1 introduce the chronological sequence of the test. This sequence of events was chosen to simulate possible borehole situations.

Table 4-1 Step-by-step sequence of experiment

1	Fill volume A with granular polypropylene
2	Fill volume B with water
3	Drain volume B
4	Empty volume A
5	Fill volume A gradually with tap water noting voltage vs. fluid level
6	Add salt to tap water to produce saline water
7	Fill volume B with water
8	Drain volume A gradually noting voltage vs. fluid level
9	Drain volume B

4.2.3 Results

The test can be divided into two parts, the first part is no 1 to 4 in Table 4-1. These results will be presented in tabular form. The values noted from the multi-meters were referenced (subtracted from the reference voltage) and the values indicating permittivity and losses were extracted from the Channel 1 and 2 readings.

Table 4-2 Results for first part of test: Centred versus probe touching one side - permittivity.

Centered		Touching	
Position in test	Voltage indicating ϵ_r	Position in test	Voltage indicating ϵ_r
Reference (both volumes filled with air)	0.309	Reference (both volumes filled with air)	0.332
Polyprop granules	0.5060	Polyprop granules	0.4852
Wet Hole (Vol. B water filled)	4.319	Wet hole (Vol. B water filled)	3.652
Volume B drained	0.518	Volume B drained	0.482
Reference with Vol. A and Vol. B drained	0.328	Reference with Vol. A and Vol. B drained	0.333

Table 4-3 Results for first part of test: Centred versus probe touching one side – Losses.

Centered		Touching	
Position in test	Indication of resistance (Channel 1/Channel 2)	Position in test	Indication of resistance (Channel 1/Channel 2)
Reference (both volumes filled with air)	1.25	Reference (both volumes filled with air)	1.298
Polyprop granules	1.303	Polyprop granules	1.246
Wet hole (Vol B water filled)	2.36	Wet hole (Vol B water filled)	1.611
Volume B drained	1.305	Volume B drained	1.237
Reference with Vol. A and Vol. B drained	1.243	Reference with Vol. A and Vol. B drained	1.248

Remarks on first part of test**1. Permittivity data**

- The sensor is sensing the granules with satisfactory sensitivity. The resulting permittivity of the granules will be less than that of the solid. According to the mixing formula (and basic algebra) the resulting permittivity will be approximately 2 ^[18, page 213]. An increase of 1.66 times the reference was obtained.
- For this specific test there seems to be no big difference in sensitivity between the centered and touching geometries.
- The probe can withstand a water filled hole without saturating.
- The test is repeatable as the value returned to the initial value in both cases.

2. Losses

- The sensor is stable and gives repeatable values
- The indication show little correlation between the expected losses.

The second part of the test results (numbers 5 to 9 in Table 4-1) will be presented in graphical form in Figure 4-5, Figure 4-6 and Figure 4-7 as the results produce a profile. The x-axis resemble the position of the water level in the "bazooka".

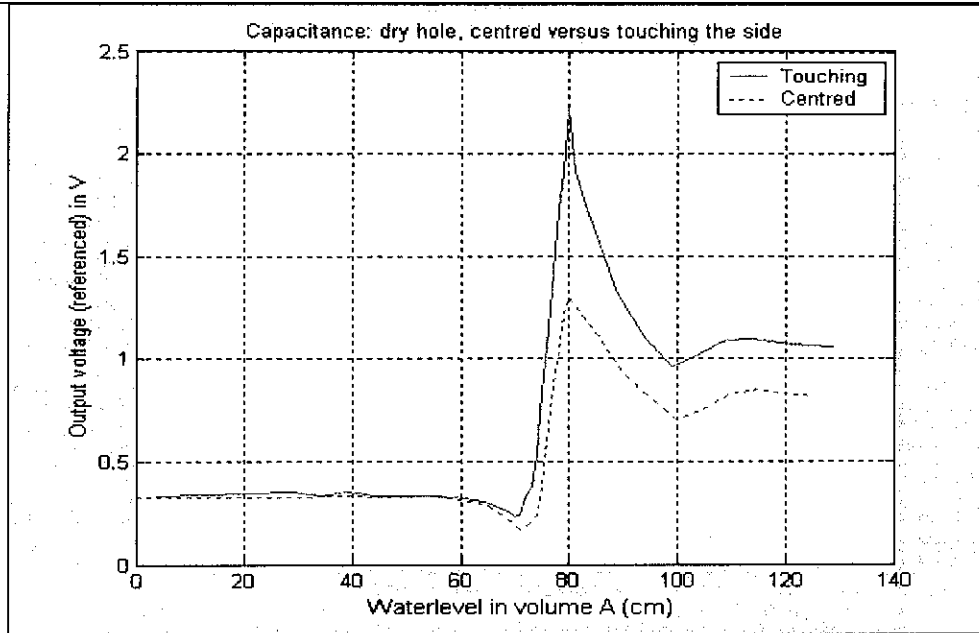


Figure 4-5 Indication of capacitance with water level changing

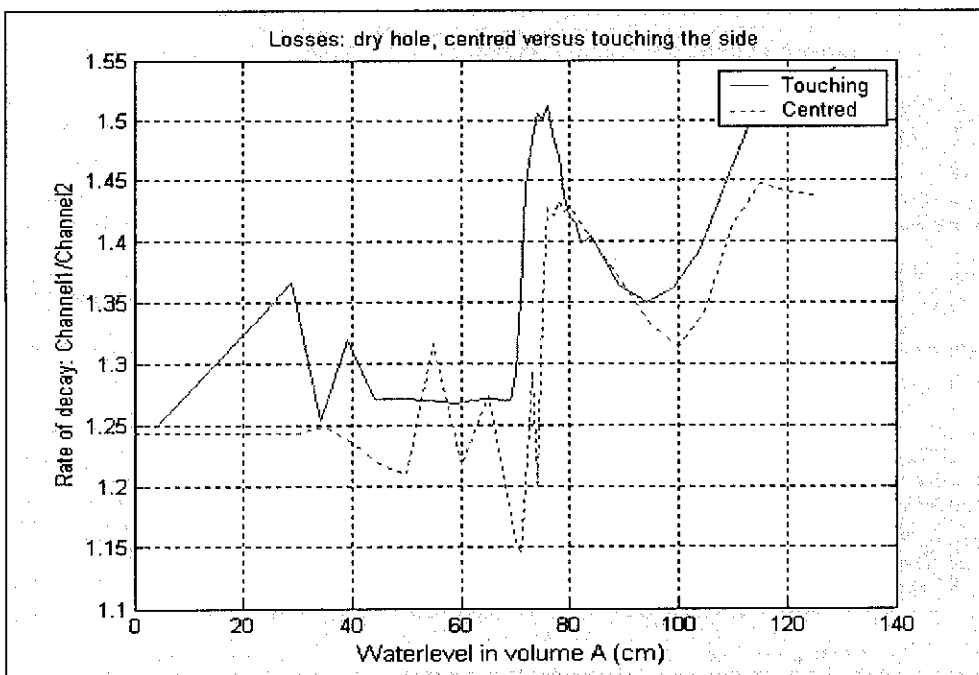


Figure 4-6 Indication of losses with water level changing

Remarks on second half of test:

1. Permittivity

- The sensor was placed at the 75 cm mark in the “bazooka” with the middle of the guard electrode taken as the center point. The driving electrode was lower and the sensing electrode higher. The transition between air and water as the water level rises can clearly be seen at this position. Four interesting characteristics can be isolated:

- If the water is more than 10 cm from the sensor, no activity is recorded
- The sensed voltage decreased by a small but notable amount just before the middle of the sensor is reached.
- A sharp, high peak (7.3 times the reference value) is formed when the water level is at the sensing electrode (just above the middle mark).
- After the high peak, a small decrease is noted after which
- the sample stabilizes at 3.3 times the reference value.
- These characteristic responses are confirmed by both Centered and Touching experiments. The touching test gives higher sensitivity. This is expected as the probe is in closer contact with the water.

2. Losses

- The rate of decay gives an indication of the losses in the system: The water has rather high (0.8 mS/cm) losses and should be a good test for the probe. From Figure 4-6 it can be seen that the sensor does indicate a material with lower losses. This decrease is contradictory as the water has higher losses than air. The author suspects that the permittivity readings influence the decay rate and the rate is not directly connected to the losses. Further investigation will be done in section 4.2.5.

Salt added to the water did not have an effect and this adds to the paragraph above.

Step 7 and 8 in Table 4-1 were specially inserted to test if the probe will be able to “see” through a water filled hole and still give an indication of the rock. The result for this test is given in Figure 4-7.

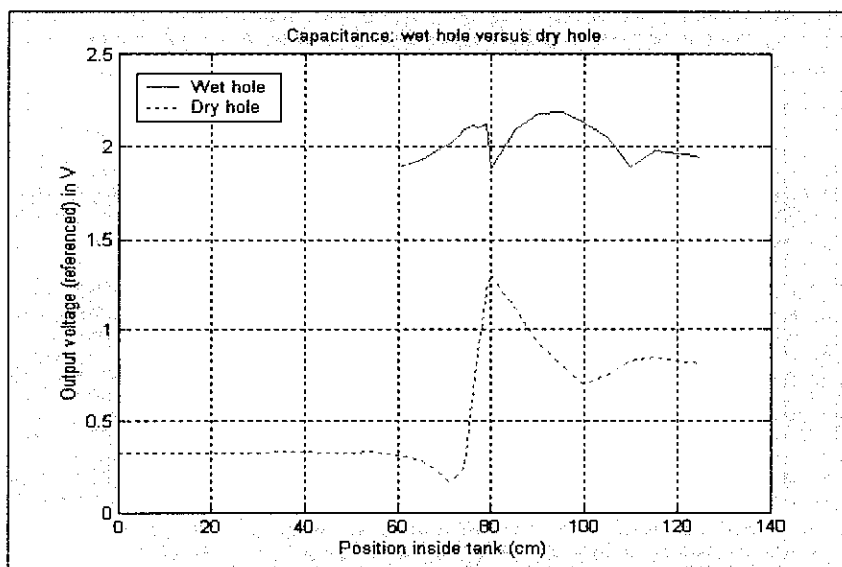


Figure 4-7 Ability (of lack thereof) of probe to sense rock in a water filled hole

This figure shows that there is no correlation between the wet and dry measurements.

4.2.4 Attributes resulting from tests: Characteristic of step response

To explain the four major characteristics of the permittivity measurement, the author will introduce four sketches that will clarify the electrode position in respect to the water position inside the tank. A practical explanation for the step response will also be given.

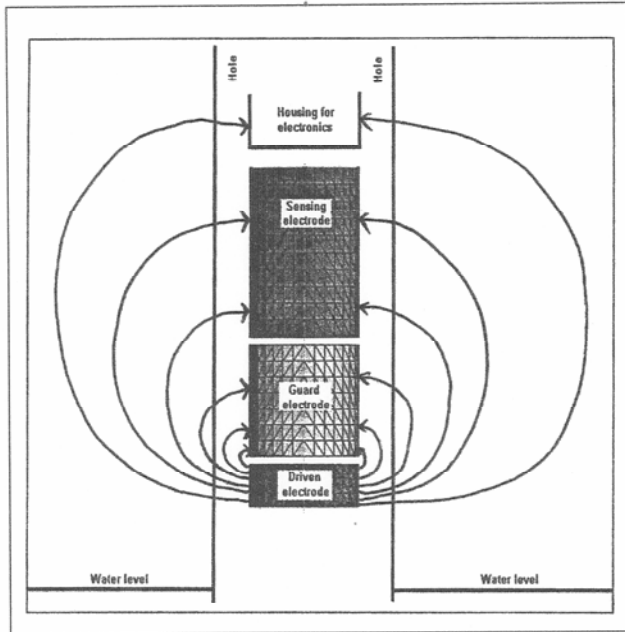


Figure 4-8 Sketch one: Homogeneous air

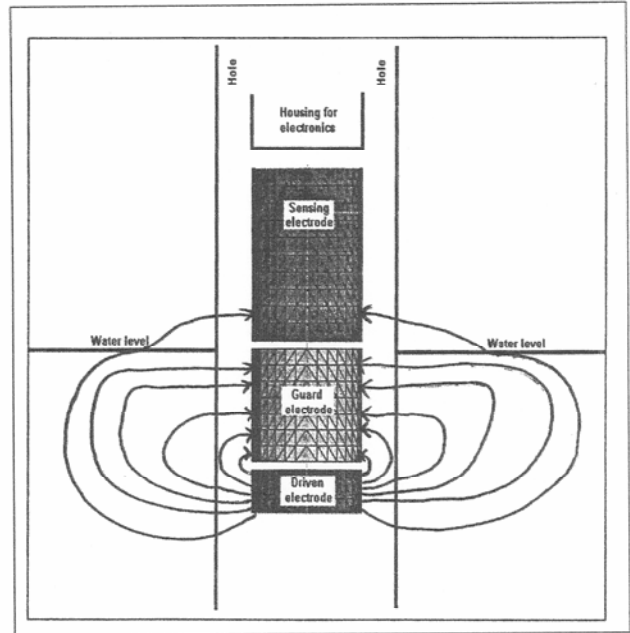


Figure 4-9 Sketch two: Water level at guard

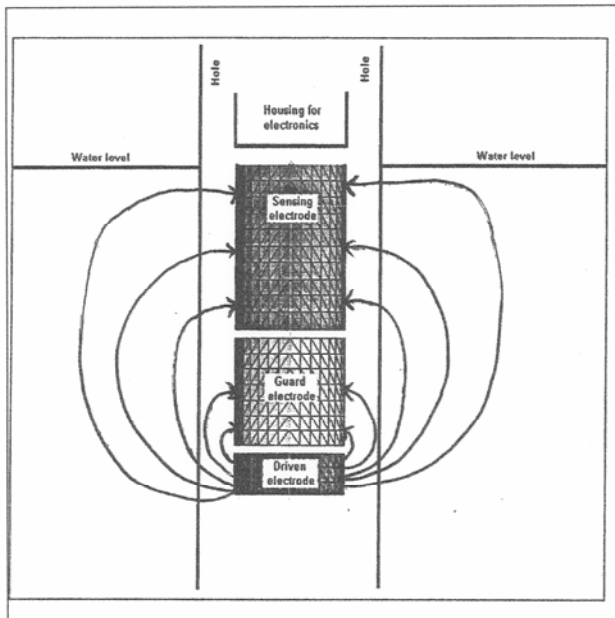


Figure 4-10 Sketch three: water level at sense electrode

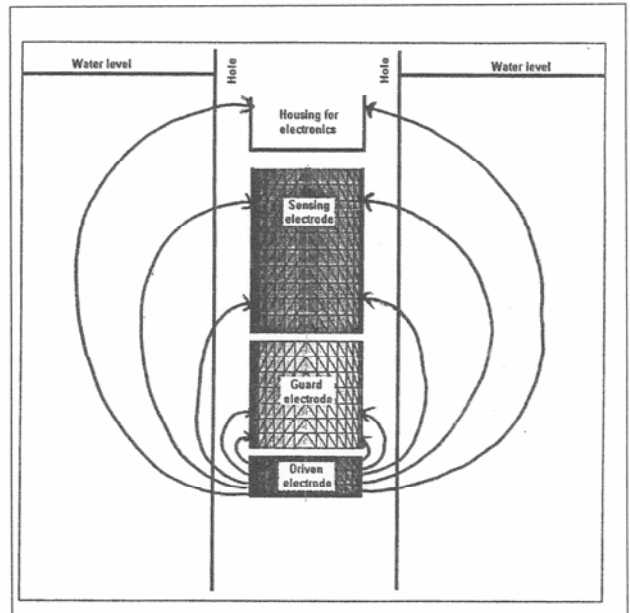


Figure 4-11 Sketch four: Homogeneous water



These pictures were drawn by hand and are only an indication of possible electric field lines. Figure 4-8 produces a reference as to the position of the field lines. This is when the water is still at some distance from the probe and the probe is not affected. Figure 4-9 shows how the field lines are "bent" back by the high ϵ_r water and how they terminate on the guard electrode. The fields are then "bent" away from the sensing electrode and the result is that the output voltage decreases. In Figure 4-10 the water level has risen to the sensing electrodes. Most of the external fringing fields terminate on this electrode and this produces the high spike displayed in Figure 4-17. The last figure (Figure 4-11) shows the final state where the fields are contained in a homogeneous material.

To verify this, a CST simulation was created to simulate the situation explained in the sketches. The results from these simulations are given in Figure 4-12 for permittivity and Figure 4-13 for losses. The observed trends in permittivity correlate with the results obtained. The effect if the water is 10 cm from the sensor is small and after this mark, the probe starts sensing the material. The gradual rise and fall while the water level is adjusted over the position of the electrodes can be seen. The fall in capacitance just before the point where the electrodes are reached, is also displayed. This fall is not as high as was seen in the test results. These main attributes that could be seen with the permittivity results could also be seen in the loss simulation, this however was not measured by the sensor and these results will be used in the next part. The simulation results produce the same characteristics that were observed in the tests.

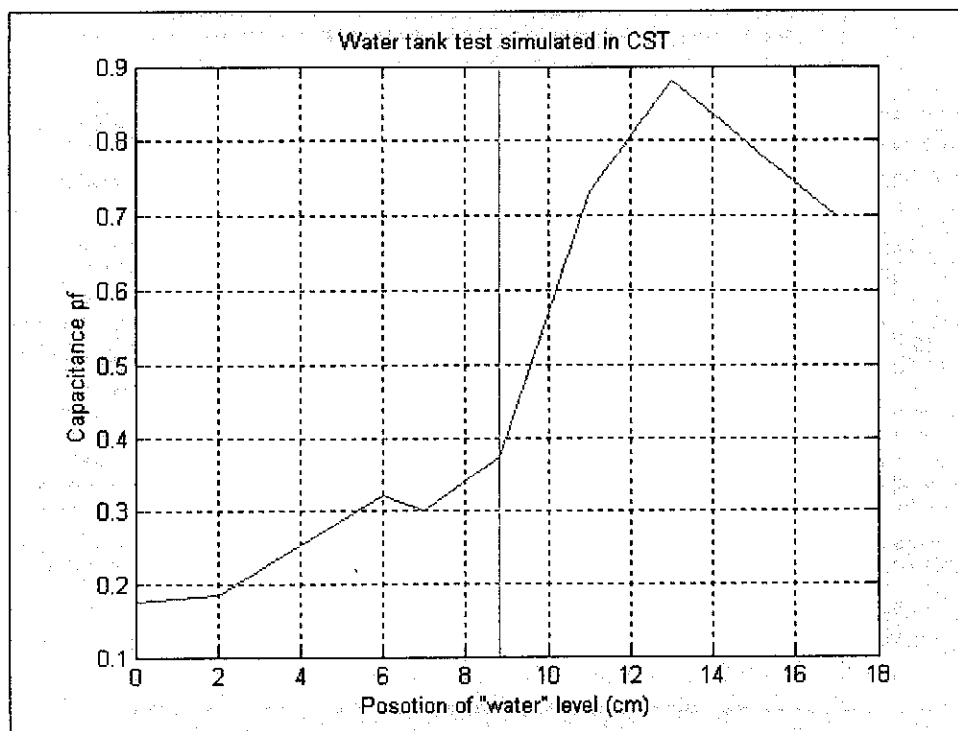


Figure 4-12 Response of probe to step function: Capacitance

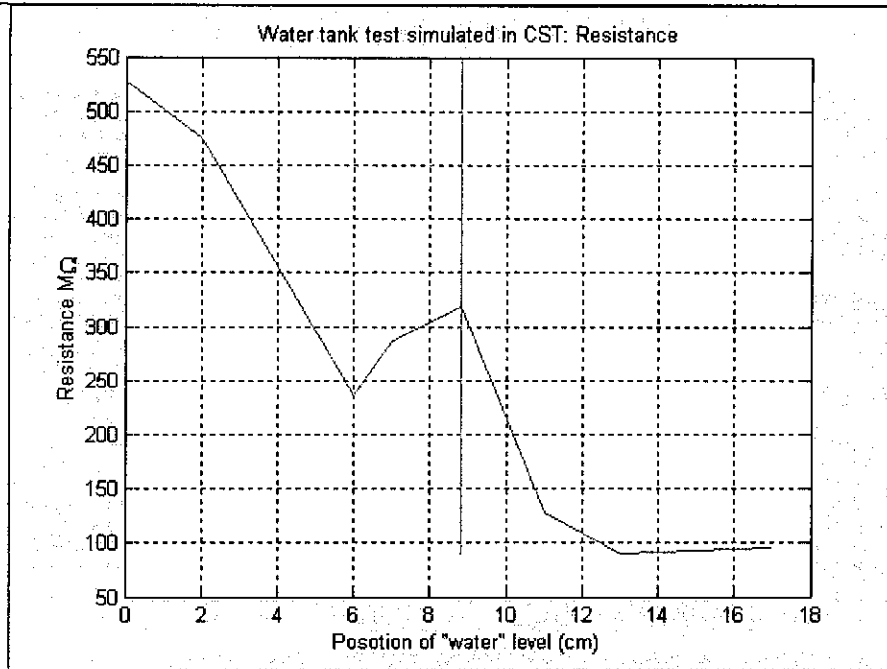


Figure 4-13 Response of probe to step function: Resistance

4.2.5 Attributes resulting from tests: Loss test

While doing tests with the "bazooka" on the characteristics of the sensor, all the permittivity tests could be explained, but none of the loss measurements results were as expected. To investigate this, the test was repeated with saline water with known conductivity and the output signal (that was sampled) was also extracted and saved. From this test it could be deduced that the sampling of the data is accurate but the output waveform did not react as expected.

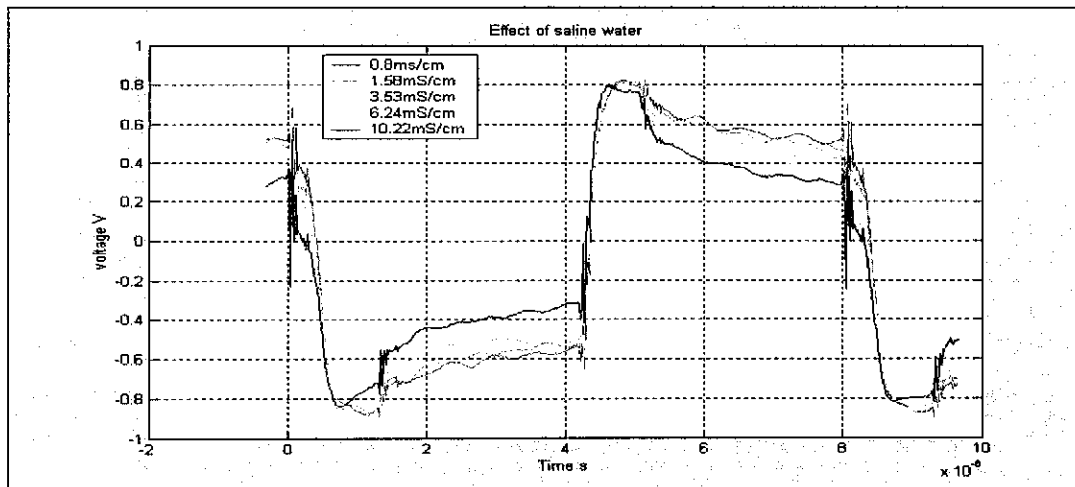


Figure 4-14 Effect of saline water on received waveform



Figure 4-14 gives the observed trace and is used to explain why the results were not as expected. The slope of the square wave is expected to be directly proportional to the losses of the medium and the slope was expected to increase as the conductivity increased. This was not the case and it can be seen that the slope decreased as the losses were increased. This explains why the tests on losses that were perceived by the probe were contradictory. The two oscillations on the positive cycle of the signal are induced by the sampling signal and indicate the timing of the hold signal.

Remarks in Figure 4-14

- The signal was noisy and the trace shown in Figure 4-14 was averaged 64 times.
- The signal did not react as expected.
- There was a jump in the amplitude that coincided with the sample command. It implied that the signal action modifies the signal itself
- The same is seen for the second sampling signal

4.2.6 Conclusions on “bazooka” tests

This test was done in laboratory, controlled environment. This will not be the case in the mine, but this test was performed to learn more about the working of the probe in similar conditions. This was successful.

The sensor was very sensitive, so sensitive that walking around the probe also influenced the samples. For this reason, the author had to step back from the probe for each measurement. The presence of a human body (high permittivity and losses) relatively close to the probe (20 cm) lowered the sampled voltage. This was interesting to note and an explanation of this can be formed by keeping the sketches presented in mind. If a body of elevated permittivity is adjacent to the probe, the fields will be drawn away from the sense electrode and hence the perceived capacitance will decrease.

Aspects of tests that were successful:

- The probe sensed the permittivity of materials in volume A (simulated rock) with high dependable sensitivity (1.6 times the reference for polypropylene and 3.3 times the reference for water).
- The probe was working under water filled hole conditions (volume B filled with water) and did not saturate.
- The difference between a centered and touching probe was measured and found to be substantial.
- The probe will be sensitive to a change in permittivity as shown in Figure 4-5 and explained in the sketches (figures 4-9 to 4-12).

Aspects of tests that were less successful:

- Changes in losses of water could not be sensed
- The probe was not able to sense through a water filled hole, this was expected but is noteworthy

4.3 Test using a characterized rock core

The permittivity and losses of water are high and the properties of rock are much lower. An attempt was made to measure the permittivity and losses of a known rock core and will be discussed now.

4.3.1 Introduction

A test was done to verify the validity of the approximation of placing rock cores next to the sensor instead of putting them inside a borehole. To do this, the probe was placed inside a hole drilled into a granite slab and again placed next to the slab. The output voltage was more sensitive to the “inside” reading than the “next to” reading by a factor of 1.4. The losses perceived also changed with position as there is more lossy material when the probe is inside the slab. Although there is a difference in amplitude of the signal, the quality of the signal does not change with position and this implies that the test using cores placed next to the rock will be valid. In fact, the performance of the probe will be better inside the hole and the core tests will give conservative results.

A rock core was measured by Rütshlin using tailor made electrodes and a Hewlett Packard auto balancing bridge. He made the results available to use as a reference for tests done with the sensor in question^[11]. The core is about 1.8m in length, has some characteristic attributes and extreme properties and correlates with a set of geological layers called the Bleskop marker, which is a system associated with the UG2 a large ore reserve near Rustenburg.

The test setup is quite apparent from Figure 4-15 and Figure 4-16. The system was placed on a piece of expanded polystyrene to produce distance from the wooden table. The sensor was powered by a battery and the data was logged using two digital multi-meters and a scope connected to the computer. The sensor was moved in 1cm intervals alongside the pipe while noting the sample voltages and occasionally storing the waveform on the scope. The mark on the probe (displayed in Figure 4-16) was taken as the middle of the sensor with the sensing electrode on the left and the driving electrode on the right.

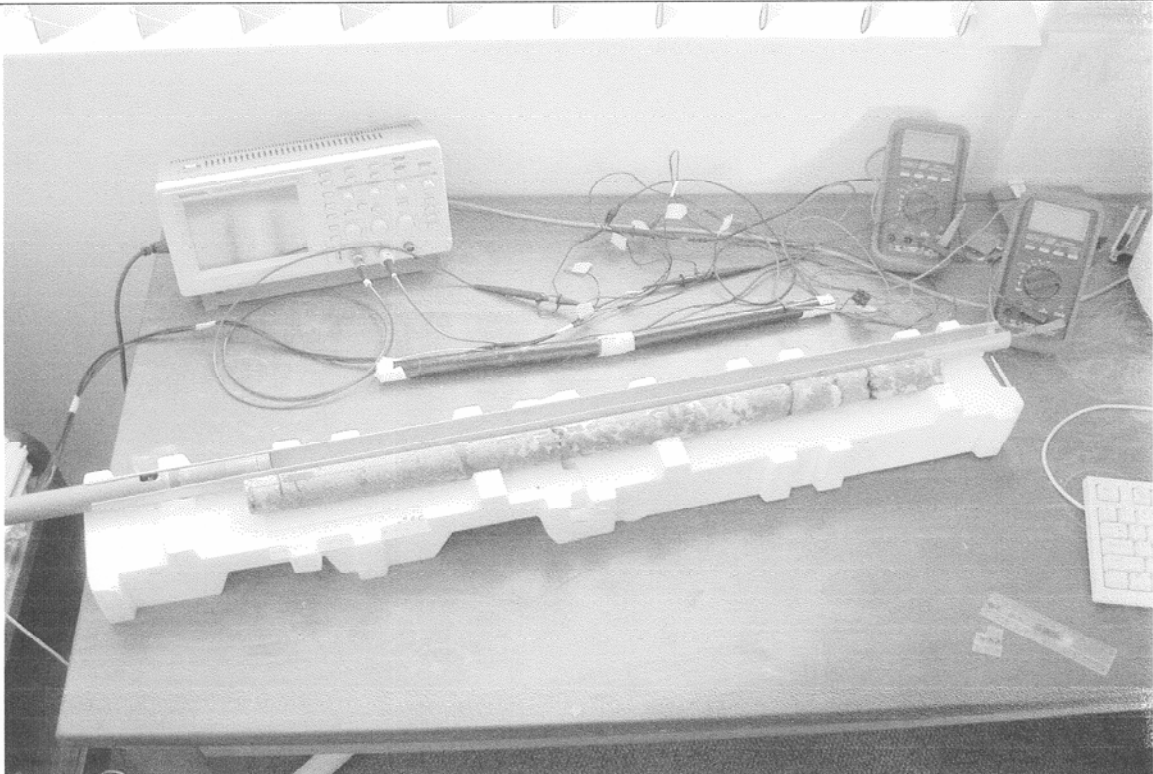


Figure 4-15 Test setup for measuring the borehole core

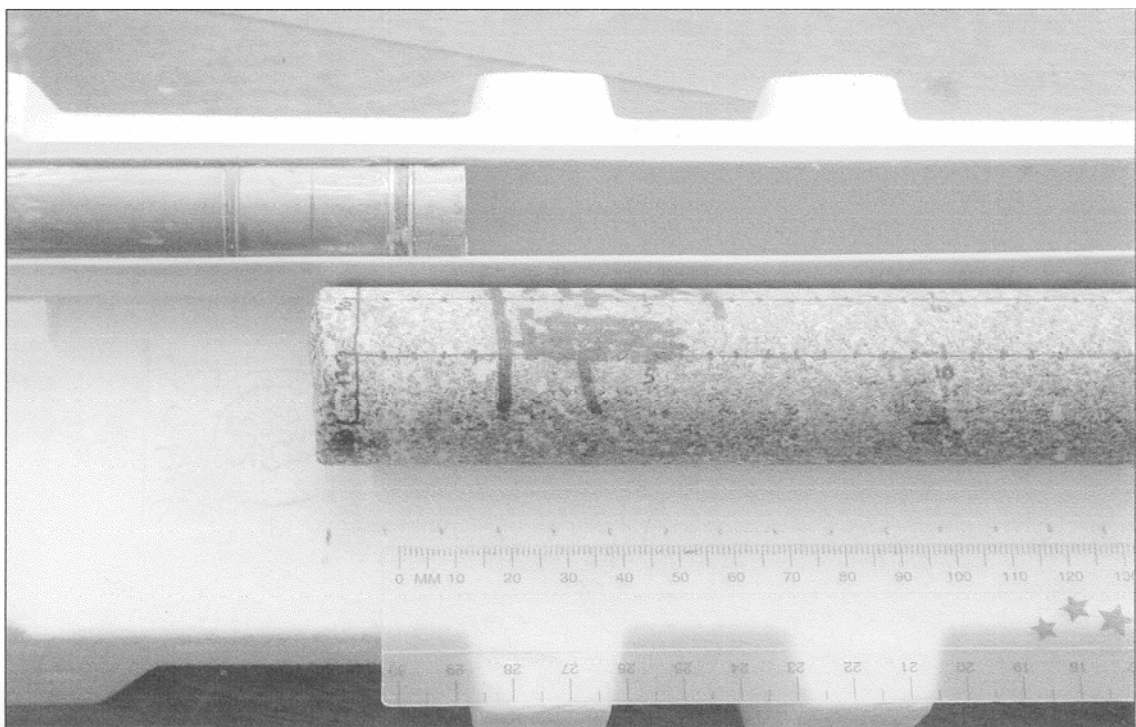


Figure 4-16 Close-up picture of the active probe elements and the core

4.3.2 Results obtained

The next two figures displays the data obtained with the sensor developed next to the results obtained by Rüttschlin.

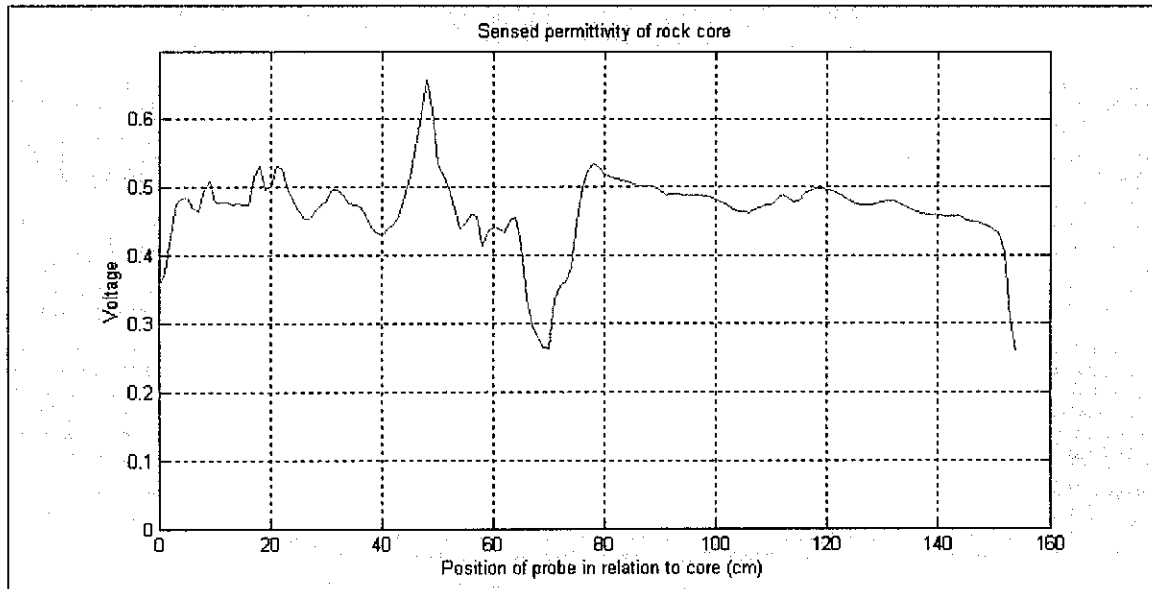


Figure 4-17 Sensed permittivity of rock core

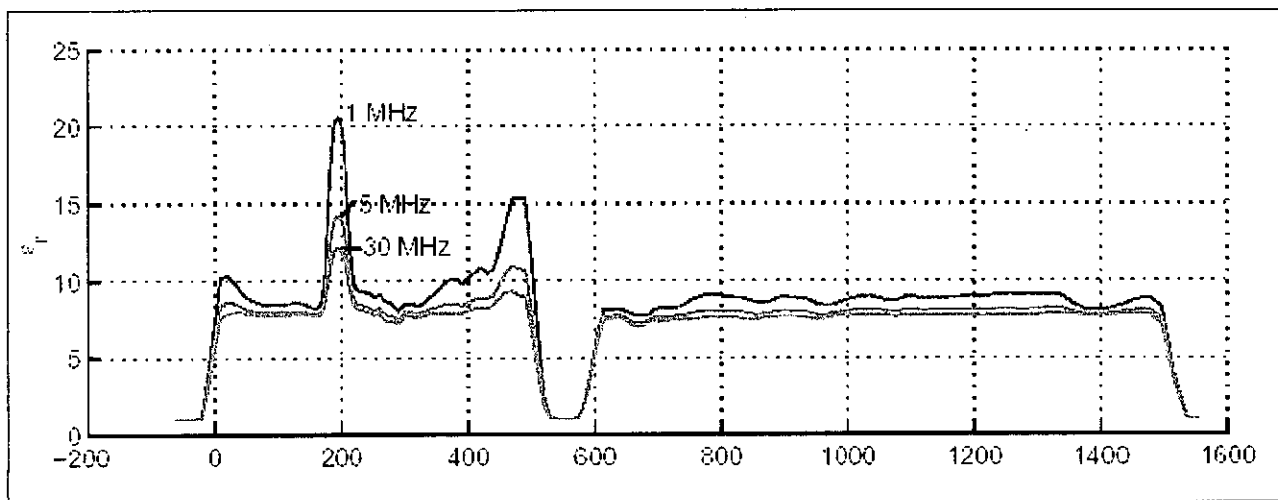


Figure 4-18 Permittivity of Bleskop marker used as reference for tests

Remarks on Figure 4-17 and Figure 4-18

- The most prominent features correlated with features displayed in the Rüttschlin results (Figure 4-18)
- Peak at the beginning correlates with the peak at the beginning in the Rüttschlin results. The two peaks that are so close together could be due to the transfer function of the sensor (see report on "bazooka" results).
- The peak at 20cm correlates with the chrome layer. The effect is small as the layer is thin.

- The large peak is at the fieldspathic pyroxenite and this is also shown in the Rütchlin results
- The negative peak corresponds with a bad break in the core.
- The rest of the graph stays constant as expected.

The losses were also measured and are displayed in Figure 4-19 with the reference data again alongside in Figure 4-20.

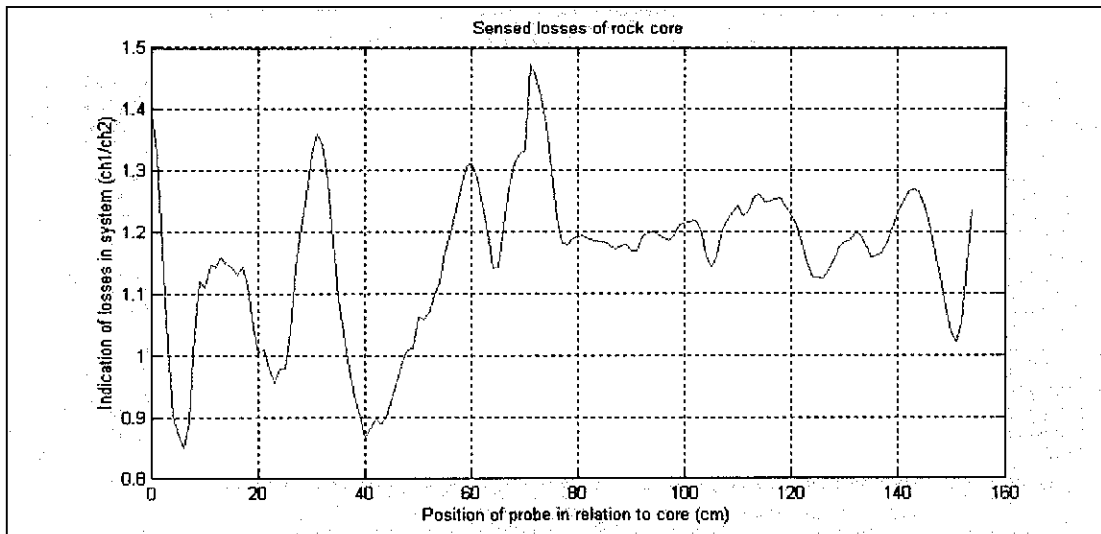


Figure 4-19 Sensed losses of rock core

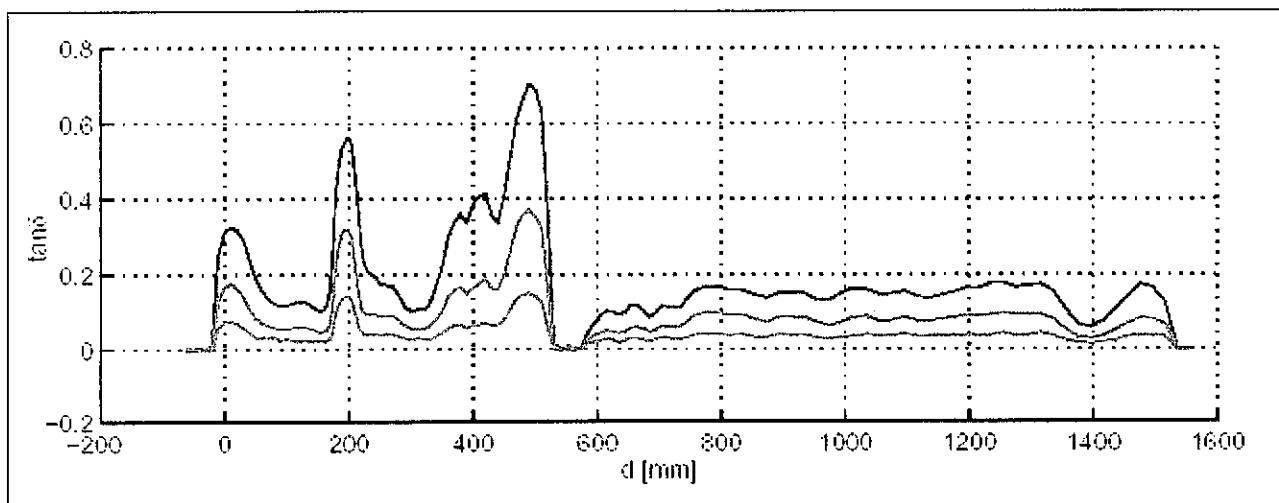


Figure 4-20 Losses of the Bleskop marker used as reference for tests

The ratio of the two samples indicate the losses perceived by the sensor. A ratio value of about 1.5 is the normal natural decaying rate and anything lower than that indicates losses. The lower the number the higher the losses. In Figure 4-19 the peaks at the beginning, at 20 cm, at 40 cm and at the end can clearly be seen as well as the low loss point where there is a break in the core. These factors can be seen in the

Rütschlin results displayed in Figure 4-20. The graphs shows that the sensor is able to sense the losses of rock core.

Two actual traces will be given now. One is measured in air and the other one was taken at the chrome layer. This was done purely for completeness and to show that the changes that were presented could be verified.

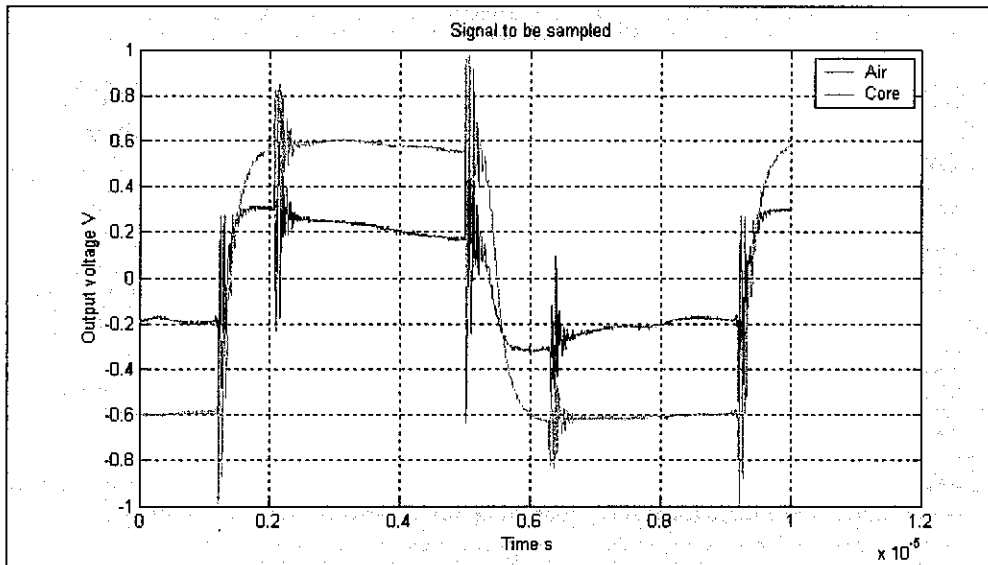


Figure 4-21 The actual received signal that was sampled

Remarks on Figure 4-21:

- The signal was sampled and not averaged.
- The changes in amplitude can be seen: indication of capacitance value.
- The changes in slope can be seen: indication of losses.
- The oscillations at the sample commands are visible but do not affect the signal amplitude and do not affect the sample output value. Power supply noise is probably the cause of this feature as the falling edge of all the sample and hold ICs produce the effect and not only the first two components that are connected to this signal. The addition of power supply capacitors at these ICs will be introduced.

4.3.3 Test on resolution of probe

Another test was done with a core that has a transition between chrome and pyroxenite. The transition is not clean and there is a layer of pyroxenite just before the transition. Figure 4-22 gives a picture of the core in the test set-up. The test was done in the same way as with the Bleskop marker. The reason for doing this test is to try and quantify the resolution of the sensor.

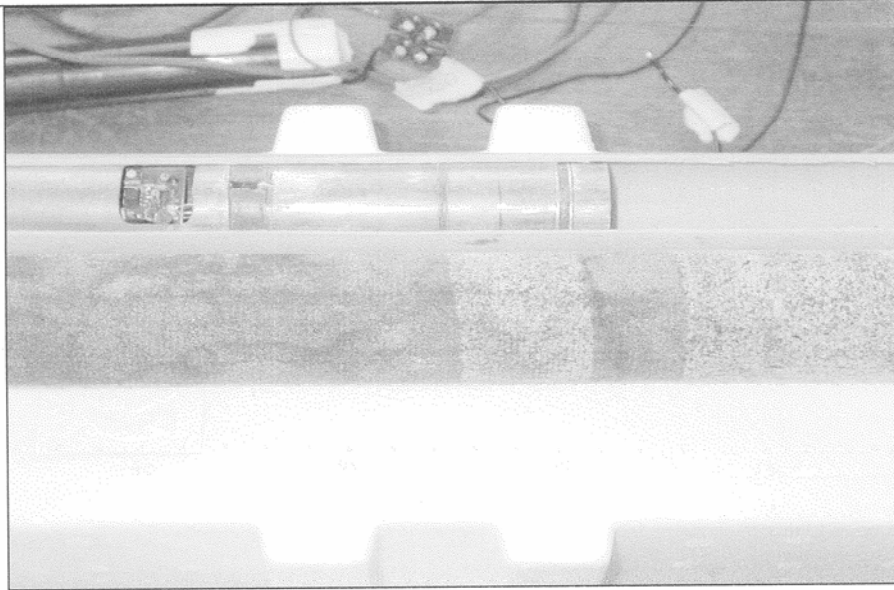


Figure 4-22 Sensitivity test setup: Chrome and pyroxenite interface

The resolution of the sensor is defined by the smallest layer of material that will be sensed accurately, implying that the output will indicate the permittivity and losses of the material. If a smaller layer is reached the output will indicate permittivity and losses that correlate to both of the layers. This implies that the sensor will have a smoothing effect on the layers. The test done here is to display and quantify this effect. A sensor with high resolution will produce the same output value for the large layer than the small layer. With the sensor implemented here this will not be the case as will be shown in Figure 4-23 and Figure 4-24. This definition of the sensitivity is harsh and the sensor will be able to indicate a layer that is smaller than the resolution but will not produce accurate permittivity and loss values. In addition to this an approximation of the properties of the material could be made if enough information is gathered in connection to the behavior of the sensor in small layers.

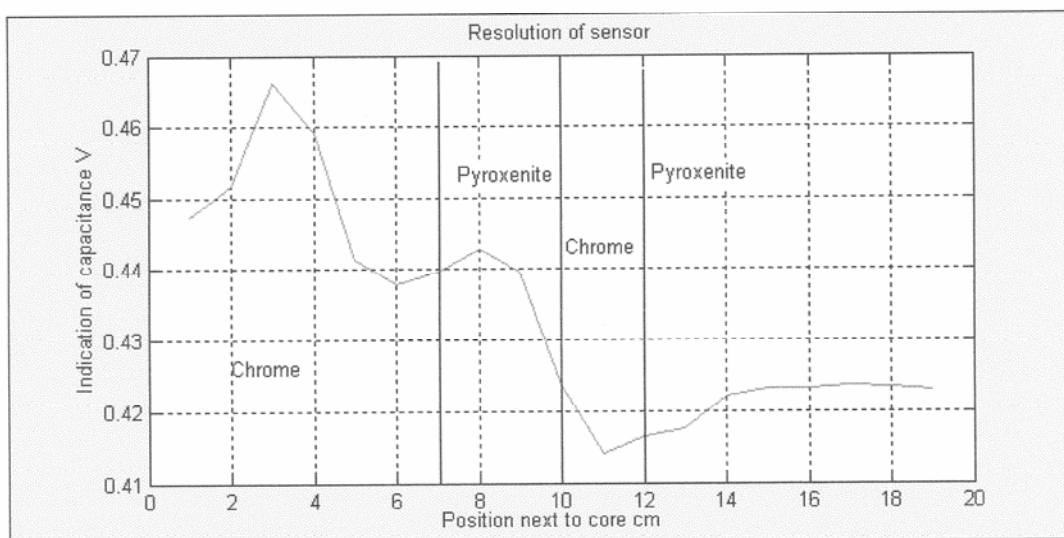


Figure 4-23 Sensed permittivity of chrome and pyroxenite interface

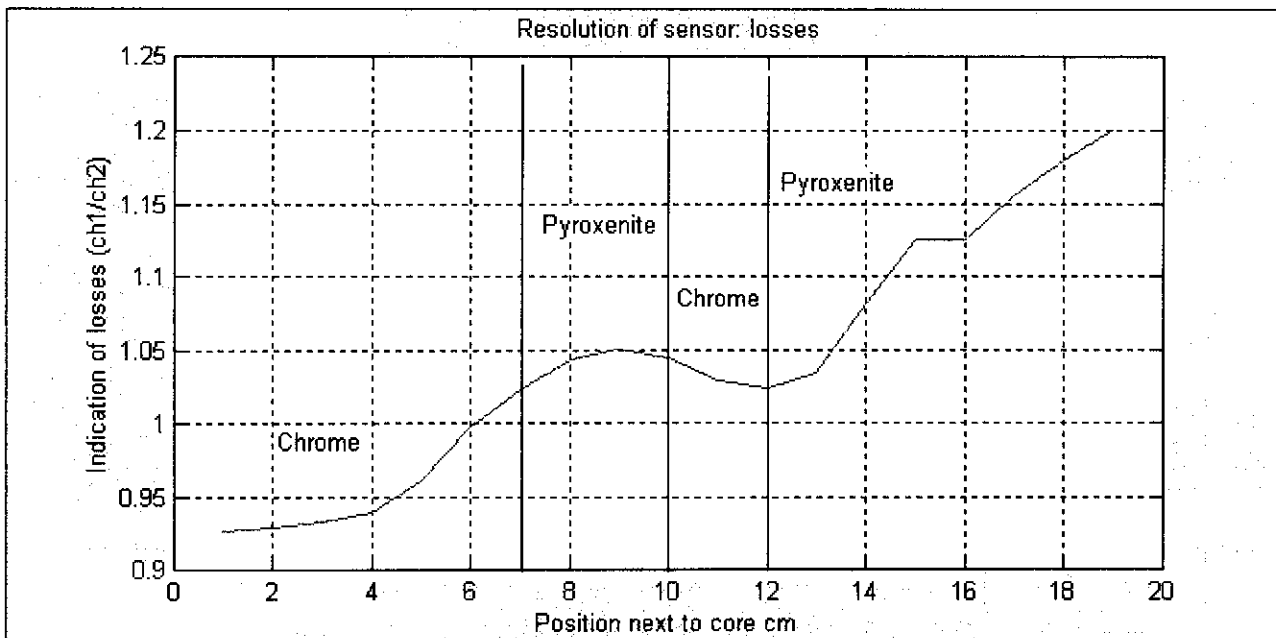


Figure 4-24 Sensed losses of chrome and pyroxenite interface

Remarks on resolution test:

- It can clearly be seen that both the losses and the permittivity indicate the layers.
- It can also be seen that the values for capacitance and losses are dependent on the total rock body and are not able to give accurate answers if the layers are small in relation to the sensor.
- The transitions between the materials are not quite the same as the measured transitions as the middle of the guard electrode is used as the reference middle while the electrical middle of the sensor seems to be in the middle of the sensing electrode (30mm to the left of the present center; to implement it in the graphs, subtract 3 from the x-axis).

4.4 Discussion of test results

The non-sinusoidal sensor is not capable of sensing the losses of saline water, but is capable of sensing losses of typical rock materials. The sensor has a complex transfer function if the transition of a material is reached. This makes it powerful to locate a change in two large materials, but if the layers are close to each other, the layers will affect each other and distinguishing between the layers will be troublesome.

The two tests that were performed had an aspect of the real life situation in them. The "bazooka" test was performed in a geometrical situation that resembles a borehole and the core tests were done on actual rock samples. Neither of them are, however, directly related to a mine situation. This made the task of producing a transfer function that could be associated with mine conditions impossible. Data points that correlated with test materials with known permittivity and losses were extracted. From these few points

and with the knowledge that the transfer function will approach an asymptote, a continuous transfer function was produced. Two sets of permittivity transfer functions were extracted according to the two tests completed and are displayed in Figure 4-25. These functions will differ as the test setups were different, but they will produce a trend that will be followed in the mine environment.

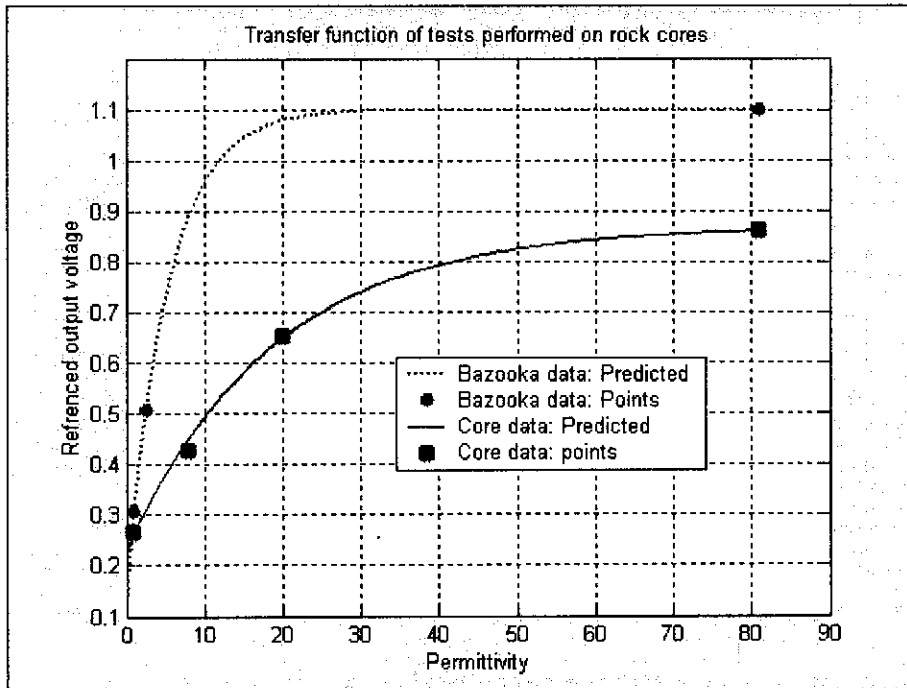


Figure 4-25 Transfer of probe for the two tests performed: Permittivity

The natural response was chosen as the base function on which the points were fitted. This function was chosen because the characteristic is asymptotic and the position of the points gave a hint to this method.

$$V = -Me^{\frac{\epsilon_r}{\epsilon_{r1}}} + K \quad (4.1)$$

Three points were needed to solve the function as there are three variables in the equation. For the core tests, four points were available and the fourth point is added but was not used to generate the function. The transfer function in borehole conditions will lie between these lines.

The same was done for the losses that were measured. The bazooka did not give results on the losses and no data was available. The core test transfer function could be predicted. This was once again done with the natural response as defined in equation (4.2) and the result is displayed in Figure 4-26.

$$\text{Ratio_of_channels} = Me^{\frac{\text{Tan}\delta}{\text{Tan}\delta_1}} + K \quad (4.2)$$

With M = 0.6263, Tanδ₁ = 0.1578 and K = 0.8737



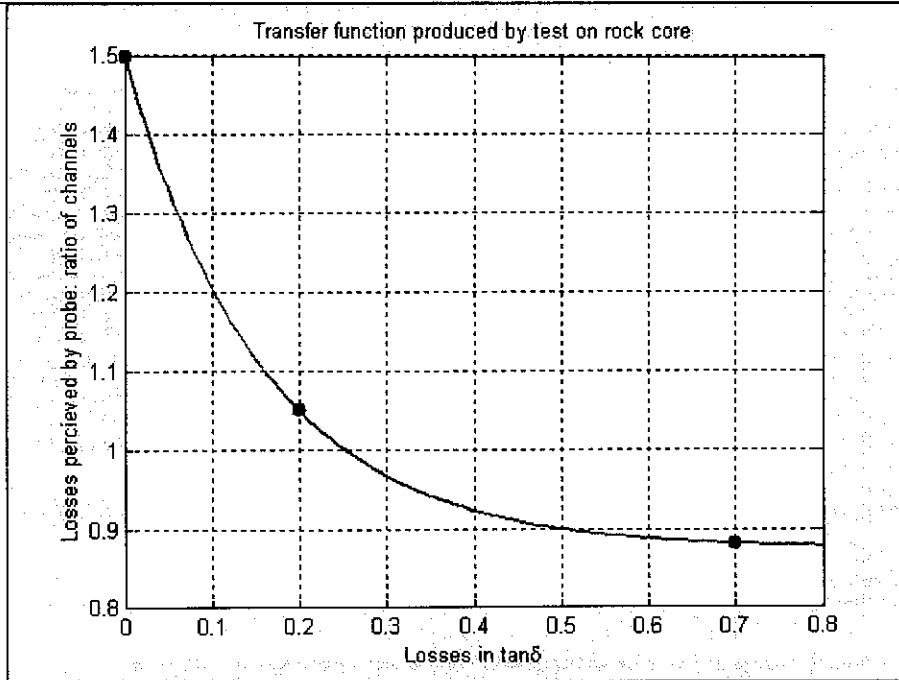


Figure 4-26 Transfer of probe for the test performed: Losses

This postulated transfer function can transform the raw data (as explained in section 3.5) to more standard units (permittivity and $\tan\delta$).



5 Conclusions

5.1 Overview

An overview of the topics covered in this report will now be given.

- The need for a dedicated sensor to produce a profile of the borehole's rock properties was stated. The properties are the hard rock permittivity and losses.
- The limitations on the design were formulated.
- The use of electrodes to couple fields into the rock was introduced. These electrodes form the heart of the sensor and produce a capacitance that is proportional to the rock permittivity as well as resistance that is proportional to the losses.
- The guard electrode concept was introduced to increase the sensitivity of the electrodes.
- Extensive simulation was performed to obtain the most suitable geometry for the electrodes.
- Three physical prototypes were built to produce tests that could verify the simulation results and to base the final design on.
- Different methods to sense small values of capacitance and large values of resistance were investigated and a specific method was chosen.
- Electronics were designed to drive the electrodes and to receive the resulting signal. Sample and hold components were used to sample the data. Buffers and level shifters were inserted to condition the output signals.
- Various tests were performed on the final probe to verify it's working.

5.2 Properties of sensor under laboratory conditions

From the final practical test results, it could be seen that the sensor was able to sense the permittivity and losses of materials with the same properties as the rock that is found in hard rock mines, in particular platinum group metals in the Bushveld igneous complex. Table 5 gives a product specification of the probe for tests conducted in laboratory conditions.

Table 5-1 Product specification under laboratory test situations

Power supply	12 Ni-Cd batteries in series producing between 13 and 15V DC
Power consumption	80 mA under working conditions (1.15W)
Probe physical size	320 mm long with diameter of 29 mm
Electrodes	Three active electrodes: Driven electrode, guard electrode and sensing electrode

Outputs	Two channels corresponding to different sampling times. One reference voltage (1V) by which the channels are referenced.
Output voltage range	From 1V to 4V
Signal driving the electrodes	Square wave
Sensitivity: Permittivity	From air ($\epsilon_r = 1$) to water ($\epsilon_r = 81$): 3.3 times
Data from test 2 on the rock core	From $\epsilon_r = 8$ to $\epsilon_r = 15$: 1.53 times
Sensitivity: Losses	Tan δ range of 0 to 0.7
Data from test 2 on the rock core	Channel ratio range of 1.5 to 0.88

If the borehole is filled with water, the functionality of the probe is lost. However, the probe will be able to produce information about the location of the water level and will recover the original functionality when removed from the water, this is acceptable to the initial problem statement.

The resolution of the probe is limited by the size of the electrodes and for the probe to be able to observe a layer of material accurately, the size of the layer must be larger than the total length of the electrodes. If a smaller layer is reached, the sensor will average out the permittivity and the layer will be sensed but the voltage will not produce a value that resembles the properties of the layer itself. The sensor is sensitive to materials removed as far as 20 cm from the electrodes. This will mean that a layer will have an effect (however small) on the probe if inside this distance.

The step response of the system is characteristic and will make the sensor exceptionally effective in observing sudden changes between two large layers of rock materials. Sensitivity increased to 7 at a water-air interchange

The radial positioning of the probe (if the probe is close to the rock body or touching it) is critical and small changes in radial positioning will affect the working of the probe.

To give an example of this: if an elevated ϵ_r material is placed broadside of the probe at a distance of 5 cm, the output voltage will decrease to a value that is lower than the value for air. If this material is brought closer until touching the probe, the voltage will increase to the expected value.

5.3 Problems associated with mine conditions

It was stated in the previous section that the probe must be in a stable radial position relative to the borehole to produce reliable results. With the present deploying mechanism this is not possible as was shown by the mine tests (appendix A). This implied that the sensor will not be able to work effectively in underground conditions with the present deployment method. If there is a borehole that is totally vertical and the tension in the pull rope is low enough to enable the probe to be pulled while lying on the bottom of the hole, the probe may produce stable results.

5.4 Future research possibilities

There is room for improvement and a few aspects that could receive attention will now be discussed.

- The deploying of the probe is being investigated and if a way could be devised to keep the probe in the same position relative to the hole, the present probe should work well in mine conditions.
- The principle that is used throughout this report is that the probe will lie on the rock and will be in direct contact. The present probe is covered with a 2 mm thick PVC. If this thickness is increased (and the electrode diameter decreased - total probe diameter stays constant) the active electrodes will be separated from the rock by a larger distance and the sensitivity will decrease. However, it could be expected that there will be an optimum radius for the pipe, hole and electrodes that would result in a probe that is position independent. The author suspects that the optimum point may be obtained by simulations similar to the simulations done in this report.
- The resonant circuit method of sensing capacitance may produce more sensitive results.
- If the deploying problem is solved, tests in mine boreholes with known properties must be done to calibrate the probe.

Bibliography

- [1] N. Braithwaite, G Weaver: "Electronic Materials", Butterworth-Heinemann, Oxford, 1990
- [2] S. Ramo, J.R. Whinnery and T van Duzer: "Fields and waves in communication electronics", Wiley and Sons Inc, New York, 1994.
- [3] J. Hargreaves: "*A multichannel borehole radar for three dimensional imaging*", PhD Thesis, Oxford University, 1995
- [4] T. Sindle, "*Design of an orientation sensor for borehole radar*", Final year B.Ing. report, University of Stellenbosch, 2002
- [5] *Netzsch Instruments, Inc.* [Online] Available at: <www.micromet.com/holometrix/m_sensors> Accessed: 31 October 2003
- [6] H.A. Haus and J.R. Melcher: "*Electromagnetic fields and energy*", Prentice Hall, New Jersey, 1989
- [7] James Clarke Maxwell, "A treatise on Electricity and Magnetism", Third edition, Vol. 1, Dover Publications Inc., New York, 1954.
- [8] FEKO [Online] Available at: <www.feko.co.ca> Accessed 05 March 2004
- [9] CST Microwave Studio version 3, *Help documentation: Getting started* Online at: <www.cst.de/content/applications>
- [10] D.M. Pozar: "*Microwave engineering*", John Wiley & Sons Inc., New York, 1998
- [11] M. Rütshlin: "*The Dielectric Properties of the Bleskop Marker*", Internal paper, University of Stellenbosch, 12 March 2003
- [12] R.E. Ziemer and W.H. Tranter: "Principles of communications", Wiley & Sons Inc, New York. 1995
- [13] W.H. Steyn: *Internal note on permittivity sensor used to measure the moist content of wood*, Dept Electric and Electronic engineering , University of Stellenbosch
- [14] Burr-Brown Corporation Datasheet: OPA 602 High Speed Difet operational amplifier

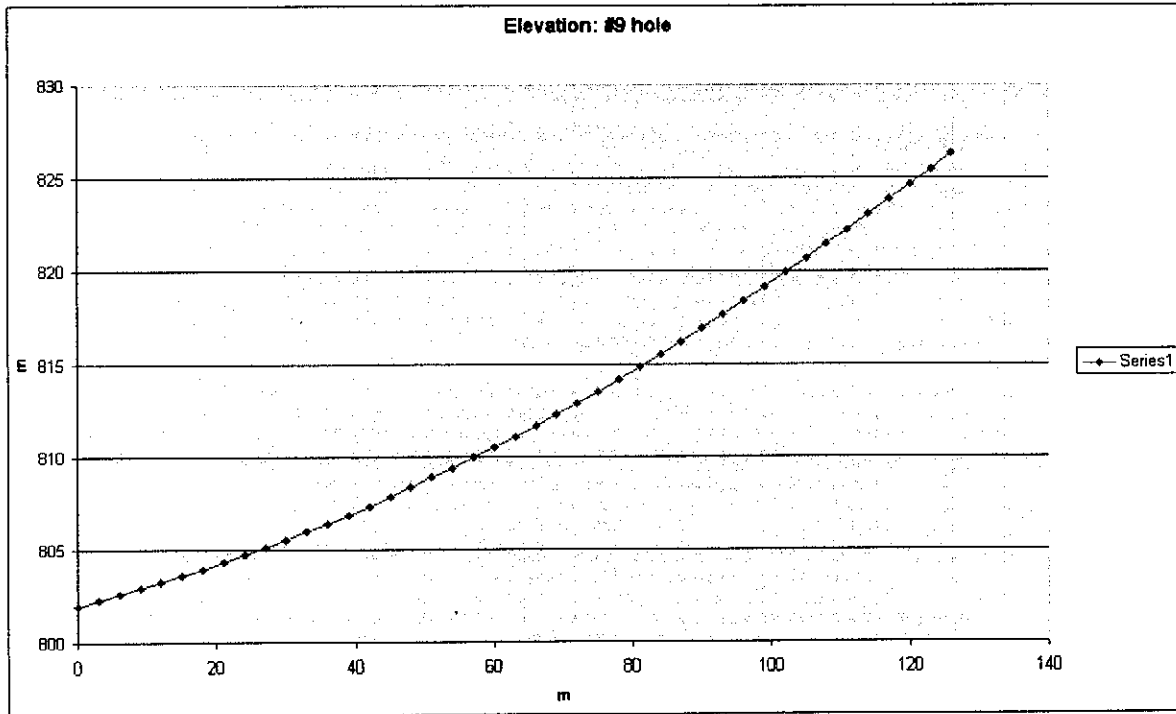


-
- [15] Neamen, Donald A: *“Electronic circuit analysis and design”*, The McGraw-Hill Companies Inc. 1996
- [16] Analog Devices datasheet: AD781 Complete 700 ns S&H amp, *Definition of specifications*.
- [17] *RS electronics Electronic catalogue*, April 2003 [Online] <www.rs-components.com/south-africa>
- [18] A. Ishimaru: *“Electromagnetic Wave Propagation, Radiation and Scattering”*, Prentice-Hall Inc. 1991
- [19] M Josh, Internal note, “Theory and usage of the Dielectric Borehole Probe”, CSIRO, Australia, 2 May
- [20] J.W. Nilsson and S.A. Riedel: *“Electric Circuits”*, Addison-Wesley Publishing Company Inc. 1996, Fifth Edition



Appendix A: Mine tests

The developed probe was subjected to tests in mine conditions. The tests were done at Bleskop Platinum mine situated close to Rustenburg. The borehole that was to be measured was 180 m long and drilled upwards at about a 6 degree angle . The trajectory was obtained from the Sindlehead navigator and is displayed in Figure A - 1.



A - 1 Vertical trajectory of borehole measured by Sindlehead navigator

The tests were not done over the entire length of the borehole and due to time and mechanical constraints the tests were stopped at 140 m. Josh^[19] also developed a probe similar to the rock sensor described in this document. Both these sensors was deployed in this borehole as field experiments. The borehole's core log will be displayed in the next figure and the hole went through the Bleskop marker.

The geological log is given in Figure A – 2. From this log, it is apparent that there is little geological features up to 116m into the hole. Then there is a lot of geological features and materials with properties that differ. There are three layers of chromite stringers that will have high permittivity and losses and might act as pointers to the position of the probe. The other materials (Norite, Anorthosite and Pegmatoid) are not characterized well and hopefully the results will shed light on these materials.



BLESKOP SHAFT GBH LOG SHEET

GHB No: Radar # 9
 Direction: RHS 61° 53' 24"
 Inclination: + 6° 06' 56"

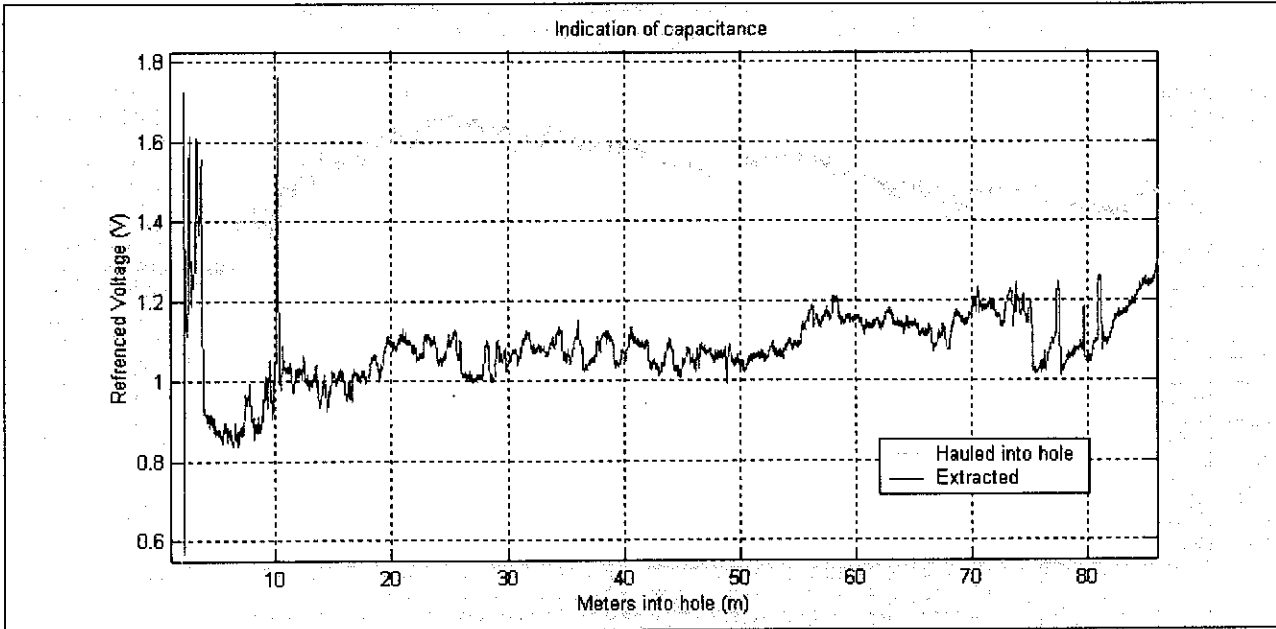
Date logged: _____ Geologist: Kabelo
 Location drilled: 12 Level 142 XIC STM Peg #: BL 502 + 22m

Collar X 2302512142 Y -89701435 Z 301936

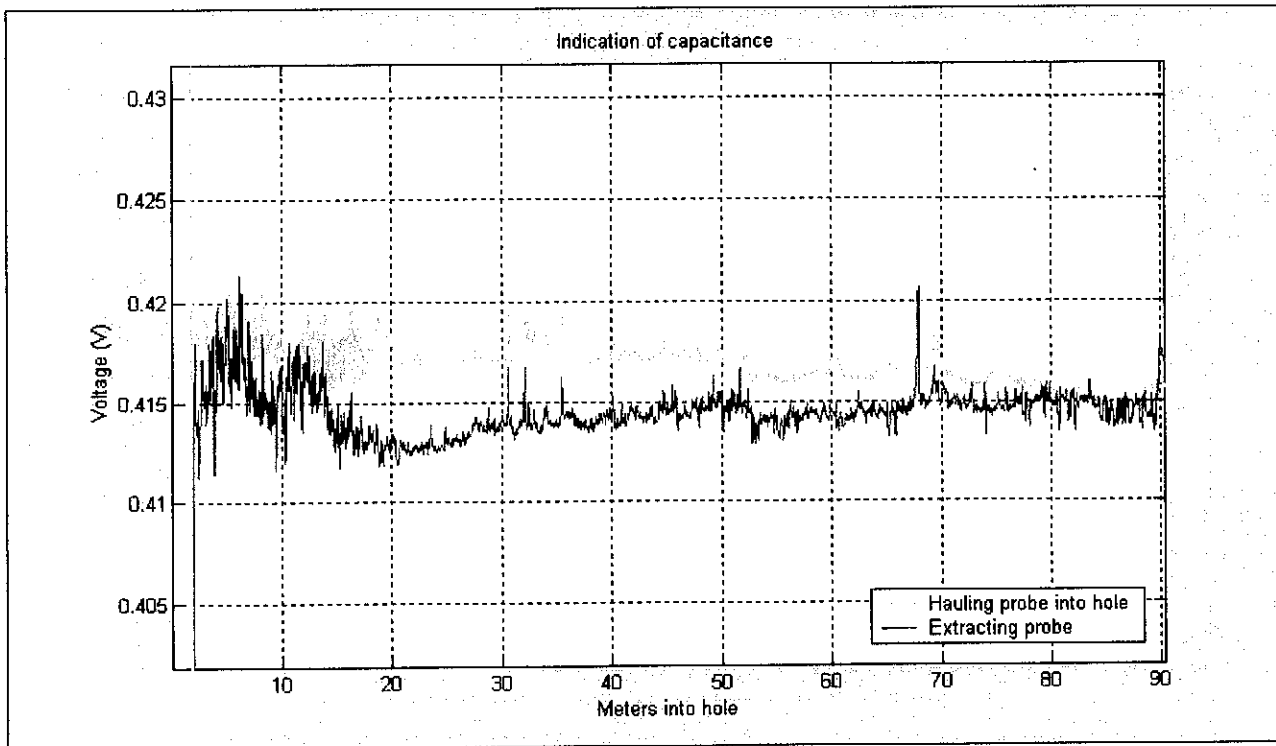
From	To	CA	Sketch	Rock Type	Description
0	10.8				
				NOI	NOHITE
116.500	117.20			MAI	MOTTLED ANORTITE
	122.0			NOI	1cm chromite stringer
122.0	124.0			NOI	NOHITE
	130.25			NOI PEG	PERCUPROID
130.25	135.00			NOI	1cm chromite stringer
	135.00			NOI	NOHITE
135.00	136.20			NOI	NOHITE
136.20	136.25			NOI	NOHITE
136.25	137.00			NOI	NOHITE
137.00	137.15			NOI	LEADER
137.15	137.20			NOI	LEADER
137.20	137.4			NOI	LEADER
137.4	137.25			NOI	LEADER
137.25	138.00			NOI	LEADER
138.00	138.05			NOI	LEADER
138.05	138.10			NOI	LEADER
138.10	138.15			NOI	LEADER
138.15	138.20			NOI	LEADER
138.20	138.25			NOI	LEADER
138.25	138.30			NOI	LEADER
138.30	138.35			NOI	LEADER
138.35	138.40			NOI	LEADER
138.40	138.45			NOI	LEADER
138.45	138.50			NOI	LEADER
138.50	138.55			NOI	LEADER
138.55	138.60			NOI	LEADER
138.60	138.65			NOI	LEADER
138.65	138.70			NOI	LEADER
138.70	138.75			NOI	LEADER
138.75	138.80			NOI	LEADER
138.80	138.85			NOI	LEADER
138.85	138.90			NOI	LEADER
138.90	138.95			NOI	LEADER
138.95	139.00			NOI	LEADER
139.00	139.05			NOI	LEADER
139.05	139.10			NOI	LEADER
139.10	139.15			NOI	LEADER
139.15	139.20			NOI	LEADER
139.20	139.25			NOI	LEADER
139.25	139.30			NOI	LEADER
139.30	139.35			NOI	LEADER
139.35	139.40			NOI	LEADER
139.40	139.45			NOI	LEADER
139.45	139.50			NOI	LEADER
139.50	139.55			NOI	LEADER
139.55	139.60			NOI	LEADER
139.60	139.65			NOI	LEADER
139.65	139.70			NOI	LEADER
139.70	139.75			NOI	LEADER
139.75	139.80			NOI	LEADER
139.80	139.85			NOI	LEADER
139.85	139.90			NOI	LEADER
139.90	139.95			NOI	LEADER
139.95	140.00			NOI	LEADER

A - 2 Detailed core log of test borehole

To display the results, the data was extracted and plotted against the position inside the borehole. If the data of the whole hole is displayed in one figure, the information is too cluttered and the hole was divided into two sections. The first section is from 0 to 90 m into the hole. This is a quiet section. The two graphs are for the insertion (dark) and extraction (light) samples.



A - 3 Capacitance of first part of borehole: measured by the rock probe

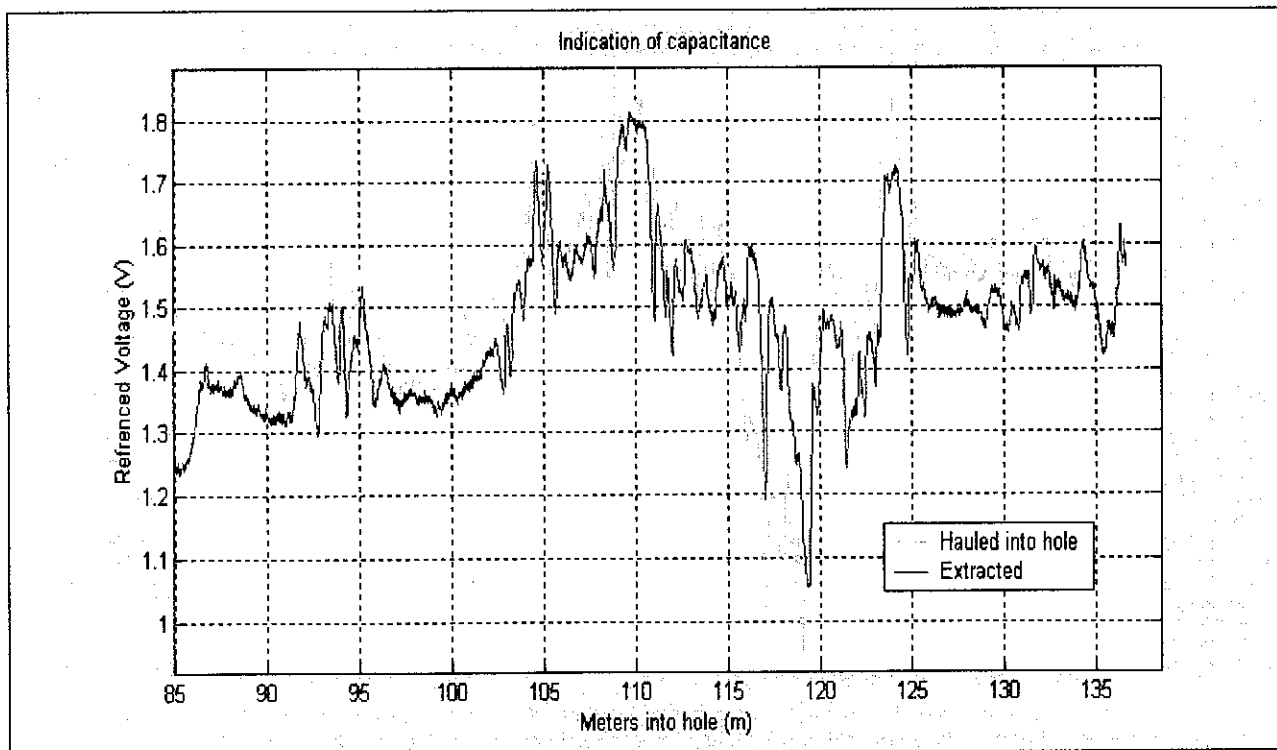


A - 4 Capacitance of first part of borehole: measured by the Josh probe



Remarks on A - 3 and A - 4:

- The rock probe's data has been processed and is referenced to ground, the Josh probe's data is raw and is referenced against 0.33 V
- The Josh data is smooth and gives an indication that nothing is happening with the properties of the rock. The traces for the insertion and extraction data is not exactly the same.
- The rock probe data shows large difference between the insertion and extraction data.
- The rock probe data shows signs of temperature dependence. This could be seen from the voltage increase after the probe was inserted in the rock body..



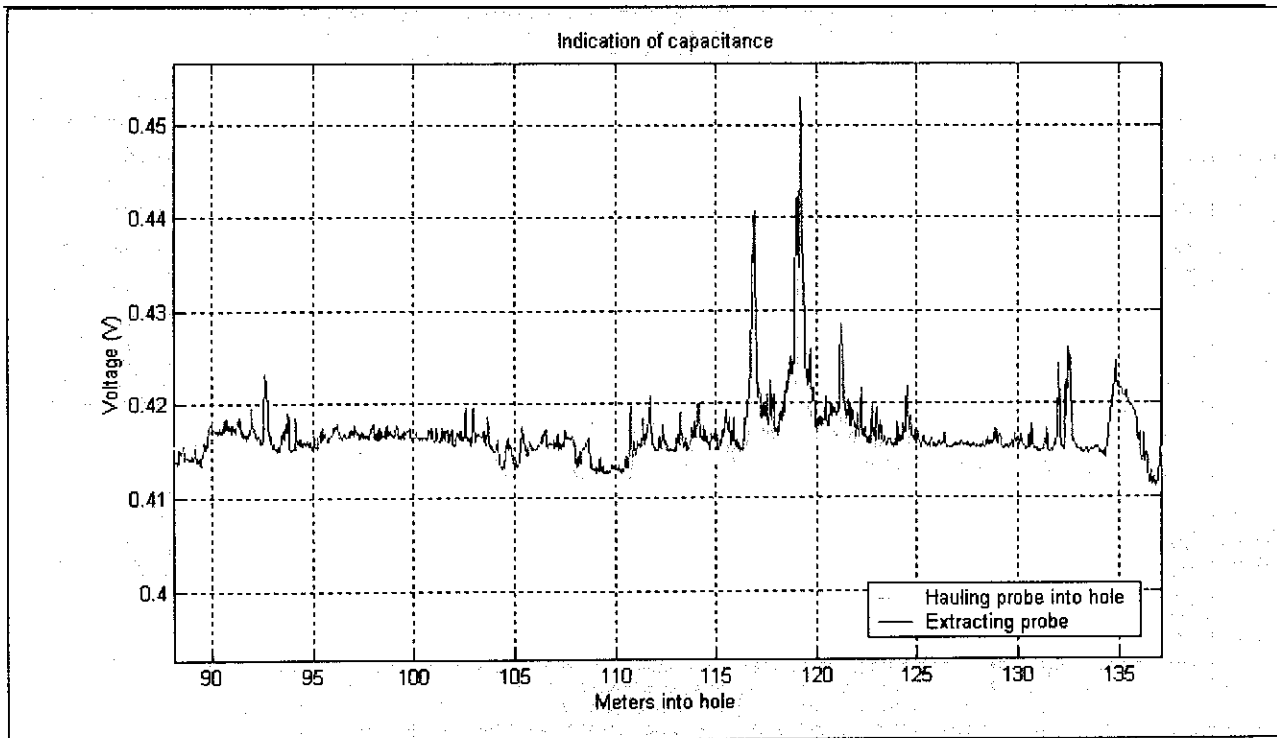
A - 5 Capacitance of second part of borehole: measured by the rock probe

Remarks on second part of borehole (A - 5 and A - 6)

- With this graph the two directions are close to each other.
- The jump in the data between 115 and 120 m into the hole was due to a problem with the reference voltage regulator.

There are six prominent features in A - 5 and A - 6

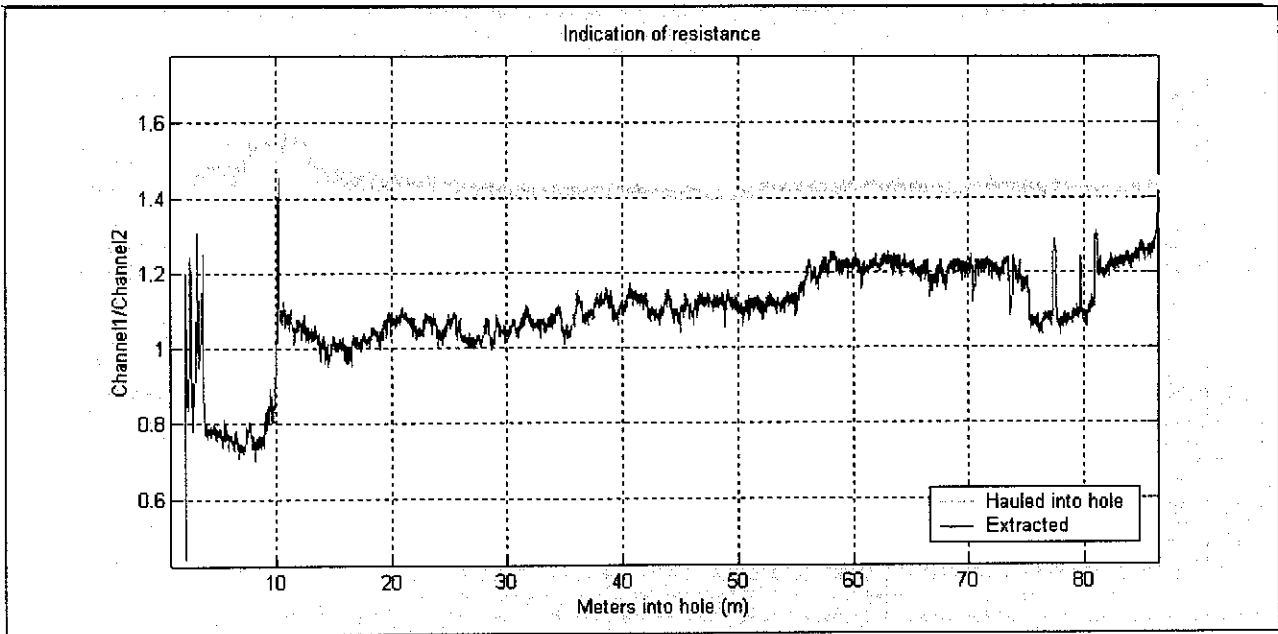
- At 95 meters there is activity that is not expected as the core log indicates that nothing is present there. There was a problem with the physical deploying at this mark as there was a "rough" patch in the hole, one probe even got stuck there. The activity could be related to this rough patch.



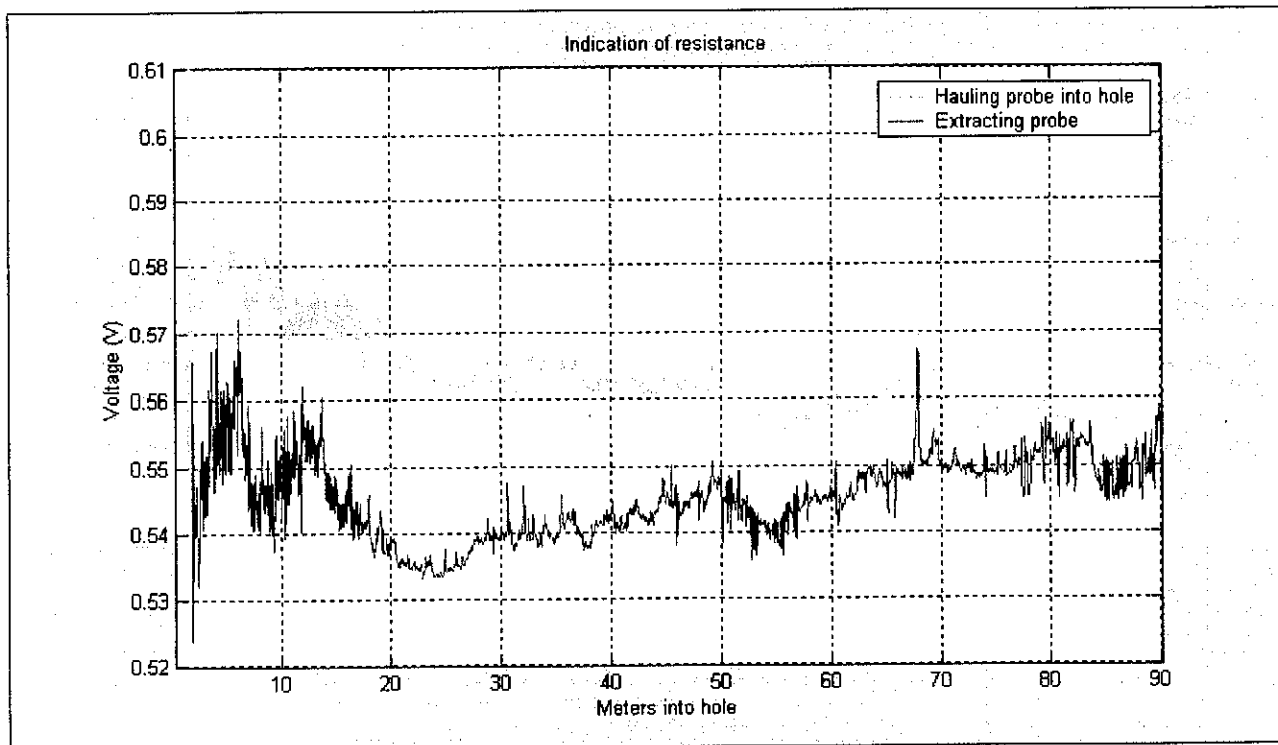
A - 6 Capacitance of second part of borehole: measured by the Josh probe

- Between 108 and 111 m the rock sensor sensed a stable high permittivity region while the Josh probe sensed a stable low permittivity reading.
- The Josh probe sensed two large peaks at 117 m and at 119 m respectively. The rock sensor sensed two low peaks at the same positions (if the extraction data is used).
- There are two stable high permittivity readings in the rock probe measurements between 120m to 122 m and 124 m to 125 m. These attributes were not measured by the Josh probe, but it did indicate a sharp point at 122 m.
- There are two peaks between 132 m and 133 m in the Josh results which are not shown in the rock samples.
- Between 134 m and 137 m both the Josh and rock probes sensed a characteristic waveform and again the signal was just inverted for the different probes.

The losses for the whole borehole were measured. Again there is a trace where the probe was hauled into the hole and one where it was extracted. Both sensors was used. Figures will follow.



A - 7 Losses of first part of borehole: measured by the rock probe

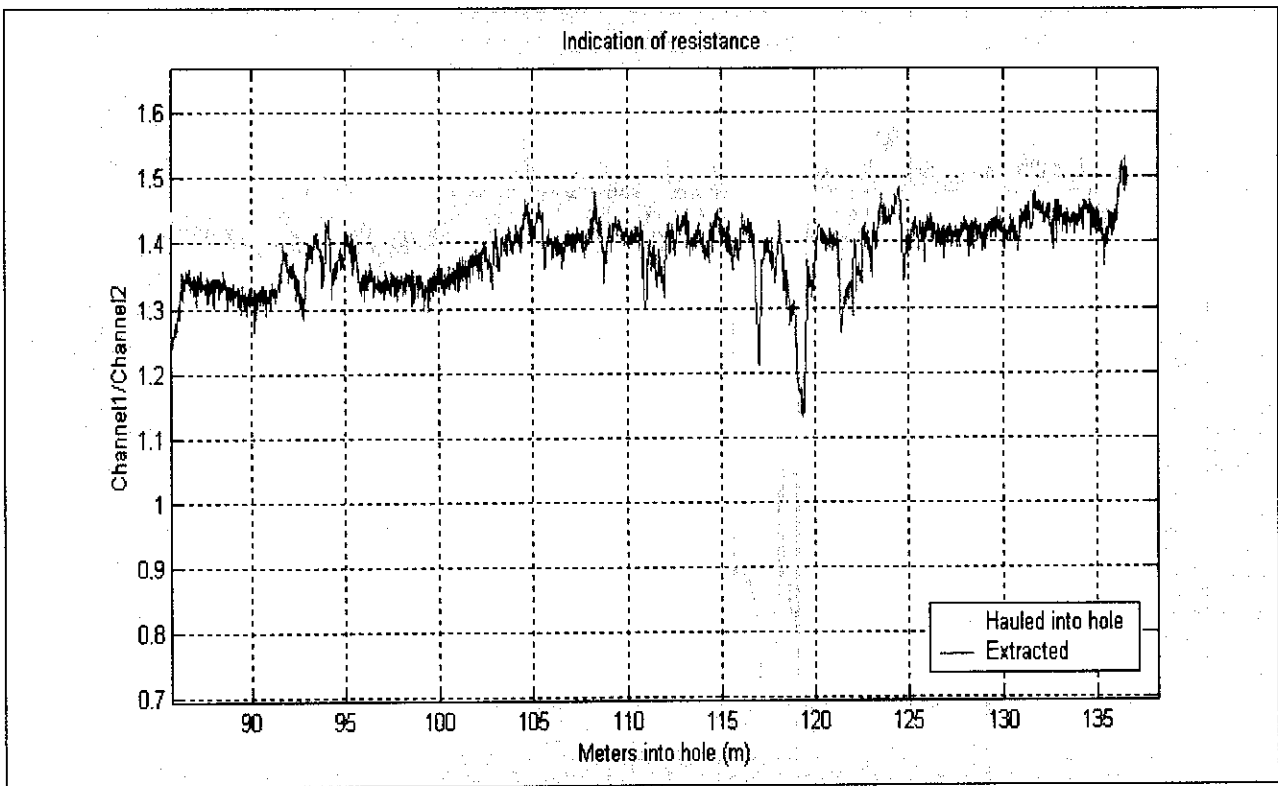


A - 8 Losses of first part of borehole: measured by the Josh probe

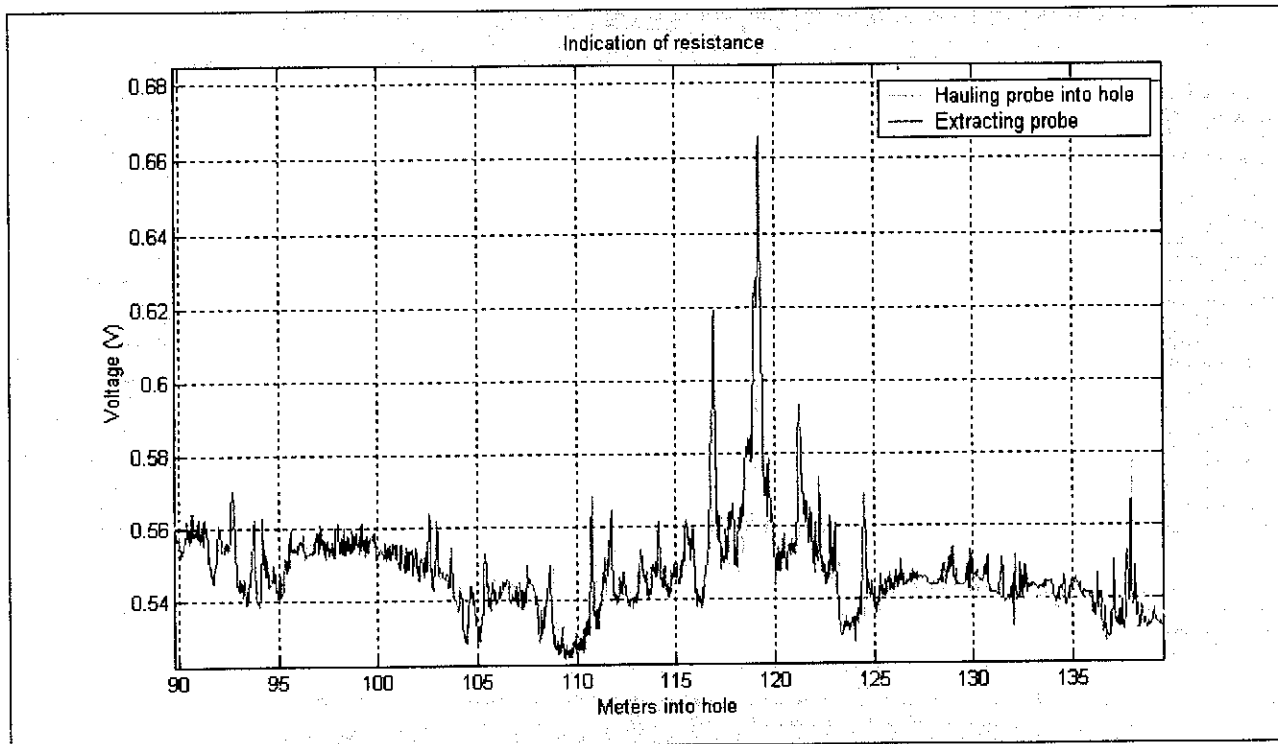
Remarks on A - 7 and A - 8

- Non-symmetry can be isolated in both the traces.
- The jump that occurred with the rock sensor is again attributed to the voltage reference.





A - 9 Losses of second part of borehole: measured by the rock probe



A - 10 Losses of second part of borehole: measured by the Josh probe



Remarks on A - 9 and A - 10.

- The rough patch at 95m can be seen in both samples.
- The Josh probe indicates a low loss layer at 110m. This is not shown in the rock probe data.
- The two high loss peaks at 117m and 119m were sensed by both probes.
- The losses between 120m and 125m have the same characteristic measured by both probes.

Conclusions on mine tests:

Temperature: To use the zener as the voltage reference was not a good decision as it is temperature dependent. This reference voltage was not sampled and saved, if this was saved, the temperature dependence could have been subtracted in the post processing of the data. This led to the use of the temperature stable voltage reference and sampling of the referenced voltage.

Symmetry: The probe should have produced the same voltage when traveling in and out of the borehole. This was not the case with either of the probes, however this feature was worse for the rock probe. One explanation to this might come from the deployment method: Because the hole is not straight and there is tension in the ropes/cables it might happen that the tension in the rope may lift the sensor off the rock. This effect is gradual as the probe approaches the end of the hole. When the probe is pulled out, the other rope is used and this will lead to further separation. As was shown in the laboratory tests done on the probe, the sensor is sensitive to radial positioning in the hole.

Capacitance: In the capacitance test, the results of the rock probe were just the opposite of what was expected: If a higher ϵ_r material is reached the probe indicates a lower ϵ_r . This contradicted the expected functionality. However, in the laboratory tests on the probe, it was shown that materials with elevated permittivity which are far away from the probe had this contradictory effect as the fields are concentrated far from the probe. This was believed to come into play when the material is about 10cm away from the probe, but from the measurements taken in the mine, this distance seems to be more in the vicinity of 2cm for a borehole. This difference may be due to the fact that the clinical tests were not done in borehole conditions. This may also add to the explanation of the non-symmetry.

Losses: The rock sensor was able to sense the losses of the material to a large extent and produce usable information. The Josh probe's sensitivity was still superior.

The mine tests were successful for it produced information that could be used and indicated that the sensor does have potential. Information was gathered on the attributes that did not work and this information was (and could be) used to solve these problems.

Very little correlation could be established between the rock core log and the results obtained by the two sensors. This point stresses the need for a sensor to measure the properties of the rock.

Appendix B: Detailed figure of "Bazooka"

